University of Kentucky

UKnowledge

2019

INVESTIGATION OF CHIP-FORM AND TOOL-WEAR IN TURNING OF HARDENED AF9628 ALLOY UNDER VARIOUS COOLING AND LUBRICATION CONDITIONS

Jason Wolf

University of Kentucky, jason.wolf@uky.edu

Digital Object Identifier: https://doi.org/10.13023/etd.2019.471

Right click to open a feedback form in a new tab to let us know how this document benefits you.

STUDENT AGREEMENT:

I represent that my thesis or dissertation and abstract are my original work. Proper attribution has been given to all outside sources. I understand that I am solely responsible for obtaining any needed copyright permissions. I have obtained needed written permission statement(s) from the owner(s) of each third-party copyrighted matter to be included in my work, allowing electronic distribution (if such use is not permitted by the fair use doctrine) which will be submitted to UKnowledge as Additional File.

I hereby grant to The University of Kentucky and its agents the irrevocable, non-exclusive, and royalty-free license to archive and make accessible my work in whole or in part in all forms of media, now or hereafter known. I agree that the document mentioned above may be made available immediately for worldwide access unless an embargo applies.

I retain all other ownership rights to the copyright of my work. I also retain the right to use in future works (such as articles or books) all or part of my work. I understand that I am free to register the copyright to my work.

REVIEW, APPROVAL AND ACCEPTANCE

The document mentioned above has been reviewed and accepted by the student's advisor, on behalf of the advisory committee, and by the Director of Graduate Studies (DGS), on behalf of the program; we verify that this is the final, approved version of the student's thesis including all changes required by the advisory committee. The undersigned agree to abide by the statements above.

Jason Wolf, Student

Dr. I. S. Jawahir, Major Professor

Dr. Fazleena Badurdeen, Director of Graduate Studies

INVESTIGATION OF CHIP-FORM AND TOOL-WEAR
IN TURNING OF HARDENED AF9628 ALLOY UNDER
VARIOUS COOLING AND LUBRICATION CONDITIONS

THESIS

A thesis submitted in partial fulfillment of the
requirements for the degree of Master of Science in
Manufacturing Systems Engineering in the
College of Engineering at the University of Kentucky

By

Jason Brian Wolf

Lexington, Kentucky

Director: Dr. I. S. Jawahir, Professor of Mechanical Engineering

Lexington, Kentucky

2019

ABSTRACT OF THESIS

INVESTIGATION OF CHIP-FORM AND TOOL-WEAR
IN TURNING OF HARDENED AF9628 ALLOY UNDER
VARIOUS COOLING AND LUBRICATION CONDITIONS

Next generation defense and commercial applications for structural steels require new alloys that eliminate or reduce critical elements from their composition to lower cost and improve manufacturability, while maintaining or exceeding high strength and toughness requirements. A new alloy, denoted as AF9628, has recently been developed for this purpose and its manufacturing characteristics and the material response in component manufacturing must be fully understood.

In the present study, hardened AF9628 alloy was turned with a coated carbide cutting tool under fixed cutting speed, feed rate, and depth of cut parameters. This work focuses on chip-form and tool-wear analysis to understand, for the first time with AF9628, these fundamental aspects of the turning process and their relationship to productivity and part quality. Current industry standard practice of flood-cooled machining for AF9628 was used during machining experiments. Dry, minimum quantity lubrication (MQL), and cryogenic machining were investigated as alternative cooling and lubrication conditions.

High-speed imaging during AF9628 turning experiments provides a new insight into the chip formation process, while the use of optical microscopy and scanning white light interferometry allowed for further characterization of chip-form and tool-wear. Chip-form is favorable as short, arc-shaped chips with new tools under all of the tested cooling and lubrication conditions. As a result of rapid wear at the end of the tool-life in all of the experimental conditions, chip-form evolves to unfavorably long, snarled ribbon-like chips and the resultant cutting force increased by as much as 64% under flood-cooled conditions.

Tool-wear types that were observed during experiments include a combination of nose wear, built-up edge, plastic deformation, and groove wear on the rake face. Due to the fixed cutting parameters and cutting tool selected for this study, which were designed for flood-cooled machining in a prior study, undesirable failure of the cutting tools under dry, MQL, and cryogenic machining occurred. Future work requires experimentation across a wider processing space, and with different cutting tools, to thoroughly evaluate alternative cooling and lubrication techniques for machining AF9628.

KEYWORDS: Chip-form, Tool-wear, Machining, High-strength Low-alloy Steel, Cooling and Lubrication

Jason Brian Wolf
_____

13 December 2019
_____

INVESTIGATION OF CHIP-FORM AND TOOL-WEAR
IN TURNING OF HARDENED AF9628 ALLOY UNDER
VARIOUS COOLING AND LUBRICATION CONDITIONS

By

Jason Brian Wolf

Dr. I. S. Jawahir
Director of Thesis

Dr. Fazleena Badurdeen
Director of Graduate Studies

13 December 2019

ACKNOWLEDGEMENTS

My opportunity to pursue graduate education full-time would not have been possible without the Air Force Research Laboratory's (AFRL) Materials and Manufacturing Directorate. I am grateful for so many individuals, at many levels of the organization, including Dr. Charles "Chuck" Ormsby, Dr. Howard Sizek, and Dr. Steven Turek, for encouraging and supporting me before this journey began and all the way up until the end. I am also grateful for the many discussions on AF9628 research that I have had with Dr. Rachel Abrahams, Dr. Manny Gonzales, and Dr. Eric Payton. There are many others that have played key roles in making the opportunity for me to pursue graduate education while on full-time leave possible. Many individuals offered technical support, provided moral support, and carried my workload while I was away at school. To all whom I have not listed or forgotten, please forgive me for this transgression. I will be forever grateful for this growth opportunity and immense support from so many members of the U.S. Air Force family.

Finally, I am thankful for the support from my family who have sacrificed so much to get me where I am today. Last but not least, I would be remiss to not express my deep appreciation for my wife, Erica. Thank you for your patience, love, and support in helping me across this finish line. You have been anxiously waiting for me to finish this work so that you can have my time back on evenings and weekends. Here it is!

TABLE OF CONTENTS

LIST OF TABLES

LIST OF FIGURES

CHAPTER 1

INTRODUCTION

We speak in strange terms: of harnessing the cosmic energy;
of making winds and tides work for us; of creating unheard synthetic
materials to supplement or even replace our old standard basics;

- *General Douglas MacArthur, "Duty, Honor, Country"*

1.1   Introductory Remarks

The work described in this thesis is focused on chip-form and tool-wear during machining of a hardened steel. The machining process of choice is turning, in which work is performed on a machine tool called a lathe. A workpiece is held in a rotating work-holding device, called a chuck, while a cutting tool traverses along the machine's axes to remove material in a controlled manner. This thesis is concerned with understanding how chips are formed during the cutting process and, just as importantly, why the cutting tool of choice wears away over time in the manner that it does. The greater aim of this work is to provide valuable insight towards more productive manufacturing of the steel of choice and other related materials.

1.2   Historical Context and Motivation

The story of materials is very much like the story of civilization. Throughout history, ages have been defined by the materials that were discovered, or created, and consequently played a critical role in shaping civilizations' development. As a result of the importance of materials throughout our history, most have heard of the Stone Age, the Bronze Age, and the Iron Age. The Iron Age is commonly believed to have begun around 1200 BC near the Middle East and southeastern Europe. By 1000 BC, the knowledge of iron metallurgy had begun being rapidly exported to other regions of the world. During this time, many people began fashioning the necessary weapons and tools for survival out of

iron and steel. Many scholars consider the Iron Age to have ended around 550 BC. However, iron and steel continue to play a critical role in modern day life.

Next generation defense and commercial applications for structural steels require new alloys that eliminate or reduce critical elements from their composition to lower cost and increase ease of manufacture, while maintaining or exceeding high strength and toughness requirements. Prior art compositions of high-strength, high-performance steels have included high weight percentages of expensive elements, such as nickel and cobalt, which contribute to the high overall cost and difficulty of processing the final steel product. A new steel alloy, denoted as AF9628, has been developed for the purposes of lowering cost, increasing the ease of manufacture, and eliminating tungsten from the material waste stream. The rise of this new material requires that its manufacturing characteristics and the material response in component manufacturing are fully understood to reduce the risk of the material's adoption by industry for various applications.

Like materials, manufacturing processes have also shaped civilization and changed over time as new materials have been created and the desire for more control during manufacturing to produce more complex-shaped products has risen. Of these processes, machining plays a critical role in component production in both the commercial and military industries. As new materials are developed to meet cost and performance demands, the need for research rises to ensure that affordable and effective manufacturing processes are employed. Machining is particularly important since it is often the last process of a manufactured component, thus making it high value. Moreover, since machining is often the final process for a finished manufactured component, the final component quality is highly dependent upon it.

1.3   Problem Statement

Since AF9628 was developed within the last few years, little research has been conducted with regard to machining this steel and characterizing its manufacturability. In metal cutting, tool-wear is an important, fundamental aspect of the process as it has significant implications on the stability of a process, the quality of the final product, and manufacturing costs. Therefore, one aspect of this thesis is focused on investigating tool-

wear to better understand the manufacture of AF9628 and move towards better processing conditions and cutting tool recommendations for finish machining in a hardened state.

Another important aspect of metal cutting processes is the means of chip-form during the process. Since the chips being formed from a metal cutting process are a bi-product and generally considered waste, many people do not consider this to be important with regard to overall machining performance. However, the manner in which chip-form occurs has an impact on the cutting forces generated during metal cutting, the temperatures generated near the workpiece and tool interfaces, and how the tool may wear over time. Much of the energy put into the machining process is used to form the chip so from an economic and practical view, understanding chip-form is important. As such, understanding chip-form, like tool-wear, can provide valuable insight into the cost and stability of the process and therefore the quality of the final product and manufacturing costs.

A variety of laboratory tools are used to qualitatively and quantitatively characterize the type of chip-form and tool-wear produced from the cutting process, all with the aim of contributing to the risk reduction for industry adoption of AF9628. The industry standard for many metal cutting applications is to use a flood of coolant during the cutting process to cool down the tool-workpiece interaction zone, provide some amount of lubrication between the tool and workpiece, and carry away the resulting metal chips from the process. Many alternative cooling and lubrication techniques to flood-coolant have been used successfully for other materials and material removal and/or finishing processes. However, these alternative cooling and lubrication techniques have not yet been performed for AF9628 machining and are therefore also investigated in this work.

Chip-form and tool-wear have not been specifically investigated during the turning process of hardened AF9628 alloy. This thesis will investigate these two phenomena to fill the knowledge gap around this aspect of machining performance. Further, the interrelationship between how chip-form effects tool-wear and how tool-wear consequently effects chip-form will be discussed.

1.4   Outline of this Work

This thesis is organized into 6 chapters. Chapter 1 provides introductory remarks and general background to the present study. The general scope and objectives of this research is described. Chapter 2 presents a brief historical background of steel making and more recent air force alloy development. A discussion of the relevant science and literature to a) metal cutting fundamentals, b) cooling and lubrication techniques in machining, c) chip-form and d) tool-wear are presented. Chapter 3 describes the experimental methods, instrumentation, and materials employed in this work to accomplish the stated objectives. The laboratory equipment used and their utility for qualitatively and quantitatively characterizing various aspects of chip-form and tool-wear is presented. Chapter 4 outlines and discusses the chip-form observations and analysis. Chapter 5 outlines and discusses the results of the tool-wear observations and analysis. Chapter 6, the final chapter of the thesis, provides a summary of the major conclusions from this study. Recommendations for future work specific to the machining of AF9628 are presented as well as future needs for broader, more pervasive machining technology capabilities.

CHAPTER 2
BACKGROUND AND LITERATURE REVIEW

We always want to create something new out of nothing, and without research, and without long hard hours of effort. But there is no such things as a quantum leap. There is only dogged persistence—and in the end you make it look like a quantum leap.

- *James Dyson*

2.1   A Brief History of Steel Making

Mankind has a long history with the presence and use of iron. Early records show that iron was used as early as 2500 BC. However, it is believed that the first uses of iron are not from intentional production but rather it was obtained from more naturally provided resources such as meteorites. It wasn't until after 2000 BC that the use of coal as a fuel in small furnaces led to the intentional development of iron. The Iron Age would be later defined around 1200 BC. Fast-forwarding several centuries, larger-scale industrial melt processes for steel production such as the Electric Arc Furnace (EAF) were first used in the early 1900s. However, it wasn't until the last three or four decades that this particular steel making technology expanded into wider use.

In addition to primary melt processes like EAF, there are secondary remelt processes, which first came around in the U.S. during the World War II era. Secondary melt processes further refine alloys for tighter composition control, improved microstructure, cleaner material by removing inclusions, and good solidification control [74, 97]. Vacuum Arc Remelting (VAR) and Electroslag Remelting (ESR) are examples of secondary refining processes that can follow a primary melt process such as EAF. However, due to the relatively higher cost of secondary melt processes, applications are typically limited to low-volume specialty alloys [100].

According to [11], the growth of EAF usage can be attributed to the lower capital costs of the technology and the reduced energy required to produce steel. EAF technology is a

88ABW-2019-5923

batch process where each batch, or heat, begins with charging ferrous scrap into the furnace. Scrap is generally layered according to size and density to facilitate the initial melt pool and protect the furnace walls from electric-arc radiation. Graphite electrodes are lowered just above the top of the scrap before power is turned on and a short arc is created. The arc starts the melting cycle as a small pool of molten steel develops under the electrode then is maintained by lowering the electrodes further into the scrap until the electrodes reach the bottom of the furnace and a large pool of liquid has accumulated.

When alloying elements are incorporated into a steel melt, many chemical and physical properties affect this process. Density, for example, can influence whether an addition floats, sinks, or becomes entrained within the melt. Alloy size and melting point can also influence dissolution rates. Alloy oxidation is a primary factor in poor or inconsistent recovery of alloys in industrial steel melting processes. Methods to deoxidize steel after melting can include ladle refining or degassing to remove nonmetallic inclusions and provide a cleaner steel product [50, 51, 94].

During the melting process, many nonmetallic inclusions such as hydrogen, nitrogen, and oxygen find their way into the molten steel. More detailed reviews of vacuum degassing and other secondary refining processes are found in literature [52, 62] but a brief overview of the salient points of vacuum degassing follows. Vacuum degassing occurs after the molten steel leaves the furnace but before it's poured into ingots. Degassing systems use argon to lift or stir the molten steel and promote the removal of hydrogen and/or nitrogen. The vacuum system then removes the hydrogen and/or nitrogen bubbles as they are lifted to the surface similar to the way boiling water creates bubbles that float to the surface of water to escape. Vacuum degassing increases the quality of the steel without the need of a remelt process. Benefits of vacuum degassing include the reduction of hydrogen, which helps to avoid common embrittlement issues in steel, improving distribution of alloying elements, and better control of the steel composition within tighter chemistry ranges [50, 94].

Despite the poorer control, relatively speaking, of EAF furnace technologies over composition ranges, compared to secondary remelting processes, its usage and capacity has been rapidly growing over recent decades. According to [11], the world steel

production from EAFs in 1975 was 20%, and by 1996 this production had grown to 39%. Emi [24] highlights significant developments in EAF technology in the last few decades, shown in Figure 2-1, such as reductions in electric energy consumption, tap-to-tap time, and electrode consumption.
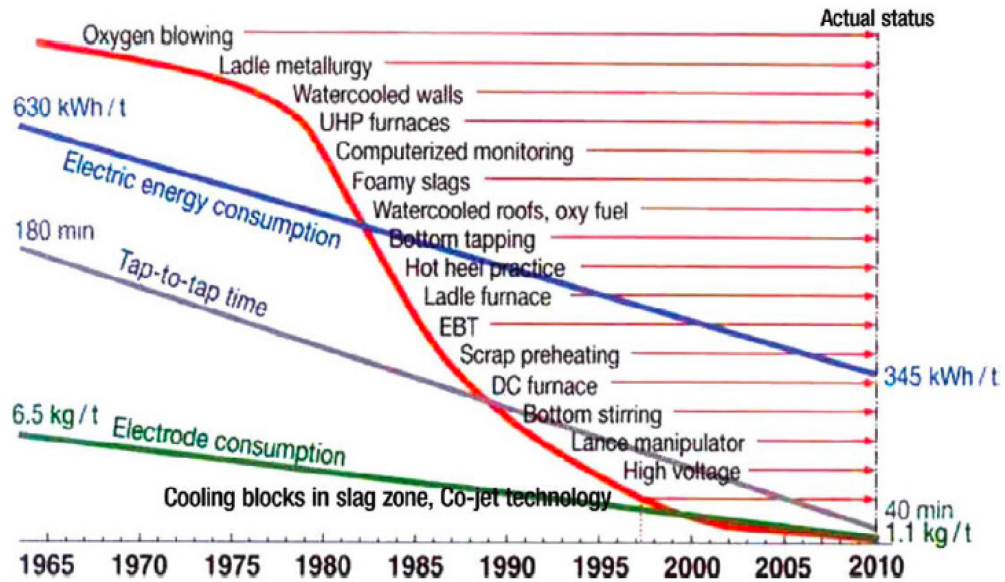
Figure 2-1. Development of Electric Arc Furnace steelmaking [24]

Controlling alloy content during melting and subsequent heat-treat processes is a crucial aspect of steel making and will, to a large degree, determine the success of other processes downstream, such as machining, as well as the final product performance. Steel can exhibit numerous properties depending on composition. Steel properties also depend on the phases and microconstituents that are present, which are dependent on the heat treatment process. Most alloys generally have three steps to the heat treating process, which include a normalizing step, an austenitizing step with quenching, and a tempering step. AF9628 alloy is no exception from this general practice of heat treating [3].

The role of the normalization step is to relieve internal stresses that form during the forging process and evens out the grain size and distribution. Normalizing is performed by heating an alloy to a temperature above the transformation range and then air-cooling to a

temperature substantially below the transformation range. The role of the austenitizing step is to develop an austenite structure in the material by heating the alloy into the transformation range for partial austenitizing or above the transformation range for complete austenitizing. The role of the tempering step is to decrease hardness and increase toughness of the alloy and is done by reheating hardened steel to some temperature below the eutectoid temperature [6].

2.2   Air Force Alloys

Steel alloys, such as HP 9-4-20 and Aermet100 alloy, having high compositions of cobalt, nickel, and/or tungsten have been used for decades in commercial and military industries. The combined high-strength and toughness properties make these alloys ideal for structural components, such as weapons casings, pressure vessels, and armor plate. Traditionally, these high-strength alloys, exhibit relatively high cost as a result of the high alloy content and expensive manufacturing processes that accompany such high-strength steels. In 2009, U.S. Air Force researchers at Eglin Air Force Base along with Ellwood National Forge Company developed a new steel alloy, called Eglin Steel. The composition of Eglin Steel has a reduced nickel content yet maintains high performance characteristics of steel compositions containing higher levels of nickel. Eglin Steel also avoided the relatively higher production costs associated with high-alloy steels [23].

In 2016, a research scientist at the Air Force Research Laboratory (AFRL) patented a new steel alloy to replace prior art steels, such as Eglin Steel, that have similar material properties but is easier and cheaper to produce. This new alloy, designated AF9628, with a low carbon content and low nickel content was been invented and can be produced at lower costs using current state-of-the-art melting techniques such as EAF [3]. Static strength is often a measure of performance in many alloys. However, in the case of the applications for AF9628, "both high strength and dynamic toughness at flight temperatures (e.g. -40°C) must be achieved" to be considered a good performing alloy [3]. The following typical values can be obtained for AF9628: an ultimate tensile strength of 245 ksi; yield strength at 0.2% offset of 187 ksi; elongation to failure of 13%; and an impact toughness measured with a Charpy V-notch test @ -40°C of 30 ft-lb. Obtaining this combination of

performance often requires steels to contain relatively high weight percentages of cobalt, nickel, and/or tungsten in its composition. These alloying elements are amongst the most expensive and tungsten is difficult to process and complicates the waste streams [102].

As with most alloys, the combinations of alloying elements are important to produce the desired effects in the alloy composition. While Eglin Steel resolved some issues with traditional high-strength, high-performance steels related to relatively high cost and difficult processing, it still contained tungsten. AF9628 contains no cobalt or tungsten and can be produced using EAF technology, further reducing the cost and ease of manufacture compared to prior alloys. Table 2-1 shows typical composition ranges of AF9628 and other prior art high-strength alloys.

Table 2-1. Composition ranges for HP 4-9-20 [82], Eglin Steel [23], and AF9628 [3]

Element	Approximate percentage by weight (%)		
	HP 9-4-20	Eglin Steel	AF9628
Carbon (C)	0.17 to 0.23	0.16 to 0.35	0.24 to 0.32
Chromium (Cr)	0.65 to 0.85	1.50 to 3.25	2.00 to 3.00
Molybdenum (Mo)	0.90 to 1.10	0.55 max	0.50 to 1.50
Vanadium (V)	0.06 to 0.12	0.05 to 0.30	0.05 to 0.35
Tungsten (W)	-	0.70 to 3.25	-
Cobalt (Co)	4.25 to 4.75	-	-
Manganese (Mn)	0.20 to 0.40	0.85 max	1.00 or less
Nickel (Ni)	8.50 to 9.50	5.00 max	3.00 or less
Silicon (Si)	0.20 max	1.25 max	1.25 or less
Copper (Cu)	-	0.50 max	0.15 or less
Phosphorus (P)	0.010 max	0.015 max	0.015 max
Sulfur (S)	0.010 max	0.012 max	0.02 max
Calcium (Ca)	-	0.02 max	0.02 max
Nitrogen (N)	-	0.14 max	0.15 max
Aluminum (Al)	-	0.05 max	0.025 max
Iron (Fe)	Balance	Balance	Balance

2.3   Machining (or Metal Cutting) Fundamentals

The terms *machining* and *metal cutting* will be used interchangeably throughout this work and no useful purpose would be served by attempting to precisely define the two. However, as Trent and Wright [92] describe it, "the term is intended to include operations in which a thin layer of metal, the *chip* or *swarf*, is removed by a wedge-shaped tool from a larger body." Machining is a term frequently used by engineers and practitioners to cover chip-forming operations. Trent and Wright [92] use the term *metal cutting* "because research has shown certain characteristic features of the behavior of metals during cutting which dominate the process and, without further work, it is not possible to extend the principles…to the cutting of other materials."

Of the many manufacturing processes used to shape metals, the operating conditions of machining are quite possibly the most varied. Machining, on its own, is a broad set of processes that includes, but is not limited to, turning, drilling, milling, broaching, shaping and planing, boring, and sawing. One of the most commonly employed processes in machining research, and heavily used in industry application, is turning. Turning is a process that is performed on a machine called a lathe and is the focus of this thesis. In the turning process, a workpiece, typically cylindrical, is held and rotated in a work holding device called a chuck. For turning, single point cutting tools are used, as opposed to multi-point cutting tools that are used in milling or drilling for example. The cutting tool for turning operations is rigidly held in a tool holder, which is rigidly mounted on a carriage that can traverse along the axis of rotation, thereby removing material from the work piece to create a cylindrical or other complex shape.

Three parameters of particular relevance to turning operations are *cutting speed*, *feed*, and *depth of cut*. Cutting speed is the relative speed at which the cutting tool travels across the workpiece surface. The feed is the distance that the cutting tool traverses in an axial direction per revolution of the workpiece. The depth of cut is the thickness of material removed from the workpiece as measured in a radial direction [92].

The surface, or face, of the cutting tool over which metal chips flow is commonly referred to as the *rake face*. The rake face intersects with a *flank face* and this intersection forms the *cutting edge*. Cutting tools are designed in such a way that the flank face provides

enough clearance during machining so that it does not rub against the newly generated workpiece surface. Single point cutting tool geometry also contains major and minor flank faces that when intersected with the rake face form major and minor cutting edges, respectively. The major cutting edge (and major flank face) is the edge that leads in the direction of tool travel during cutting while the minor cutting edge (and minor flank face) trails in the cut direction. The intersection of the rake face, major flank face, and minor flank face forms the *nose* of the cutting tool. While the nose can theoretically come to a nearly perfect sharp point, it is often designed with a nose radius for increased mechanical strength.

In reality, cutting tool design includes a seemingly infinite number of different shapes making the specifications and vernacular very complex to the reader that lacks practical machining experience. It should also be noted that cutting tool performance is highly dependent on the shape and features that they exhibit. As such, these simple descriptions are intended to only provide the reader with a basic understanding of the common cutting tool features that will be described through the rest of this work.

Figure 2-2 illustrates some of the more common cutting tool terms that will be used later in this work. Other terms will be illustrated and discussed in corresponding figures and tables at the time of discussion. It should also be noted, that in Figure 2-2, the workpiece travel direction, relative to the cutting tool, is from left-to-right and at some velocity, V_c. The chip can be seen forming in an upward manner along the rake face.
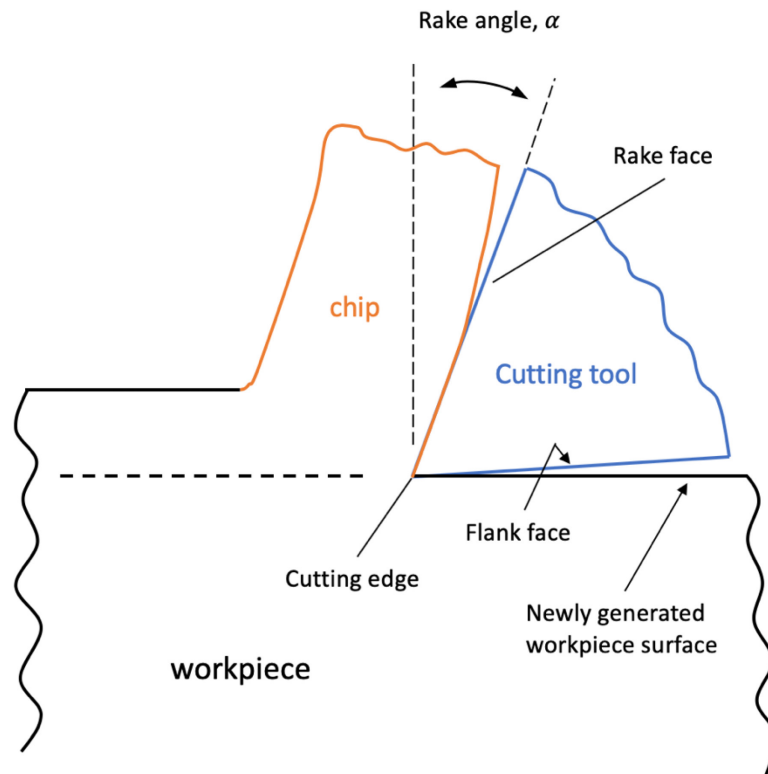
Figure 2-2. Common cutting tool terminology.

2.3.1 Metal Cutting Theory

Metal cutting has roots that can be traced back to the Industrial Revolution. By the mid-1800s, many manufacturing processes had relatively robust machine tools capable of performing various machining operations. It wasn't until the late-1800s when specific focus and attention would be placed on the practice and art of metal cutting. In 1906, Frederick W. Taylor published a notable paper entitled "On the Art of Cutting Metals", which was a compilation of experimental investigations that started 26 years earlier [86]. Taylor sought to answer very fundamental metal cutting questions that machining practitioners must still ask themselves today, such as "What tool shall I use?", "What cutting speed shall I use?", and "What feed shall I use?"

By the late 19th century and mid-20th century, many pioneers in metal cutting, were publishing more proper, quantitative understandings of metal cutting mechanics and chip formation [25, 56, 57, 65, 66]. Metal cutting can be basically classified into orthogonal

88ABW-2019-5923

(two-dimensional) and oblique (three-dimensional) cutting processes shown in Figure 2-3. The simpler of the two metal cutting classifications is orthogonal cutting where the inclination angle of the cutting tool edge is perpendicular to the direction of the cutting action. As a material removal process that is characterized by chip formation due to plastic deformation, metal cutting consists of a wedge-shaped cutting tool that exerts compressive stress with high strain rates ($\sim 10^3$-10^6 s^{-1}) and continuous material flow. Ignoring more complex features of the cutting tool geometry and geometrical relationship to the workpiece and cutting direction makes the orthogonal cutting model an ideal, simplified model to describe the mechanics of the cutting process. However, it should be noted that in most practical metal cutting applications, oblique cutting is the general case.
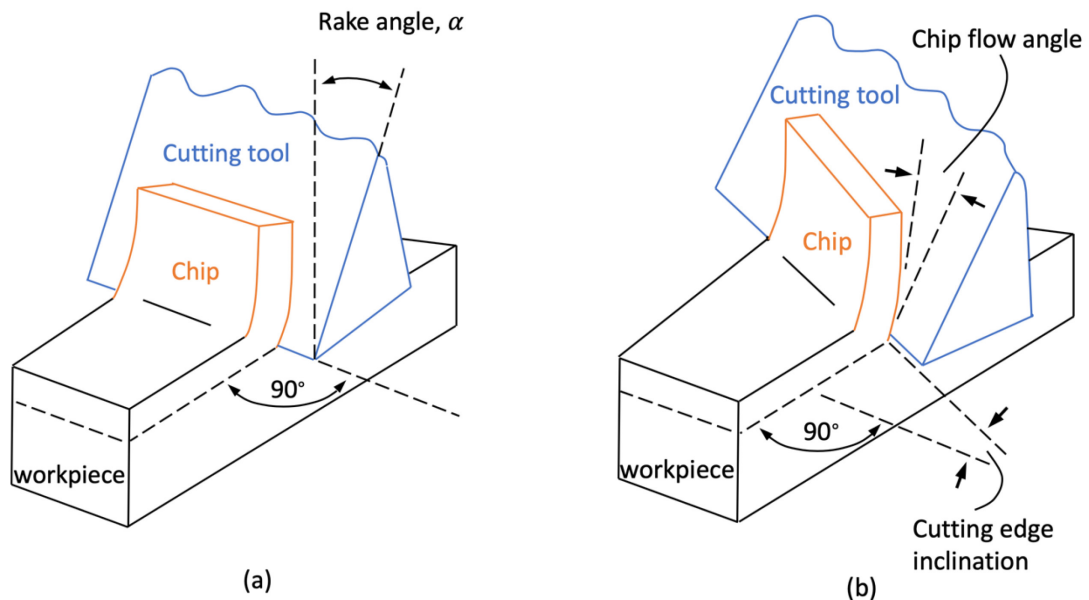
Figure 2-3. Orthogonal cutting model (a) on left and oblique cutting model (b) on right; adapted from [49]

Many metal cutting historians contribute the work by Piispanen [65] to be the first paper to use the so-called "stack of cards" model for understanding shear plane and chip formation shown in Figure 2-4. The card model depicts the workpiece material as a stack of cards inclined at an angle that corresponds to the shear plane angle, ϕ. As the cutting tool moves relative to the workpiece, it engages one card at a time and causes it to slide over the neighboring card. Merchant also describes the card model in his early work [56], where the card-like elements are assumed to have a finite thickness, ΔY, however in actual cutting, ΔY is approaching zero. Each card-like element is then displaced a distance, ΔS, with respect to its neighboring card-like element along a plane extending from the cutting edge of the tool to the surface ahead of the tool, called the *shear plane*. The material's crystal structure, represented by the "bubbles" drawn along the sides of the card-like elements in Figure 2-5, is elongated in the direction of the major axis of the ellipses produced in the resulting chip from the cutting process.
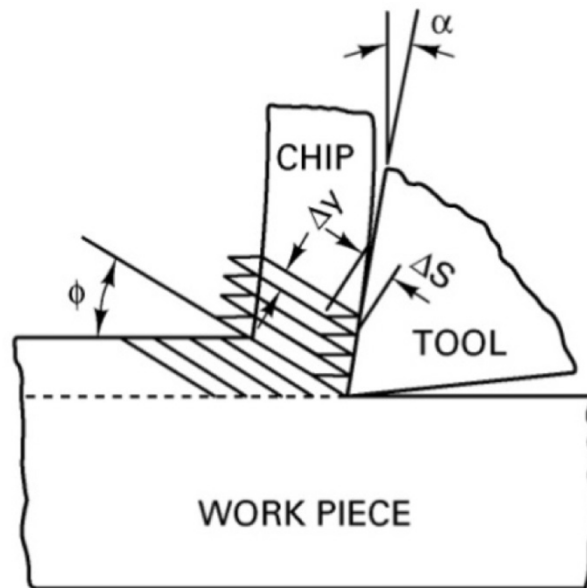
Figure 2-4. Stack of cards model for understanding concept of shear plane and chip formation. Adapted from [56]
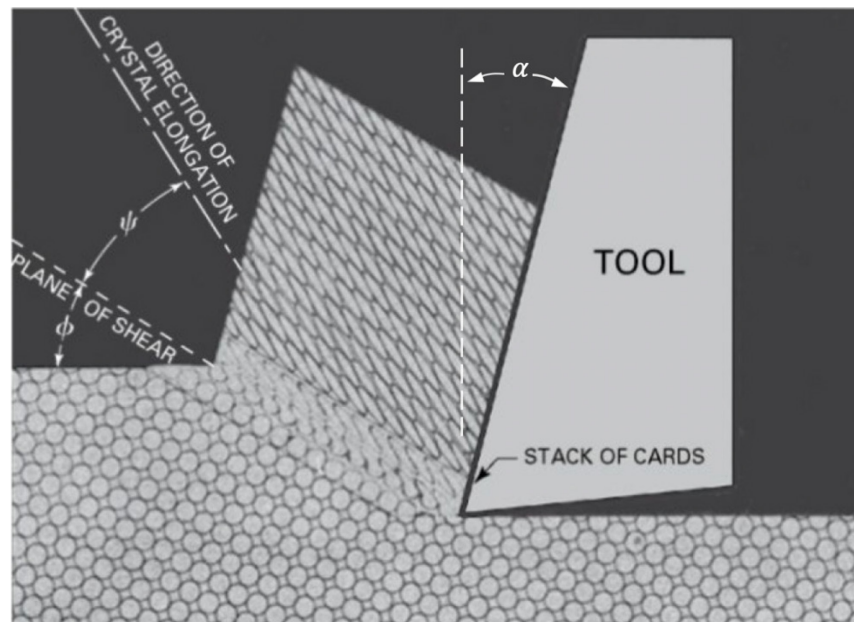
Figure 2-5. Stack of cards model, with bubbles, illustrating the mechanism of continuous chip formation and the resulting deformation of the workpiece material crystal structure. Adapted from [56]

Ernst and Merchant describe three types of chip-form from metal cutting processes, see Figure 2-6. The type of chip that is formed during the metal cutting process can depend upon a number of variables related to the cutting tool geometry, process parameters (i.e. cutting speed, feed, and depth of cut), and workpiece material. Type 1 is a discontinuous or segmented chip more common in brittle materials that don't undergo continuous plastic deformation, but rather exhibit more of a fracture behavior. Type 2 is a continuous chip formed by continuous deformation of the workpiece material more common is steels and alloys with more ductile behavior. Type 3 is also a continuous chip but includes a so-called "built-up edge" between the chip and cutting tool, near the cutting edge. Built-up edge (BUE) is the adhesion, and growth of, workpiece material onto the cutting tool near the cutting edge, commonly resulting from low-to-intermediate cutting speeds, which can vary depending on workpiece material [92].

88ABW-2019-5923
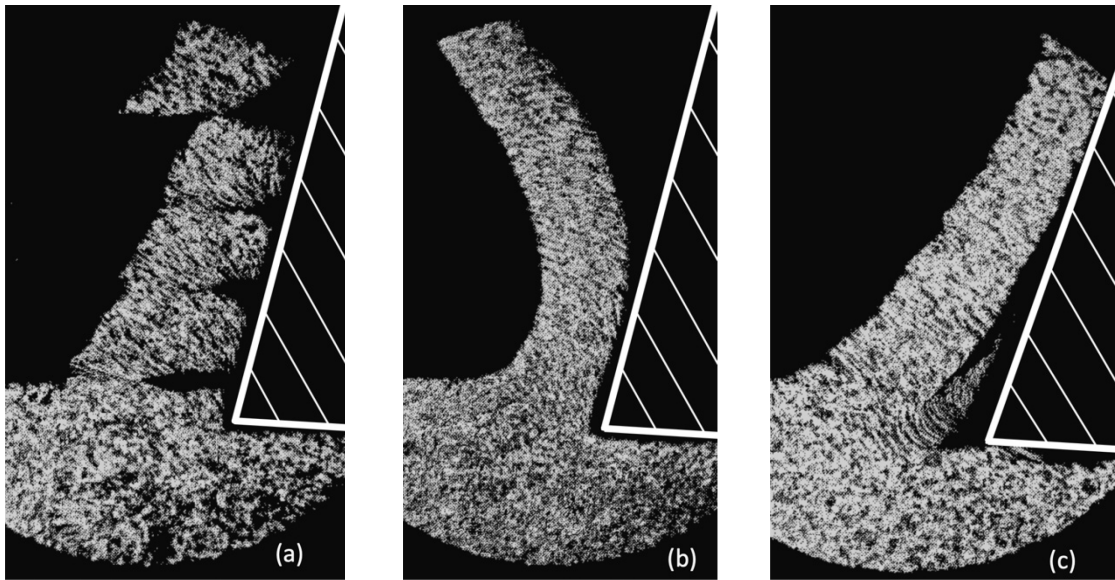
Figure 2-6. The three basic chip types according to Ernst: (left to right), Type 1 (a), discontinuous or segmental chip; Type 2 (b), continuous chip without built-up edge; Type 3 (c), continuous chip with built-up edge. Adapted from [25]

Technically speaking, this background analysis of metal cutting [56] is primarily based on the type 2 (continuous) chip and confines the shear in chip formation along a single-shear plane, when in fact shearing takes place in a *shear zone* close to this plane [33, 64]. Furthermore, many practical limitations exist within the cutting models discussed, due to numerous assumptions. Amongst these assumptions are [63, 78]:

- perfectly sharp cutting edges,
- the chip does not flow to either side (no side flow), only up along the rake face,
- depth of cut is constant,
- a continuous chip with no built-up edge is generated, and
- shear occurs on a perfectly plane surface extending from the cutting edge.

Despite the limitations in early metal cutting models, the single-shear plane model has survived time and remains the go-to as a basic foundation for understanding metal cutting theory. This is because it is easy to teach, and simple numerical examples for various cutting parameters can be easily calculated with basic geometric and trigonometric understanding, as will be seen later in this section [7]. In more recent years, more realistic

16

slip-line models have been developed by Jawahir and colleagues [37, 39]. The development of the universal slip-line model, based on rigid-plastic and plane-strain assumptions used in classic slip-line theory, accounts for curled chip formation and chip back-flow phenomena while incorporating previously developed slip-line models [26]. Moreover, these models consider grooved tool geometries with finite rounded cutting edges [95].

However, back to the basics. It is common in machining research to define a term called the *chip thickness ratio*, r, which is the ratio of the undeformed chip thickness, t_1, to that of the deformed chip thickness, t_2. Since chip thickness is related to the tool rake angle and shear plane angle, we can use this to derive a formula for the shear plane angle. Additionally, these angles, along with other geometric features of the cutting tool and chip-form, provide the basis in the derivation of equations for velocity vectors and cutting force components during the cutting process. From Figure 2-7, it can be shown that,

$$AB = \frac{t_1}{sin\phi} = \frac{t_2}{cos(\phi - \alpha)}$$

and given that $r = \frac{t_1}{t_2}$, we can rearrange to obtain

$$\frac{t_1}{t_2} = \frac{AB \sin \phi}{AB \cos(\phi - \alpha)}$$

Solving for ϕ,

$$\phi = tan^{-1}\frac{r \cos \alpha}{1 - r \sin \alpha} \tag{2-1}$$

The three velocity vectors at play in the cutting process can also be seen in Figure 2-7. The cutting velocity (or cutting speed), V_c, is the velocity of the workpiece relative to the cutting tool. The shear velocity, V_s, is the velocity of the chip relative to the workpiece along the shear plane. The chip velocity, V_f, is the velocity of the chip relative to the cutting tool along the rake face. Therefore, from the velocity-vector diagram on the right side in Figure 2-7, it can be shown that,

$$V_f = V_c \frac{sin\phi}{\cos(\phi - \alpha)} \qquad (2\text{-}2)$$

$$V_s = V_c \frac{cos\alpha}{\cos(\phi - \alpha)} \qquad (2\text{-}3)$$
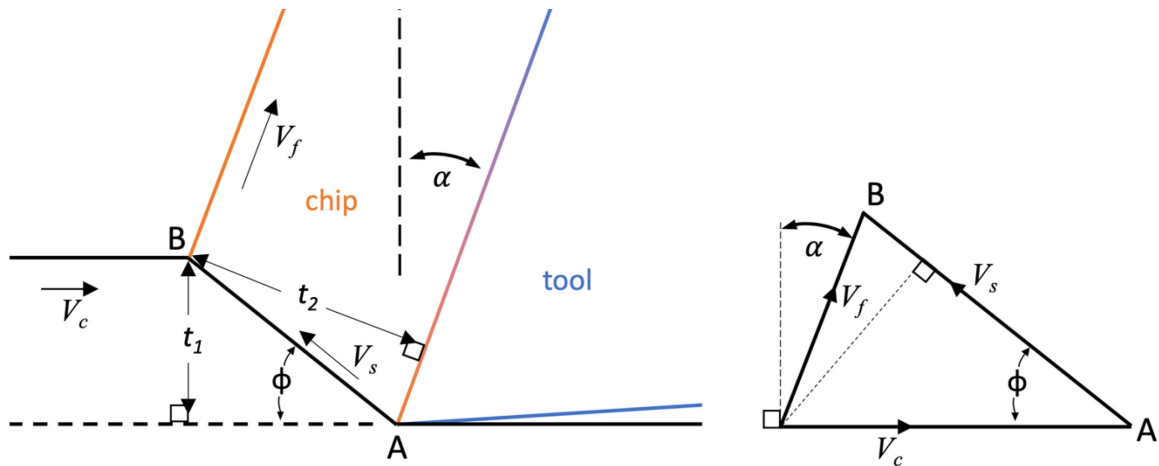
Figure 2-7. Velocity-vector diagram showing the relationship between shear angle, chip thickness, and velocities.

Another important aspect of metal cutting theory are cutting force components that can be calculated by understanding geometric and trigonometric relationships as well as directly measured from the cutting process. One of the most widely used descriptions of forces in metal cutting is that of the pioneering work by Merchant in 1945 [56], although in his publication, Merchant mentions a similar force diagram developed by Piispanen a few years earlier [65]. Merchant's two-dimensional force model for orthogonal cutting depicts a number of force components acting on the cutting tool and chip.

The free body diagram in Figure 2-8 shows that when the chip is isolated, only two forces need to be considered – the force, R, between the workpiece and the chip along the shear plane and the force, R′, between the tool's rake face and the chip. When the forces in Figure 2-8 are rearranged and applied at the tool's cutting edge, this condensed force diagram shows the relationships between force components, known as Merchant's circle, in Figure 2-9.

$$F_s = F_C \cos\phi - F_T \sin\phi \tag{2-4}$$

$$F_N = F_T \cos\phi + F_C \sin\phi \tag{2-5}$$

$$F = F_T \sin\alpha + F_C \cos\alpha \tag{2-6}$$

$$N = F_C \cos\alpha - F_T \sin\alpha \tag{2-7}$$

The ratio of a force in the direction of sliding, to the force normal to the sliding interfaces is known as the coefficient of friction. In looking at the rake face of the cutting tool, in which the chip is sliding across, the coefficient of friction, μ, can be found using components F and N as follows.

$$\mu = \frac{F}{N} = \frac{F_T \sin\alpha + F_C \cos\alpha}{F_C \cos\alpha - F_T \sin\alpha} = \frac{F_C + F_T \tan\alpha}{F_C - F_T \tan\alpha} \tag{2-8}$$

This method assumes that the force components, F and N, are uniformly distributed across the tool-chip interface. However, in the reality of metal cutting, this is far too simple of an analysis to adequately describe the more complex tribological interactions of sticking, slipping, and seizure that occur at the interface. For the purposes of this basic background, it remains a sufficiently useful way to think about the energy required for metal cutting and how the resulting workpiece material deformation will take place.
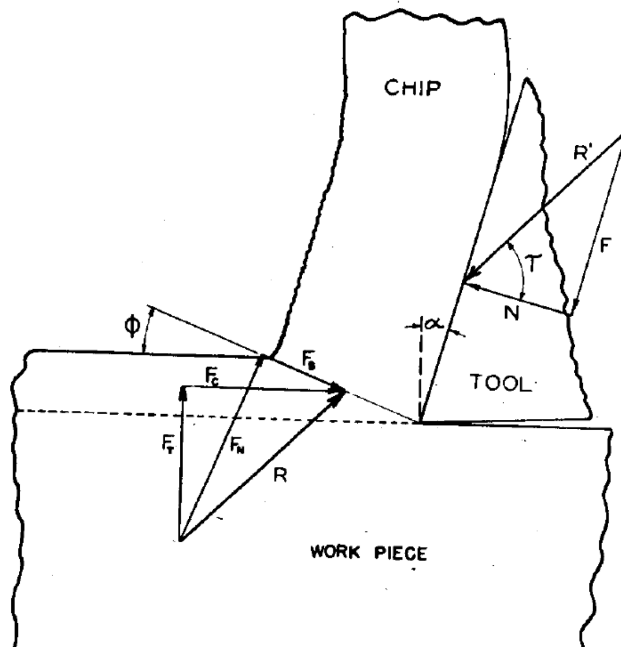
Figure 2-8. Free body diagram of chip-form during 2D metal cutting [56]
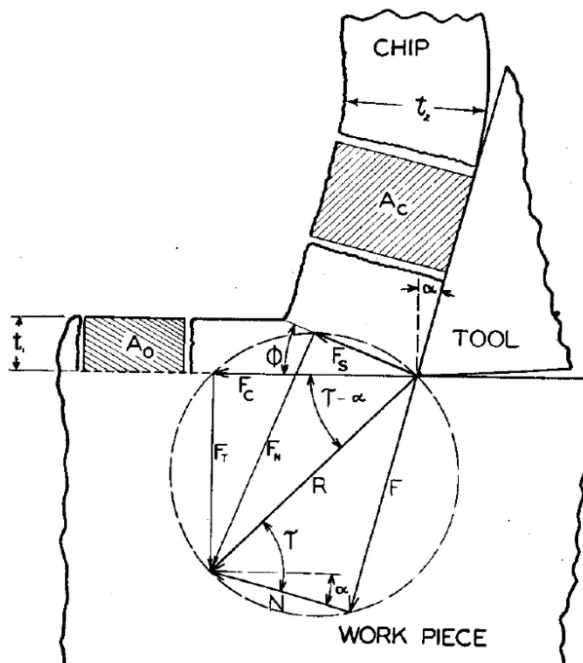
Figure 2-9. Combined force diagram, Merchant circle [56]

2.4   Cooling and Lubrication Techniques in Machining

Brinksmeier [15] defines metalworking fluids (MWFs) "as liquids, which are supplied to a manufacturing process in a way that allows for increased productivity based on lubricating and cooling effects." In this section and other parts of this thesis, commonly used terms such as coolant and lubricant are summarized as MWFs. Two main functions in metal cutting are served by the application of MWFs. First, is to provide cooling at relatively high cutting speeds where temperatures are likely to be higher. Under relatively high cutting speed conditions, MWFs have practically no time to infiltrate the tool-chip interface or the wear land on the tool in order to provide lubrication. Second, is to provide lubrication at relatively low cutting speeds where cooling is generally insignificant. MWFs are employed to achieve many objectives, including to reduce friction between the tool and the workpiece, increase tool life, improve surface finish, facilitate chip removal from the cutting area, and to prevent the tool, workpiece, and machine from overheating [92]. It should be noted that chip removal is another primary function served by the application of MWFs. These objectives help a manufacturer achieve the primary desired outcome of either reducing per-part costs or increasing production rates. Considerations for MWF selection must also consider cost, health and safety of the operator, and to inhibit workpiece corrosion or rust [78].

Many challenges are presented during the metal cutting process. Heat in a cutting process is primarily generated on the primary shear plane and at the tool-workpiece interface, especially in the flow-zone on the tool rake face [92]. In most cutting processes, this generated heat will be mostly removed in the chip and a smaller portion is conducted into the workpiece. Coolants typically cannot gain direct access to the primary heat source zones, however, they can efficiently reduce temperatures on the surfaces of the workpiece, chip, and cutting tool.

In machining processes, effective material removal is a primary objective. Thus, cooling and lubrication techniques play a major role in helping the engineer or machine operator to control chip-form and chip-flow over the cutting tool, obtain predictable tool-wear and tool-life, provide the necessary chip removal from the cutting area, and provide adequate quality of the finished surface. As such, several cooling and lubrication

techniques have been developed over the years and are available to manufacturers. The selection of the right cooling and lubrication technique can vary based on the material being machined, cutting tool materials, and processing parameters. Needless to say, the future role of MWFs in machining operations will remain an important topic of discussion [81].

Brinksmeier et al. [15] provide an extensive summary of metalworking fluids and present the current state of the art regarding the working mechanisms and performance of MWFs. The multi-disciplinary interrelationships and complexity of MWFs discussed include tribological (physical and chemical) aspects, effects of MWF-composition and concentration on machining performance, and advanced approaches for more sustainable application of MWFs. Brinksmeier et al. provide historical context to the evolution of MWFs over time including the drivers for change and effect on MWF-composition. Figure 2-10 summarizes the MWF development chronology.

	Driver	Effect on MWF-composition
< 1800	Demand to machine metals	Development of first MWFs based on natural products e.g. water, animal or vegetable oils
1800 - 1899	Industrialization (machine tools) Availability of mineral oil	Replacement of natural MWF-components First investigations on the lubrication ability of the used MWFs
1900 - 1999	Superior tool and workpiece material Advanced machine tools Mass-production	Addition of numerous chemical substances to increase the technical performance Application of chlorinated MWFs containing boric acid and further harmful chemicals First approaches to reduce amount of mineral oil in MWFs (driven by the rising oil-price)
2000 - today	Regulation Energy- and resource efficiency	Substitution or elimination of chlorine and further harmful substances Assessment of the sustainability of MWFs Interdisciplinary assesment of MWFs

Figure 2-10. Chronological development of MWFs [15]

2.4.1 Flood-coolant in Machining

One common cooling technique used in many industrial machining processes is the application of flood coolant. In 1906, F.W. Taylor investigated the effect of cooling the tool by a "heavy stream of water" at the point of tool engagement to increase cutting speeds by 40 percent [86]. In the 20th century, with the progress of industrialization, the addition of many natural and synthetic substances have been made to MWFs. Nowadays, coolants are commonly emulsions of mineral oil concentrates that can effectively dissolve in water and contain added emulsifiers, biocides, corrosion inhibitors, and antifoaming agents [87]. These emulsions typically have oil-to-water ratios between 1:10 and 1:60 [92].

It has already been stated that coolants are relatively effective at reducing temperatures on the surfaces of the workpiece, chip, and cutting tool. It should also be stated that this effectiveness depends significantly on the location and method of the coolant delivery. Proper placement is one such that the coolant is directed towards accessible surfaces of the cutting tool where temperatures are the highest. In cutting conditions where temperatures are more evenly distributed over a larger area of the cutting tool surface, a flood of coolant, hence the term flood-coolant, can be applied at the rake face of the tool, allowing coolant to provide consistent cooling action over the rake and flank face surfaces. In cutting conditions where temperatures may be hottest near the cutting edge, a high-pressure jet of coolant can be applied as close to that heat source zone as possible. In this thesis, flood-coolant under relatively lower pressure is used in the experiments discussed in future chapters.

It is well known that the constant use and exposure to certain coolants can have adverse health impacts ranging from minor skin irritations to respiratory problems. Over the last couple decades, environmental protection and occupational health regulations have restricted the use of certain chemical substances found in MWFs. Guidelines, such as "The European Union REACH Regulation for Chemicals: Law and Practice" [12] and "Prevention of Metalworking Fluid Pollution: Environmentally Conscious Manufacturing at the Machine Tool" [80] are amongst these guidelines and regulations. Some fear that more serious skin conditions and potentially different types of cancer can result from long-term exposure. Tolbert [87] reviews the epidemiologic evidence on the relationship

between mineral oil exposure and cancer in metalworking. Additionally, the costs associated with coolant and coolant delivery systems, as well as waste management costs and environmental concerns has driven a trend towards alternative cooling and lubrication strategies.

In recent machining research, flood-coolant is explored in so far as to serve as a baseline in which other MWF techniques are compared against. Much research has been done particularly in comparing flood-coolant, often referred to as a "conventional" cooling approach, when machining metallic materials of interest to the aerospace industry, such as for nickel alloys [35] and titanium alloys [84].

The remainder of this section will highlight alternatives to traditional flood-coolant methodologies starting with dry machining, then discussing minimum quantity lubrication (MQL), and finally cryogenic cooling.

2.4.2   Dry Machining

In the effort to remove cutting fluids from machining processes, dry machining is perhaps the ultimate goal. Dry machining is the act of machining without the use of an applied MWF. However, proper implementation of dry machining cannot be done by simply turning off the coolant supply. Previous works have summarized dry machining to greater lengths [48, 98] and emphasized this point.

There have been a number of dry machining approaches to achieving successful metal cutting while obtaining sufficient surface finish, geometric accuracy, good chip-breaking characteristics, and chip removal from the cutting area. Klocke and Eisenblätter [48] reviewed dry machining within a wide range of machining of cast iron, steel, aluminum, and titanium and superalloys. For cast iron machining, cubic boron nitride (CBN) tools are highly suitable for dry machining since their relatively high thermal conductivity can efficiently move heat from the cutting edge engagement zone.

Dry machining is often recommended for many machining processes in so-called superalloys, which are typically nickel- or titanium-based alloys, when using ceramic tools. The use of flood coolant with ceramic tools, and in some cases with carbide tools, is not

typically performed since thermal shock can be induced into the process, causing catastrophic tool failure. However, research continues to investigate dry machining with carbide tools since they are also commonly used when machining these superalloys [21, 31, 61, 70]. Klocke and Eisenblätter conclude that moving towards dry machining requires careful consideration and understanding of the complex interrelationships between the process parameters, cutting tools, workpiece material, and the machine tool.

As discussed during the previous section on flood-coolant applications, dry machining has been a focus of research for comparative studies with various MWF techniques. Kaynak and colleagues [46] compare dry machining to cryogenic cooling and MQL techniques in turning operations of a NiTi alloy to compare tool-wear performance. Pu et al. [69] employ dry machining and cryogenic cooling of a Mg alloy to investigate the effect of tools with various cutting edge radii on the resulting surface integrity. Rotella and colleagues [73] compare results of machining a Ti-alloy using coated carbide tools at varyious cutting speeds and feed rates under dry, MQL, and cryogenic cooling conditions to investigate the effects on resulting surface integrity.

Weinart and colleagues [98] summarize dry machining technology and the machining applications where it can influence future development. Turning processes are included in such machining applications. The authors conclude that many machining technologies (e.g. tool design, coatings, machining strategies, and machine design) have advanced because of the growing interest in dry machining. While high-volume industries such as automotive manufacturing have required special solutions to implement dry machining, further research activity of dry machining will ultimately expand solutions and technologies to the small and medium manufacturers that are especially challenged with a huge variety of machining tasks.

2.4.3 Minimum Quantity Lubrication in Machining

Minimum quantity lubrication (MQL) is another recent approach in the effort to remove, or limit, cutting fluids from machining processes. A normal rate of consumption per machine hour for consideration of an MQL system is typically between 10-50 ml of the MQL medium (i.e. lubricant). The heightened interest to limit the amount of MWF,

known as near-dry machining (NDM), has led many to explore MQL as a solution to also combat the relatively high production costs of traditional MWFs, which can be as high as 16% of an operations cost.

Astakhov provides a thorough summary of machining using Minimum Quantity Lubrication (MQL) as an alternative approach to deal with the costs and health and safety concerns of MWF. MQL machining supplies small quantities of lubricant to the machining zone where droplet diameters of 1-5 µm are generated "as a mixture of air and an oil in the form of an aerosol (often referred to as the mist)." Astakhov emphasizes the need for system-level consideration of the machining process when considering NDM as an alternative process and technology, particularly the total energy required by the metal cutting system to determine if MQL becomes feasible for a particular material and process space [8].

Maruda et al. study droplet sizes in MQL to determine potential heat exchange and find that when the distance of the delivery nozzle from the workpiece increases and volumetric air flow increases, the surface wettability decreases. In their work, coefficient of droplet deformation and wetting angles were experimentally determined. The authors also defined thresholds where droplets do not evaporate completely in one second if droplet diameter is greater than 30 µm and the emulsion mass flow is greater than 60 g/h. The quantity of dissipated heat from the cutting zone decreases beyond this threshold [55]. Suda et al. [83] evaluate synthetic ester's secondary performance characteristics such as biodegradability, oxidation stability, and storage stability. Particle diameters from their system are on average about 1 µm and typically under 2 µm. Oil was supplied at a rate between 2 and 30 ml/h with the nozzle angle at 60 degrees from the tool rake face and a distance of 20 mm from the nozzle to the tool. The authors conclude that synthetic esters are optimal lubricants for MQL machining in terms of these secondary performance characteristics.

Dhar [22] conducts turning experiments on AISI 4340 steel under MQL, dry, and flood-cooled conditions. Turning was performed with a cutting speed of 110 m/min, feed rate of 0.16 mm/rev, and depth of cut of 1.5 mm. The MQL was supplied with an air pressure of 7.0 bar at a delivery rate of 60 ml/h for the lubricant. The author found that

with MQL, tool-wear was reduced, tool-life increased, and surface roughness improved compared to dry and flood-cooled machining. The authors do not mention the hardness of the material or other processing conditions of the steel used during experiments, so it is assumed to be in an annealed condition based on the resulting tool-life curves. Detailed information regarding the orientation (i.e. inclination angle) of the MQL nozzle or distance to the tool is also missing in his work.

As with many manufacturing process technologies, science-based modeling is a valuable tool to use for enhancing the understanding and thus further development for NDM techniques. Marksberry and Jawahir [54], present a new method to predict tool-wear and tool-life performance in NDM by extending a Taylor speed-based dry machining equation in an effort to provide a more science-based modeling approach for wider NDM consideration and adoption.

Weinart and colleagues[98] discuss MQL technology as being a central element for many applications that are approaching dry, or near-dry, machining. MQL will ultimately experience the same challenges as dry machining for successful implementation. That is, continued research needs to be performed for continued development in tool design, coatings, machining strategies, and machine design. These aspects, which make up some of the many variables in a machining system, must be understood for a given machining process for successful implementation. With the expansion of MQL technology development, similar potential benefits to dry machining exist to significantly reduce total machining costs and improve process sustainability.

2.4.4   Cryogenic Cooling in Machining

Cryogenic machining involves the application of a cryogenic coolant, typically liquid nitrogen (LN_2) supplied at -196 ºC (-321 ºF), to the cutting area of the machining process. In 1919, the first reported use of a liquified gas, carbon dioxide (CO_2), was used as a coolant in machining [72]. The term cryogenic processing is believed to have been first used in 1966 by the CryoTech Company (Detroit, MI, USA), where they used cryo-tempering to obtain a 200-400% increase in tool life [38].

Cryogenic machining offers many advantages over the conventional use of flood-coolants, such as lower potential health and safety issues like skin or respiratory effects since nitrogen is an inert gas and is approximately 78% of the air that we breathe. Additionally, chip management can be easier since the chips will be dry and less "sticky" from the absence of an emulsion-coating from coolants or lubricants. While it seems like a minor issue, removing chips from the machining center and processing them for disposal can be a major issue for many machine shops. Dry, non-sticky chips make it easier to move around a shop and process for disposal. A large amount of time and resources are expended in the management of coolant and chips.

There have been many technical benefits of cryogenic cooling reported in the last couple decades, typically in the area of improved tool-life and desirable surface integrity results [34, 45, 84, 93, 96]. Much of the machining research, particularly with cryogenic cooling has been done on commonly used aerospace alloys that are titanium- and nickel-based. Biček et al. [14] compare cryogenic cooling with conventional flood-coolant and dry machining in turning of normalized and hardened AISI 52100 bearing steel. The authors conclude that tool life is improved up to 370% in the normalized steel and thermally-induced residual stresses were reduced in the hardened steel, while tool-life improved.

Cryogenic machining has also been explored for biomedical materials manufacturing, such as for Ti alloys, Co alloys, and Mg alloys [43]. In the context of biomedical implant materials, cryogenic machining provides a cleaner process and eliminates potential contaminates that conventional flood-coolant may introduce, while providing many of the engineered surface benefits mentioned in previous work. Cryogenic machining has also seen application in the manufacture of complex materials such as porous tungsten, as an alternative to the traditional practice of machining the plastic infiltrated workpieces [76]. More advanced research has gone into understanding the effect of depth of cut and pre-cooling when cryogenic cooling is used with porous tungsten [77].

Jawahir and colleagues [38] provide an extensive overview and summary of the current state-of-the-art regarding cryogenic cooling applications for machining, forming, grinding, and burnishing. The authors discuss implications of cryogenic cooling on surface integrity characteristics and product performance. Operational performance of cryogenic

cooling is compared with conventional flood-cooling and MQL in terms of the effectiveness and limitations relating to tool-wear, surface roughness, chip control, etc. Analytical and numerical predictive modeling capabilities are discussed, as are safety and health related issues.

A summary of cryogenic cooling and the other cooling and lubrication techniques discussed in this section are shown in Table 2-2. The table illustrates the effect of the various cooling and lubrication strategies on several primary and secondary interests during the machining process. Rankings of either poor, marginal, good, or excellent are given for each strategy's effect on the various items of interest.

Table 2-2. Effectiveness of various cooling and lubrication techniques on primary and secondary interests during machining [38]

	Effects of the cooling and lubricating strategy	Flood (emulsion/oil)	Dry (compressed air)	MQL (oil)	Cryogenic (LN_2)	Hybrid (LN_2 + MQL)
Primary	Cooling	Good	Poor	Marginal	Excellent	Excellent
Primary	Lubrication	Excellent	Poor	Excellent	Marginal	Excellent
Primary	Chip Removal	Good	Good	Marginal	good	Good
Secondary	Machine Cooling	Good	Poor	Poor	Marginal	Marginal
Secondary	Workpiece Cooling	Good	Poor	Poor	Good	Good
Secondary	Dust/Particle Control	Good	Poor	Marginal	Marginal	Good
Secondary	Product Quality (Surface Integrity)	Good	Poor	Marginal	Excellent	Excellent
	Sustainability Concerns	Water pollution, microbial infestation, and high cost	Poor surface integrity due to thermal damage	Harmful oil vapor	Initial cost	Initial cost, oil vapor

2.5   Machining of AF9628 Alloy

Little has been published to date on the machining of AF9628 alloy. Primarily because it is a relatively new alloy and its use has not been widespread outside of intended applications within the United States Armed Services. Limited studies have been performed that have looked at fundamental machining performance aspects of AF9628 in milling, drilling, and turning in comparison to a surrogate alloy such as AISI 4340. In recent years, a couple contracted efforts have been funded and managed by the US Air Force to study various aspects of AF9628 machining performance. On such study, under contract FA8650-14-C-5517 [44], explored drilling, milling, and turning processes.

Recently, data from the above contracted effort was presented in a paper [101] on milling experiments performed on AF9628 and AISI 4340 under flood-cooled and dry conditions. Force measurements were obtained for comparison between the two alloys under the same machining parameters. The study also investigated the impact that flood-coolant would have when compared to dry machining on surface integrity, including surface roughness, micro hardness, and sub-surface microstructure evolution. The authors found that flood-cooled and dry conditions affect the resulting generated surface as well as microstructure. Microhardness was found to be over 9% higher in flood-cooled milling than in the dry milling condition. Also, a more refined microstructure resulted from the flood-cooled condition. The authors conclude that this is likely due to the rapid cooling of the machine-generated surface, which effectively quenches the material, resulting in a more refined microstructure and increased hardness near the surface from the formation of martensite.

More recently, a study was performed under Air Force contract FA8650-18-F-5573 [5] at TechSolve Inc. in Cincinnati, OH, USA to evaluate machining performance in terms of tool life, energy consumption, and cost. This effort fundamentally sought to understand the processing space for turning AF9628 in a soft and hardened state. To do so, the study evaluated several different carbide and ceramic cutting tool inserts from multiple cutting tool manufacturers. Screening tests were performed using the different inserts across varying cutting speeds to identify the best performing tools with regard to tool-life as a function of cutting speed. Turning tests for AF9628 were performed with these cutting

tools along with a commonly known surrogate steel alloy, AISI 4340, so that the resulting machining performance could be compared between the two steels. The screening tests concluded with two ideal cutting tools for turning operations that demonstrated potential for further studies and potential use in a production environment. Of these two tools, one is a coated carbide tool (ISO designation CNMG432-MF2) and the other tool was ceramic.

The TechSolve study made significant findings on what cutting tools perform best when using finish machining conditions for AF9628 in a hardened state (51 HRC) and quantified this performance in terms of tool-life, energy consumption, and cost. However, the number of experimental tests for finish turning experiments were very limited due to the scope of work and the extensive number of different tools being evaluated. One test for each tool type was performed at various cutting speeds in order to develop the tool-life curves. It is well known that tool-life is not always consistent due to a number of factors related to the workpiece, cutting tool, and machine tool setup. Moreover, while tool-life curves were generated based on the limited experimental tests at various cutting speed, the mechanism by which the cutting tools wear was not fully addressed as this was also outside the scope of the study. Figure 2-11 shows an example tool-life curve developed during the TechSolve study with the recommended carbide insert (ISO designation CNMG432-MF2).
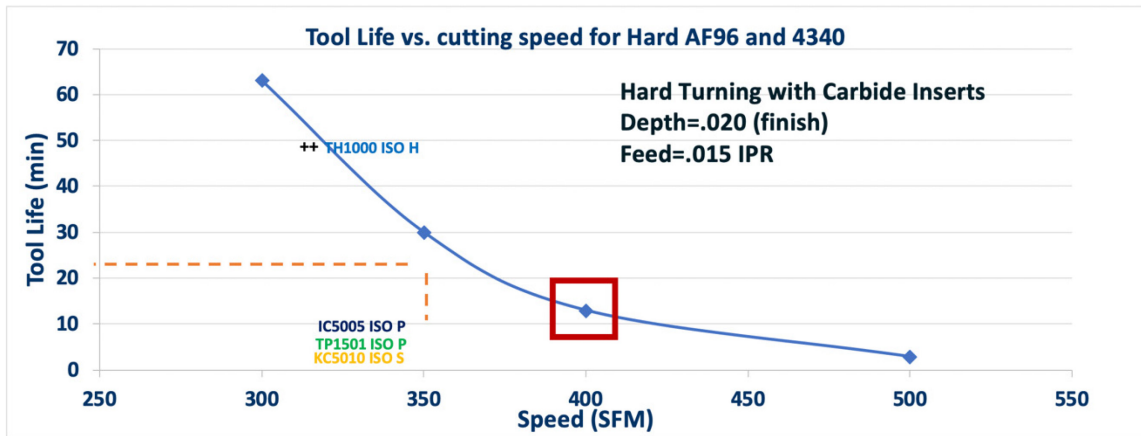
Figure 2-11. Tool-life curve developed by TechSolve Inc. illustrating expected tool-life in minutes as a function of cutting speed. This figure was generated under Air Force contract FA8650-18-F-5573 [5]

Following the initial machinability study at TechSolve, several machined specimens were identified for surface integrity characterization. A sub-contract was awarded to the University of Kentucky to perform characterization of machining-induced surface integrity on AF9628. The identified specimens were those that experienced the harshest processing conditions during the experiments at TechSolve. Harsh conditions were considered those where relatively higher cutting speeds are used, as this will likely increase the total temperature generated during the process as well as higher cutting forces. Higher temperatures and higher cutting forces have the greatest likelihood of producing undesirable surface and sub-surface characteristics, which must be understood. Residual stresses and changes in the hardness of the material at the surface and at some measurable depth into the sub-surface of the machined component are two such characteristics that can be modified by the machining process.

Machining-induced surface integrity is an area of manufacturing all in itself. Over the years, much research has been published on surface integrity of machined surfaces under various conditions and the importance of understanding its impact on the functional performance of manufactured components [2, 9, 16, 28-30, 32, 40, 60, 69, 75, 85, 99]. However, this type of work is only just beginning with AF9628. With the limited knowledge of machining AF9628, and the lack of any study diving deeper into chip-form and tool-wear mechanisms for this alloy, this thesis will help fill a critical gap in the known literature. The contribution of this work, dovetailed with previous machining research with AF9628, will provide a more robust foundational knowledge source of information to further reduce the risk for industry adoption of the steel.

2.6   Chip-form

Chip control plays a critical role in machining to ensure reliable operation in automated machining systems. Understanding and predicting chip-form and chip breakability is a challenging task. In turning operations of ductile materials, such as steels, the continuous cut can lead to long and unfavorable chips being formed. Therefore, cutting tool geometry, chip breaker design, and the cutting parameters play a critical role [98].

When hardened steels are machined, a saw-toothed chip is commonly produced. The cause of this chip-form has drawn much attention over the years. Shaw and Vyas review the hard turning of steels and seek to provide understanding of the events that occur in the formation of the saw-toothed chip. The authors discuss two competing theories on the origin of the saw-toothed chip and discuss the significance in understanding the fundamental chip-form mechanisms [79]. Mabrouki and Rigal [53] look at the thermo-mechanical effects on chip morphology by modeling the case of (orthogonal) turning of hardened AISI 4340 at 47 HRC to explain the effects of chip-form on tool-wear behavior. The authors model the saw-tooth formation on the back of the chip due to adiabatic shear banding, which also produces a cyclical variation in the cutting force magnitude corresponding to chip segmentation. The authors conclude that the oscillation in cutting forces due to chip segmentation causes fatigue of the tool and may result in fracture. Morehead et al. [59] study the effect of tool-wear and cutting conditions on the saw-toothed chip-form while dry turning 52100 bearing steel at 62 HRC to further promote hard turning as a viable technology option.

The growing interest in machining components in a hardened state has led research to explore the chip-form mechanisms and the relationship to tool-wear. Poulachon and Moisan [67] investigate 52100 steel across a hardness range of 180 to 750 HV_{10} and across various cutting speeds and feed rates. A relationship between the chip geometry and the cutting parameters was such that chip morphology was primarily influenced by the material hardness and cutting speed. Poulachon et al. [68] use a shear instability criterion to understand the major cutting parameters influencing shear localization and perform hard turning experiments on AISI 52100 bearing steel to confirm the results. Their study of understanding and modeling the chip-form process is in anticipation of growing interest in hard turning technologies.

Prediction of chip-form and chip breakability across a range of machining conditions, materials, and with various cutting tools is a challenging task. Developing the predictive theories and capabilities that will be suitable for use on the shop floor is even more challenging. Fang et al. [27] present an Artificial Intelligence (AI)-based hybrid algorithm to characterize various chip shapes and sizes, and to quantify the chip-form/chip breakability in the machining of steels. The model uses a reference database developed

from machining experiments along with the fuzzy predictive model to achieve a quantitative estimate of chip-form/chip breakability. Jawahir and Wang [36] present a summary of modeling and optimization developments of machining processes including predictive models for 2D and 3D chip formation, and chip-form/chip breakability prediction. The authors propose a new modeling approach for predictive evaluation of machining performance.

2.7   Tool-wear

Tribology is the study of the interaction between two or more bodies in relative motion with one another, particularly the friction, wear, and lubrication phenomena associate with the interaction. Machining is a tribological problem at its core. Friction and wear of cutting tools have a detrimental effect on the performance limit in any cutting process. Tool-wear can be any one, or combination, of the following, but not limited to: flank wear, crater wear, nose wear, notching, chipping, and plastic deformation of the cutting tool tip. Multi-pass operations, which are most real-world applications, require the same tool to be used for multiple passes across a workpiece. Therefore, the need for understanding tool-wear as it relates to product quality is critical. Industry and researchers have had interests in understanding tool-wear and tool-life as long as metal cutting has been around.

Early work by F. W. Taylor [86] made major discoveries that related tool-wear rate to the temperatures at the tool cutting edge. Over the years, many others have continued to study the fundamental aspects of tribology in metal cutting [10, 71, 91]. De Melo et al. provide a nice summary of different wear types and damage that can occur in carbide tools. Using numerous examples from literature, the authors highlight tool-wear types including plastic deformation, crater wear, attrition wear, notch wear, abrasion and built-up edge, mechanical fracture and chipping, and thermal and mechanical fatigue [17]. In the last couple decades, more sophisticated measurement techniques have become available that allow for more advanced qualitative and quantitative analysis of tool-wear. Devillez et al. [20] successful measure crater wear developed during orthogonal cutting of a steel material with an uncoated carbide tool using white light interferometry.

The increasing interests in the application of various cooling and lubrications techniques during machining have led many to investigate tool-wear performance under these techniques. Marksberry and Jawahir [54] present a model to predict tool-wear/tool-life performance in near-dry (MQL) turning operations. Kaynak et al. [47] investigate progressive tool-wear of a Ni/Ti alloy under dry, MQL, and cryogenic cooling conditions. The authors find that progressive tool-wear is enhanced by cryogenic cooling, which was applied by two nozzles from the rake face and the flank face. However, after four minutes of cutting, all of the conditions obtained similar surface roughness results. Sun et al. [84] investigate cryogenic cooling during turning operations on Ti-5533 alloy and compare tool-wear to similar experiments under flood cooling and MQL. Two tool-wear types found under all conditions were abrasion and built-up edge, although cryogenic cooling applied to the rake face of the tool resulted in less nose wear due to reduced material adhesion.

Grooved cutting tools have become more common over the last several decades and much research has been performed to assess the chip-flow and tool-wear associated with these tools. Grooved tools often produce three-dimensionally curled and broken chips. It has been found through experimentation with grooved tools that flank wear is often not the most dominant factor. Jawahir et al. [42] present a methodology for evaluating tool-wear for a typical grooved tool. By observing variations in the chip-groove interaction by changing the cutting speed, feed rate, and depth of cut, a chip-groove effect factor was developed for new tool-life relationships. Additional work on grooved tools have identified tool failure resulting from improper groove utilization by the chip as a result of either poor chip-groove design or inappropriate cutting conditions for the chip-groove. Mechanical action of the chip-flow can cause tool-wear in grooved tools more so than adhesion or diffusion wear [41].

At the conclusion of this literature review, it is clear that despite all of the prior research that has been conducted to understanding chip-form and tool-wear, no work has been done to understand these aspects of machining for the recently invented AF9628 alloy. With an understanding of this gap in the known literature, this thesis seeks to fill a knowledge gap in the following areas:

- Perform chip-form analysis for turning of hardened AF9628 alloy with a coated carbide tool.
- Perform tool-wear analysis for turning of hardened AF9628 alloy with a coated carbide tool.
- Provide an understanding of the interrelationship between chip-form and tool-wear for turning of hardened AF9628 alloy with a coated carbide tool.

It is the desired goal that filling this knowledge gap will provide a foundation for continued research in machining of AF9628 alloy. In addition, the data that is generated from this work is expected to merge with the other limited existing data from prior machining studies on AF9628. By doing this, a more robust data set will be of immediate interest and potential value for industry's consideration of adopting AF9628 alloy for industrial applications. The following chapter will discuss the experimental methods and instruments used for analysis as well as the workpiece and cutting tool materials.

CHAPTER 3

EXPERIMENTAL METHODS AND MATERIALS

As the true method of knowledge is experiment, the true
faculty of knowing must be the faculty which experiences.

- *William Blake*

3.1   Turning Setup for Flood and Dry Machining

Various cooling and lubrication techniques were explored in this study of turning the outside diameter (O.D.) of AF9628 in a hardened state. The experimental setup in Figure 3-1 shows a Haas TL-2 CNC lathe with a bar of AF9628 alloy setup for machining. Due to the length of the AF9628 bars, and the necessity for a rigid setup, the bars were prepped to be supported by a three-jaw chuck on the left-hand side and a live center on the right-hand side of the bar. More detail on the AF9628 bar stock preparation for the experiments is described later in the chapter.

For flood-cooled experiments, a soluble oil emulsion type coolant, Trim® E206, was mixed with water to a 9.0% -10.0% concentration for all flood-cooled experiments. An American Optical model 10440 hand refractometer was used to measure the coolant before flood-cooled experiments. Figure 3-2 shows the typical flood-cooled machining setup for a turning operation and the position of the coolant nozzle relative to the cutting tool and workpiece. In these experiments, the coolant nozzle was positioned such that there would be a constant flow of coolant, at a rate of 2 l/min, directed at the rake face of the cutting tool, near the cutting edge. This allows the coolant to flood the cutting tool surfaces while also contacting the workpiece near the tool-workpiece interface.

Dry machining, or machining in the absence of any cooling or lubrication medium was also performed. The setup for dry machining is identical to that shown in Figure 3-1.
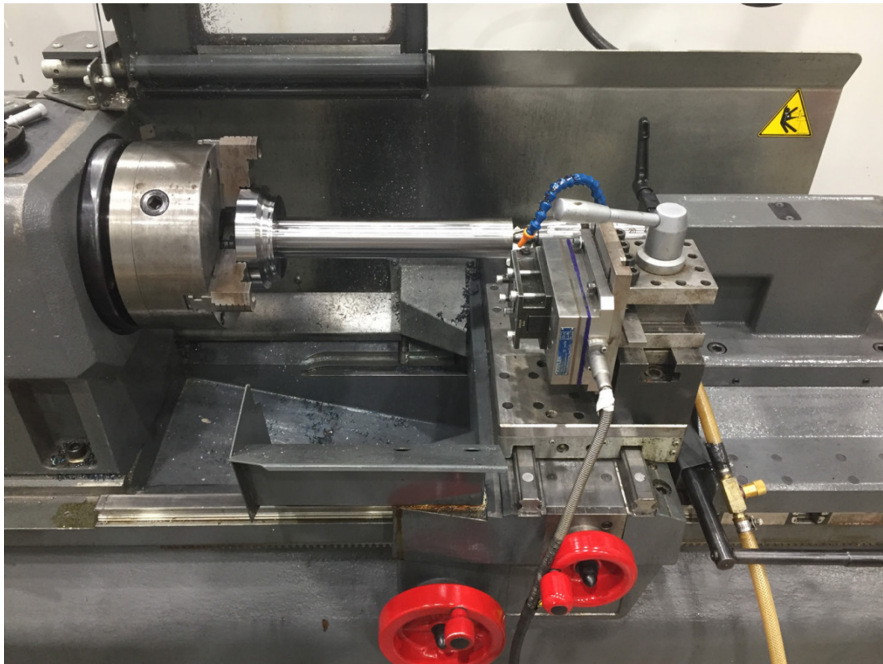
Figure 3-1. Haas TL-2 CNC lathe used for experimental tests under various cooling and lubrication conditions.
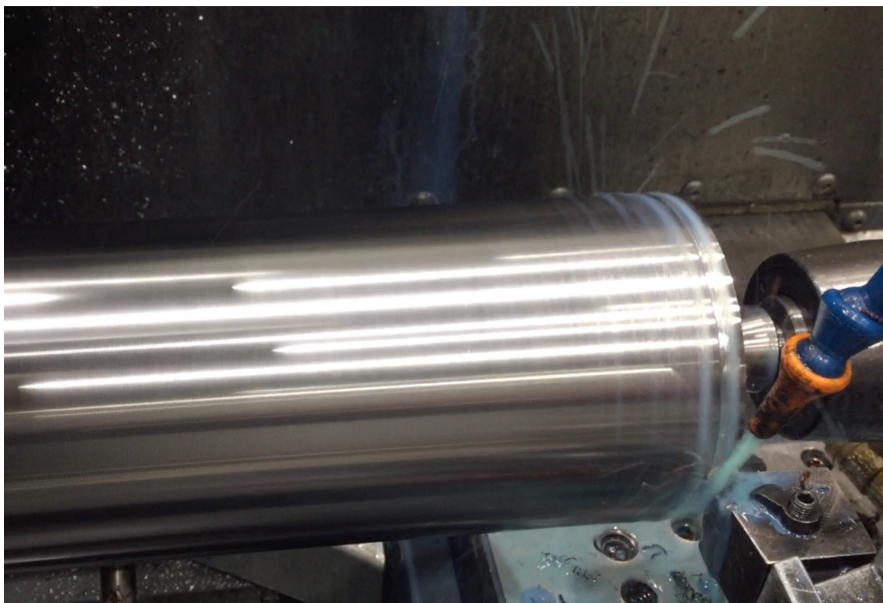
Figure 3-2. Experimental setup for flood-cooled machining on Haas TL-2 showing the position of the coolant nozzle relative to the cutting tool and workpiece. The cutting tool traverses along the axis of rotation from right to left.

3.1.2 Turning Setup for Minimum Quantity Lubrication Machining

A Unist Coolubricator™ MQL system was used for experiments along with Coolube® 2210EP lubricant, which is based on vegetable oils and natural esters. The Unist Coolubricator™ system has an adjustable, pneumatic displacement pump to control the pump cycle rate and a pump stroke adjustment knob to control the volume of fluid delivered per stroke. For experiments, the MQL system was adjusted to deliver 0.01 ml of oil per cycle at 84 cycles per min, resulting in a flow rate of approximately 50 ml of oil per hour. The MQL system also has an adjustable pressure regulator that can adjust the delivery pressure of the oil lubricant through the system. The pressure was adjusted to 0.38 MPa (55 psi), which is comparable to prior machining research with MQL to investigate progressive tool-wear during turning experiments on nickel-rich NiTi alloys. The Unist Coolubricator™ system is shown in Figure 3-3 below.
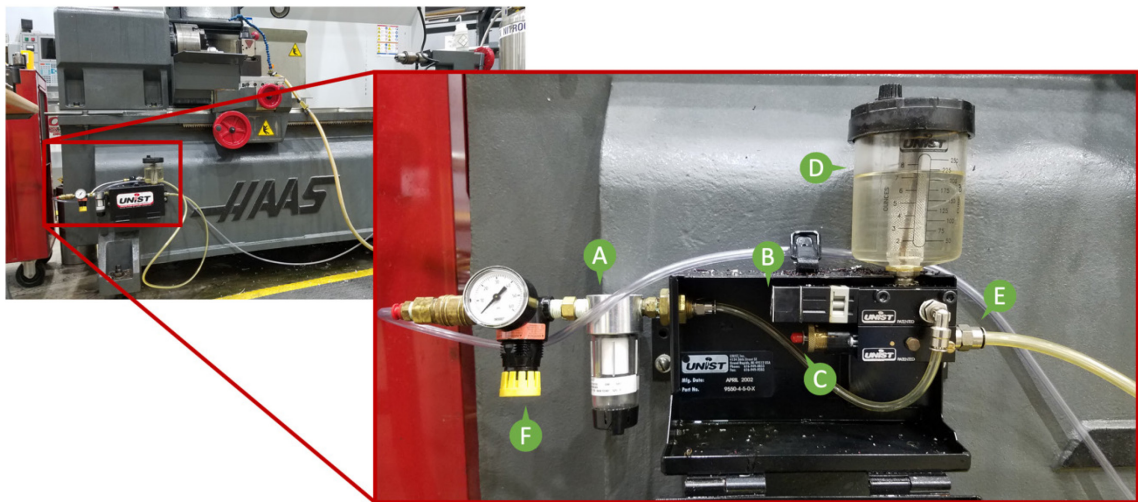
Figure 3-3. Unist Coolubricator™ MQL system on Haas TL-2 CNC lathe

The MQL system shown in Figure 3-3 operates pneumatically. From the figure, the bubble with the letter F is the pressure regulator for controlling the incoming pressure from the air supply. Bubble A is an air filter, bubble B is a pneumatic pulse generator used to control the rate at which the system pulses to releases a mist of lubricant. Bubble C points to the pump stroke adjustment knob, which controls how much lubricant is effectively

dispensed with each pulse. A fluid reservoir can be seen at bubble D and bubble E shows an output port where the lubricant travels through a tube to the application zone.

The experimental setup for MQL is shown in Figure 3-4. In that figure, the MQL delivery nozzle can be shown near the cutting tool, where it is directed at the rake face of the cutting tool and near the cutting edge. The end of the nozzle, where the lubrication exits, is positioned 8.9 mm (0.350 in) from the cutting edge at approximately 40° relative to the rake face.
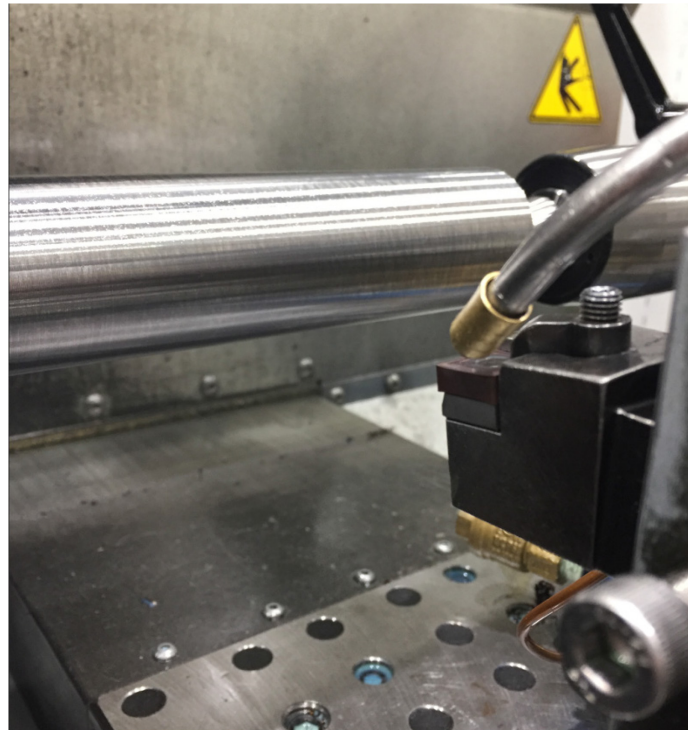
Figure 3-4. Experimental setup for MQL machining on Haas TL-2 showing the position of the MQL delivery nozzle relative to the cutting tool and workpiece. The cutting tool traverses along the axis of rotation from right to left.

3.1.1 Turning Setup for Cryogenic Machining

To reduce the cutting temperature during cryogenic machining experiments, liquid nitrogen, which has an approximate temperature of -196°C (-321°F), was delivered as a coolant. A 3mm diameter copper tube was used to deliver the liquid nitrogen from a

standalone dewar beside the lathe to the metal cutting zone. The dewar was maintained at a pressure of 200 psi during tests. Figure 3-5 shows the cutting tool on the right side of the figure, with the copper nozzle directed at the rake face of the tool to deliver LN_2. The copper nozzle was also positioned along the flank face of the tool during one experiment. This position was explored in an attempt to deliver the LN_2 more directly into the cutting zone during machining by delivering it from the underside of the chip being formed. This was attempted since LN_2 delivery from the top of the tool has potential to be blocked out from the cutting zone by the chip forming on top of the tool.
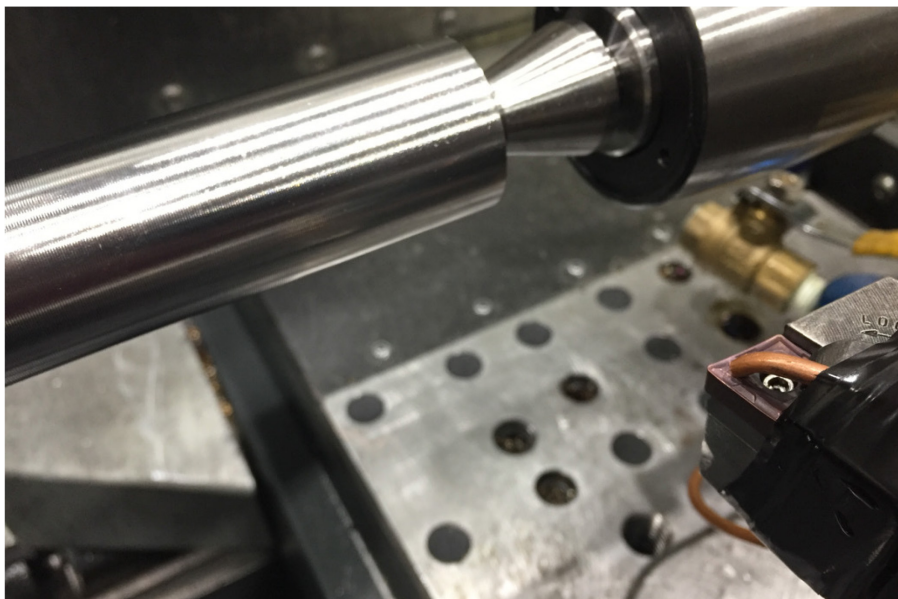
Figure 3-5. Experimental setup for cryogenic machining on Haas TL-2 showing the position of a 3mm nozzle for liquid nitrogen delivery relative to the cutting tool and workpiece. The cutting tool traverses along the axis of rotation from right to left.

3.2   AF9628 Bar Stock

Several bars of AF9628 material were used to conduct the turning experiments under various cooling and lubrication conditions. Figure 3-6 shows three (3) bars that were remnants from a machining study performed by TechSolve. These bars were electric arc furnace melted, forged, and rough turned at Superior Forge & Steel (SF&S) to an O.D. of 140 mm (5.5 inch). The bars were also heat treated at SF&S to a hardness of 51 HRC using

41

a standard heat treat procedure starting with a normalization step, followed by an austenitization step with a water quench, then finished with a tempering step. It should be noted that since these bars were remnants from the TechSolve study, the effective O.D. for machining in the current study was closer to 70 mm (2.75 in).

Figure 3-6. AF9628 remnants from TechSolve machinability study

An additional bar, produced by Timken Steel that was electric arc furnace melted, forged rolled, and rough turned in an annealed condition to an O.D. of 101.6 mm (4.0 in), was used for turning experiments. Material compositions are shown in Table 3-1 for both the SF&S- and Timken-produced material. Before performing experiments, the bar in Figure 3-7, was heat treated to a hardness of 49 HRC using a standard heat treat procedure starting with a normalization step, followed by an austenitization step with a water quench, then finished with a tempering step. The exact heat treat specifications cannot be described here since the furnace charts for the heat treatments are not available. However, from comparing the outcome of final hardness of the two bars machined in this study to hardness values measured in prior heat treatments for AF9628, it is assumed that the following heat treat procedure is representative of what was used for the material in the current study. A

typical heat treatment procedures is as follows: normalize at 633 ºC for 4 hours followed by air cooling, austenitize at 1015 ºC for 1 hour (+30 minutes per inch thickness) followed by a water quench, then finally normalize at 227 ºC for 4 hours followed by air cooling.

Table 3-1. Composition for AF9628 steel bars used in turning study

percentage by weight (%)		
Element	SF&S	Timken
Carbon (C)	0.29	0.27
Chromium (Cr)	2.60	2.74
Molybdenum (Mo)	0.94	0.95
Vanadium (V)	0.06	0.06
Manganese (Mn)	0.6	0.6
Nickel (Ni)	0.93	1.01
Silicon (Si)	0.91	0.97
Copper (Cu)	0.11	0.16
Phosphorus (P)	0.015	0.011
Sulfur (S)	0.001	0.004
Nitrogen (N)	not reported	0.0068
Aluminum (Al)	0.0116	0.008
Iron (Fe)	Balance	Balance

Figure 3-7. Timken-produced AF9628 bar after heat treatment

The Timken bar, since it was heat treated prior to initial machining at the University of Kentucky, had a decarburization layer that is typical of heat-treated steel. To prepare the bar for experiments, one end was mounted in the lathe chuck so the opposite end could be turned down in diameter on the lather across a length of 70 mm until the bar was visually "cleaned up" to produce a new, clean surface that is concentric to the lathe spindle. Then, the bar was flipped around with the newly generated surface (70mm long) being held in the chuck, and the face of the bar on the opposite end, perpendicular to the axis of rotation, was center drilled and countersunk to accommodate a live center to support the size and weight of the bar during experiments and provide rigidity. Once the bar was supported with the live center, the O.D. was turned down by an amount of 2 mm per side with a sacrificial insert that was not used to study tool-wear, to remove the decarburization layer that results from the heat treatment process. This is a critical step in sample preparation for experimental work since the decarburization layer is a layer at, and near, the surface of the steel that becomes depleted of carbon during heat treating and is consequently of lower hardness to some depth from the surface.

The depth of the sacrificial layer was determined by taking a slice off of the end of the bar before preparing it to be mounted for tool-wear experiments. This slice was roughly 13 mm thick. The bar was then setup on a surface grinder to grind and produce two flat, parallel, and relatively smooth surfaces on the cross-section of the sliced bar. The decarburization layer was found to be about 1.4 mm in depth from the surface, which was observed by grinding the surface incrementally and taking hardness measurements of the ground surfaces until the final, expected hardness was reached.

The final hardness was measured for both AF9628 bar products (SF&S and Timken) and graphed in Figure 3-9. As can be seen, the SF&S bar had a measured bulk hardness of 51 HRC while the Timken bar had a measured bulk hardness of 49 HRC. The differences in the resulting harnesses of the two AF9628 bars are minor and could come from the fact that they are two different "products", melted at different times, in different locations by different suppliers, and have slightly differing compositions, but are both within the acceptable composition ranges. Additionally, the bars were heat treated at different times, but at the same location under similar heat treatment conditions for AF9628 as previously described.

Bulk material hardness measurements were performed on a Future-Tech FR-3 hardness tester using ASTM E18 procedures for obtaining hardness Rockwell C (HRC) values. A 120° diamond indenter was applied at 150 kgf for HRC measurements. The bar slices, as previously described, from each of the SF&S and Timken bars were measured a total of five times on each slice to obtain an average hardness value. The five measurement locations on each bar included one in the center of the bar, two more locations about half-way to the outside of the bar in the radial direction and 90 degrees from each other, and two more near the outside of the bar and 90 degrees from each other. The measurement locations are illustrated in Figure 3-8. The O.D. of the bar slices were either 70 mm (2.75 in) or 101.6 mm (4.0 in) depending on which bar was being measured for bulk hardness.
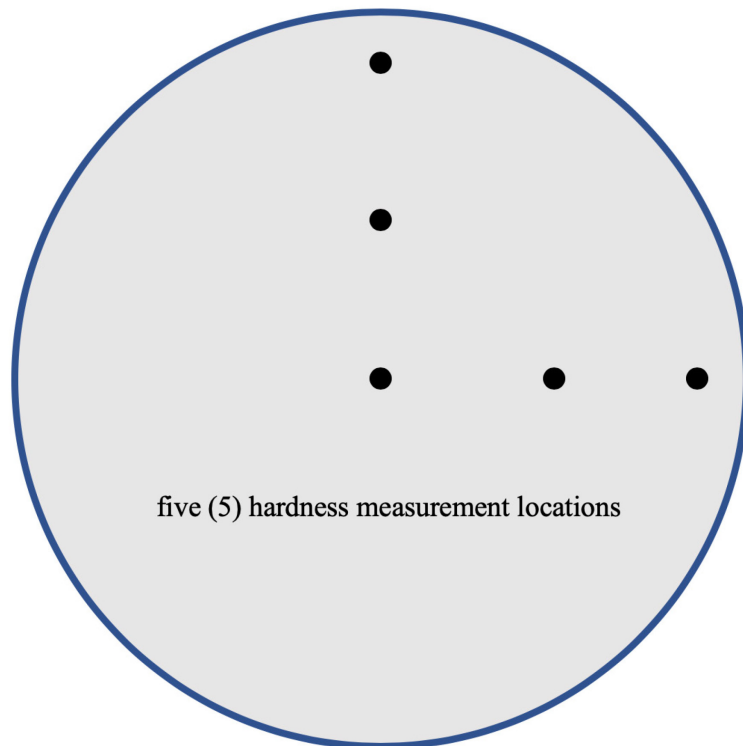
Figure 3-8. Measurement locations on bar slice for bulk hardness (HRC)
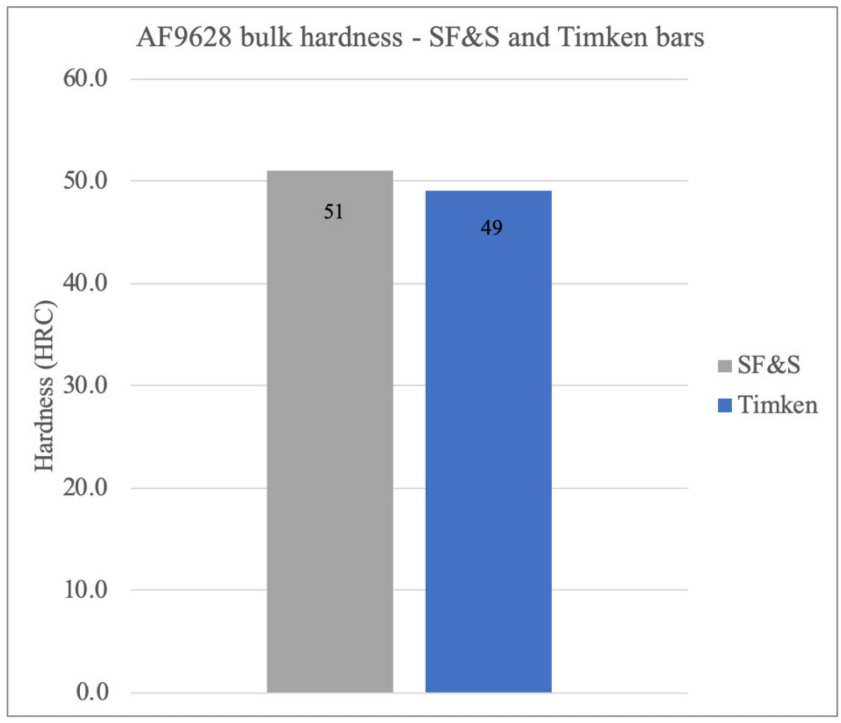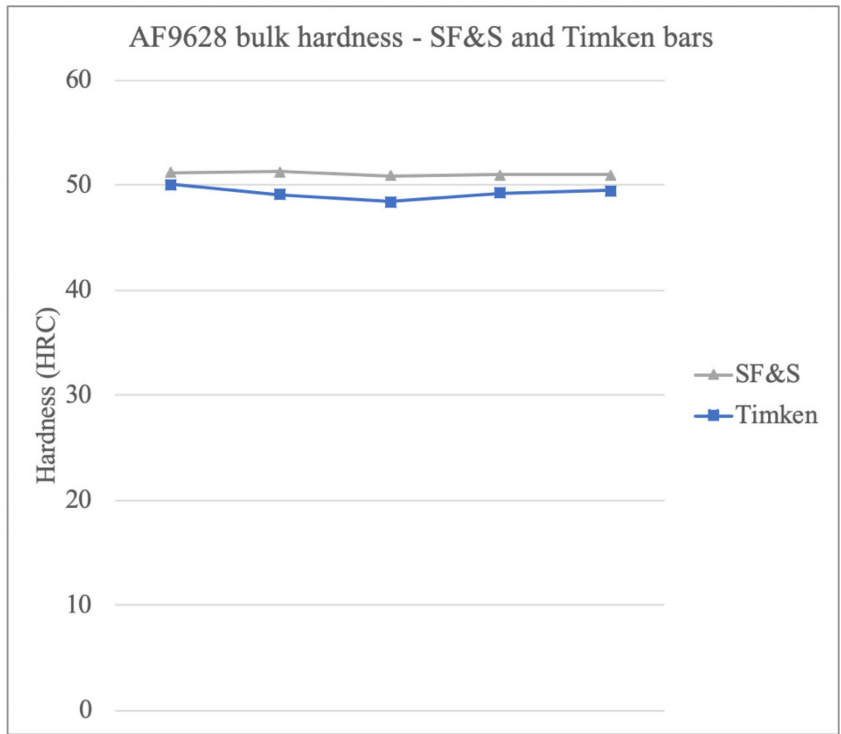
Figure 3-9. Bulk hardness graphs for AF9628 bars. Top: actual measured values at five locations on each bar. Bottom: average bulk hardness for each bar

3.3   Cutting Tools

The coated carbide cutting tools, often referred to as inserts, used during this work were manufactured by Seco. The insert type used is designated as a CNMG432-MF2 using Seco's TH1000 grade carbide. Insert designations describe many aspects of the cutting tool such as shape, clearance or relief angle, tolerance, cutting edge length, thickness, nose edge radius, and chip breaker type. Chapter two alluded to the complexity of cutting tool design that includes a seemingly infinite number of combination of shapes, sizes, and geometric features that make the specifications and vernacular very complex. Resources from cutting tool manufacturers and standards such as the ANSI B212.4-2002, attempt to provide a standard description of the tools for use by the process engineer and end-user.

It is worth noting that the selection of the CNMG432 carbide insert during this work was motivated by the aforementioned machining study on AF9628 performed by TechSolve. In an effort to extend the knowledge gained during TechSolve's study of turning AF9628 in a hardened state, and eventually merge all of the available AF9628 turning data into a more comprehensive data set, as many variables in the experiments presented in this thesis were kept constant with the conditions from the TechSolve study. Therefore, as the TechSolve turning study used this insert, so does this work. Moreover, other machining variables selected in this work such as cutting speed, feed rate, and depth of cut were kept the same as in the TechSolve study. Furthermore, the tool holder and flood coolant type were also kept the same.

Figure 3-10 shows an illustration of the Seco CNMG432-MF2 insert on the left, and an actual insert image on the right. The golden color of the insert illustration (left) can be easily misled for a common TiN coating found on cutting tools. However, this is an illustrative misrepresentation from the cutting tool manufacturer's website. In reality, the cutting insert is a TiAlN coating, which appears closer to black in color to the human eye, shown on the right side of Figure 3-10. From the illustration in Figure 3-10, RE = 0.8 mm (0.031 in), IC = 12.7 mm (0.500 in), L = 12.9 mm (0.508 in), EPSR = 80º, D1 = 5.16 mm (0.203 in), and S = 4.75 mm (0.187 in). The tool holder used was Kennametal's DCLNR-164D. While there is little value in illustrating the tool holder, and describing its geometric characteristics at length, it is most important to reiterate that the tool holder used in this

work is identical to the tool holder used in the TechSolve study. The selection of the tool holder is to ensure that the overall machining performance of this work has the greatest probability of replicating the machining performance from the prior study.
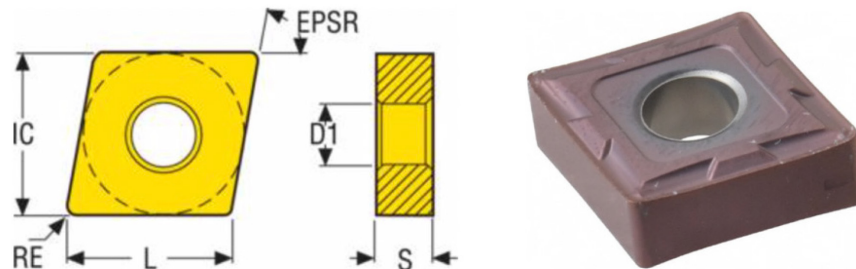
Figure 3-10. Seco CNMG432-MF2 carbide insert [1]

One feature of cutting tools that is not generally reported by cutting tool manufactures is the cutting edge radius, which is different that the radius of the nose edge, RE, from Figure 3-10. Cutting edge radius can have a significant effect on chip-flow and tool-wear. It also has other critical implications of the machining performance such as the temperatures generated during machining and the mechanical strength of the tool. To measure cutting edge radius, a scanning white light interferometer at the University of Kentucky was used. The scanning white light interferometer will be discussed in more detail in a later section.

In this work, several inserts were used during experiments. Each insert has four cutting edges that can be indexed in the tool holder. Inserts were numbered 1, 2, 3…N and the four cutting edges on each insert were identified as either A, B, C, or D. As such, inserts are identified as 1A, 1B, 1C, 1D, 2A, 2B… and so on. Figure 3-11 shows the resulting measurements for various cutting edges used during experiments in this work and it can be seen there is an average cutting edge radius of 37 μm. Also, measurements range from about 30 μm to about 45 μm, which is a fairly tight spread of measurements for production inserts that have not been custom made and honed to a specific size.

It should be noted that the inserts used in the TechSolve study were not measured prior to machining and therefore cannot be compared to the inserts used in this work. However, since the inserts were of the same type, it is fair to assume that the measurements

would fall within the range measured in this work. Finally, it should be noted that measuring edge radius as a single value is too simplified. This is because rarely is the radius on the cutting edge a constant value if one where to look at a cross-section of the edge. Instead, edge geometry profiles can have varying radii and sometimes even flat regions. Discussion on a more proper characterization of cutting edge prep geometry will occur in the conclusions and future work chapter of this thesis.
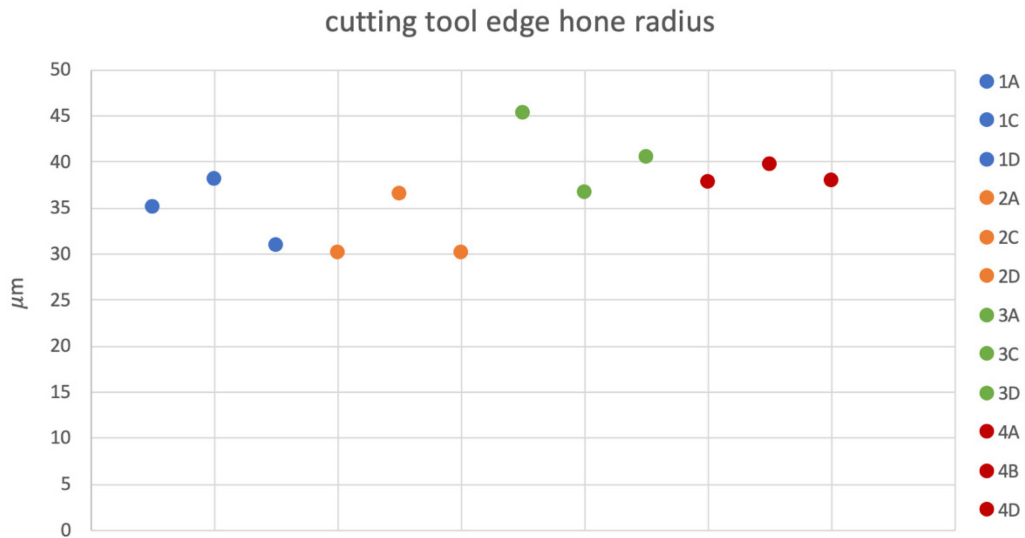
Figure 3-11. Cutting tool edge radius measurements for inserts used in experiments

3.4   Cutting Force Data Acquisition

There are certain observations that must be made before, during and after the metal cutting process to perform quantitative analysis. However, there exist limited observations that can be made during metal cutting. A common measurement made during machining experiments is that of cutting force components. Cutting forces were measured with a Kistler type 9257B three-channel dynamometer. The dynamometer is mounted on the tool post of the lathe with a custom fixture to accommodate the cutting tool, shown in Figure 3-12. While cutting forces are not a major focus of this work, it can provide value for other studies, and the only time to obtain this data is during experiments. Therefore, the data was captured and will be discussed minimally in this thesis. As such, it is worth introducing the cutting force data acquisition setup here.
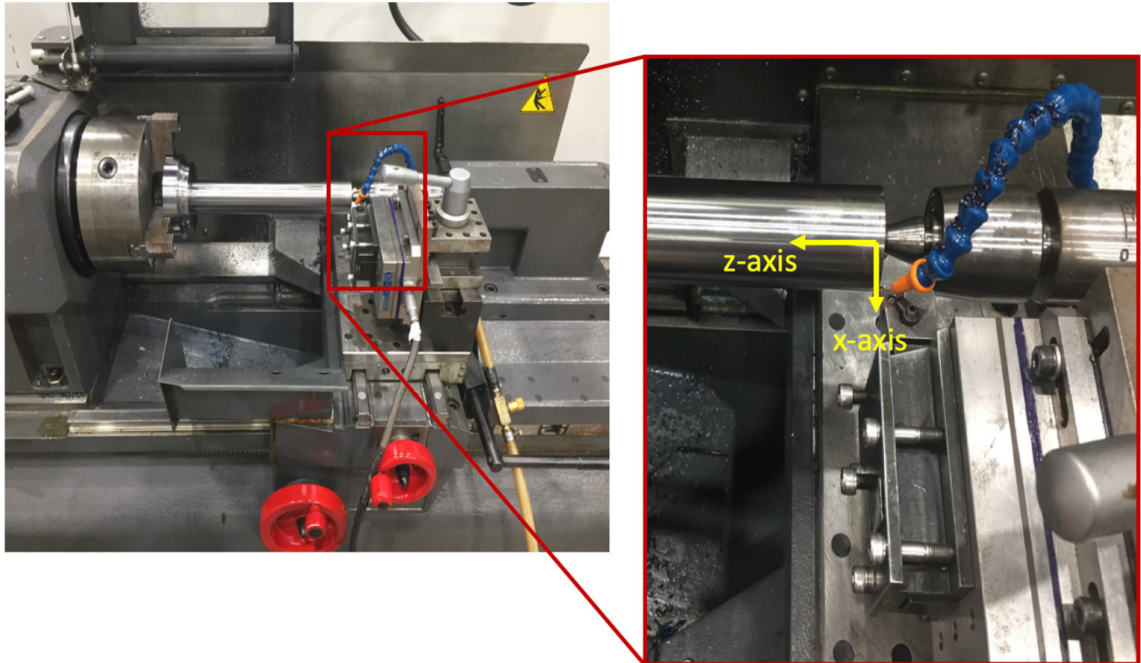
Figure 3-12. Kistler type 9257B three-channel dynamometer mounted on Haas TL-2 lathe

3.5   Characterization of Chip-form and Tool-wear

Since the major focus of this work is investigating chip-form and tool-wear, it is important to be able to qualitatively and quantitatively measure these aspects of the machining process. Industry experience with AF9628 is extremely limited at the present date, therefore little is known about tool-life and chip-form under various cutting conditions. To investigate chip-form and tool-wear from turning AF9628 in a hardened state, the following characterization instruments were utilized.

3.5.1   Optical Microscopy

Optical microscopy was performed using a Nikon SMZ800 stereo microscope in conjunction with a Leica DFC 425 digital camera for capturing images, see Figure 3-13. The Nikon SMZ800 is equipped with a 0.5x objective, 10x eyepiece, and 1x-6.3x zoom range. These attributes, along with providing great contrast of features and sufficient depth of field, made it ideal for capturing the relatively larger feature sizes (> 0.1 mm) on the cutting tools and chips from the machining process. An AmScope MR095 stage

micrometer, Figure 3-14, was used at various zoom magnifications to "calibrate" length scales that would later be used with an image processing program, ImageJ, to measure tool-wear and chip features from experiments.
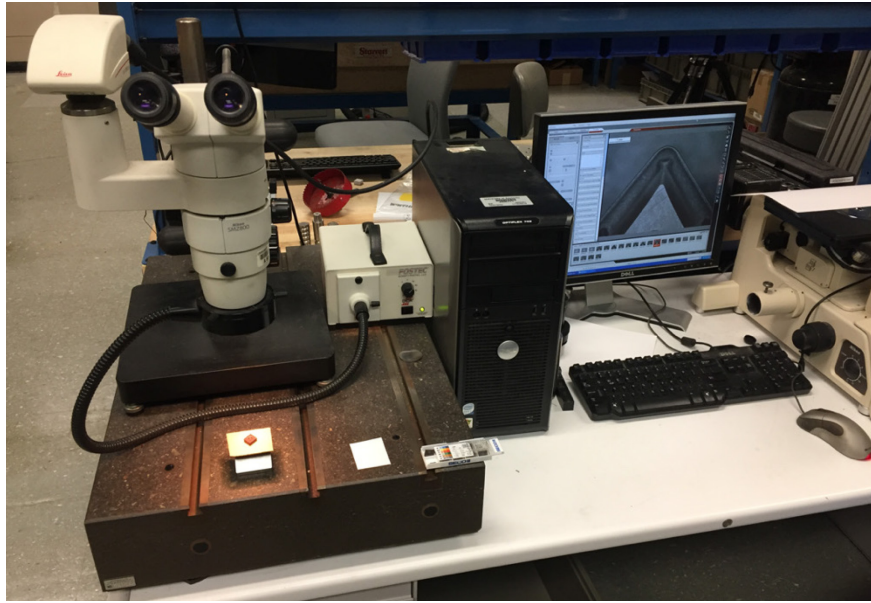
Figure 3-13. Nikon SMZ800 stereo microscope with Leica DFC 425 digital camera
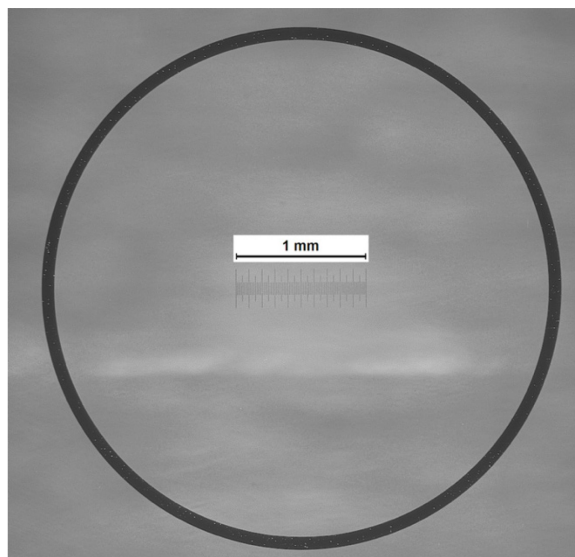
Figure 3-14. AmScope MR095 stage micrometer at 5x zoom

3.5.2 Scanning White Light Interferometry

Optical microscopy is a powerful tool that can provide a large amount of significant data in research. However, a more detailed understanding of the surface features and defects that often occur on cutting tools and machined surfaces at the micron- and sub-micron-levels require tools that can capture this information with greater resolution. Additionally, optical microscopy is an ineffective method for characterizing features such as a built-up edge or crevices that may be present on a surface where the necessary line-of-sight cannot be obtained, or the feature sizes make it difficult to obtain measurements confidently. Furthermore, many surface characterization tools contain probes and can be destructive to features that may be sensitive to contact with another body. Features that are smaller than the tip of the probe cannot be effectively measured. Therefore, a non-contact technique can overcome the limitations with optical microscopy for characterizing surface features that may be present and of interest during chip-form and tool-wear analysis.

For this purpose, a Zygo NewView 7300 scanning white light interferometer (SWLI) was used. The SWLI is equipped with a 20x and 50x objective to obtain 3D profiles of surface topography and roughness of samples. This is done with a white light source projected towards the surface of interest, and the interferometer scans through some vertical height range, along which light intensity interference fringes are produced. By analyzing the intensity fringing, a 3D contour map at nanometer-length resolution can be produced that is representative of the surface that was scanned. These 3D contour maps can be used for characterization of chip-form and tool-wear features with higher fidelity than optical microscopy.

The utility of SWLI for characterizing tool-wear is well served for studies such as in this work. Zygo can be used for obtaining different types of measurements depending on the user's interest. For this study, two measurements of particular interest were cutting edge radius and surface topography profiles of the rake face of the cutting tool. Each of these measurements can be obtained on the Zygo instrument with the use of different applications within the Zygo software. Figure 3-15 shows the Zygo instrument with representations of the data that can be generated for cutting edge radius and rake face surface profiles using an image stitching technique.
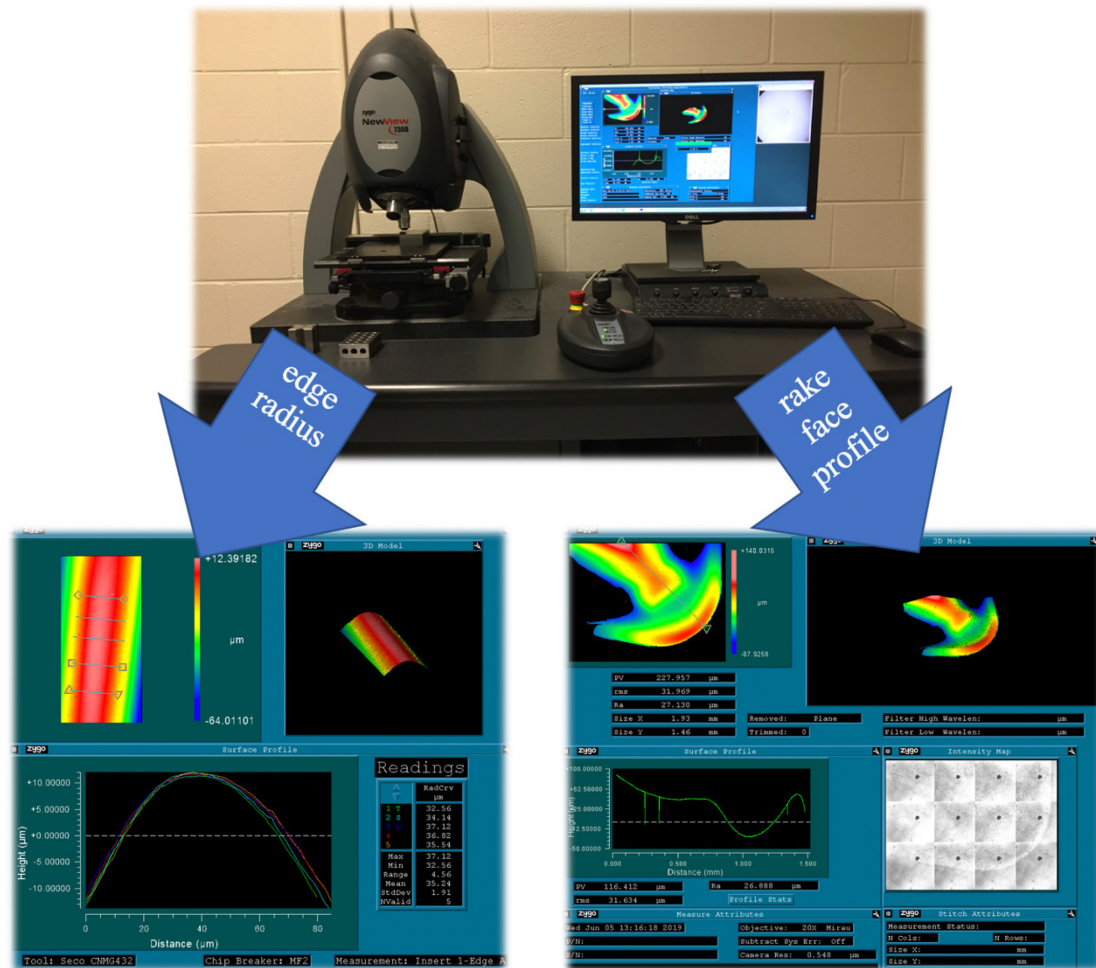
Figure 3-15. Zygo scanning white light interferometry instrument

3.5.3 High-speed Imagery

During the machining process, chips are formed so quick that it is impossible to observe and understand what is happening with any detail by the naked eye. To better understand how chip-form occurs in this work, a high-speed camera was used. The Photron FASTCAM SA-Z type 2100K-M-34GB high-speed camera is capable of providing megapixel resolution up to 21,000 frames per second and reduced resolution at frame rates up to 2.1 million frames per second. In order to provide the necessary continuous light at a sufficient intensity to capture images at higher frame rates, a Thorlabs HPLS345 light source was used with a 5mm liquid-cooled light guide. Figure 3-16 shows the high-speed imaging setup used during the turning experiments. High-speed imagery was only captured

during dry machining to keep the coolant or lubricant used during the other tests from obstructing the view of chip-formation due to the close proximity of the camera to the machining process.
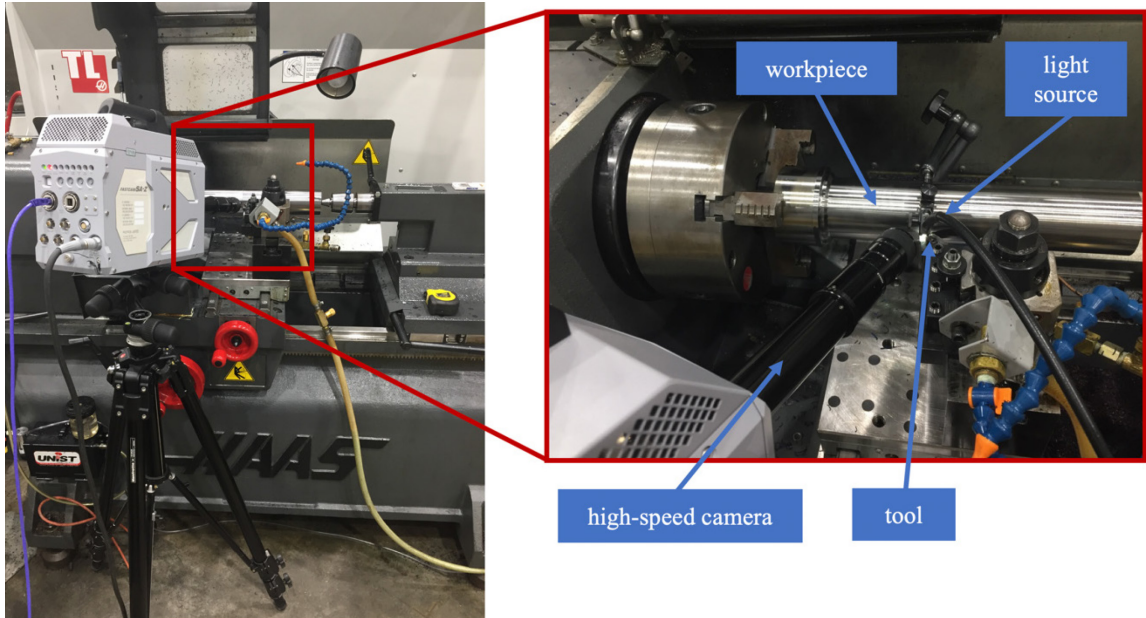
Figure 3-16. High-speed camera setup during dry machining experiments

CHAPTER 4

CHIP-FORM ANALYSIS

We shape our tools and afterwards our tools shape us.

- *Marshall McLuhan*

4.1   Introduction

In everyday life, most people are familiar with the process of cutting relatively soft matter, such as butter or bread, with tools such as a knife. The knife-edge is formed by two faces that meet at a small included angle that can then be forced into the matter being cut. Sharp tools provide a clean cut, and require minimal effort, into the matter causing the one body to split into two pieces by the faces of the cutting tool. Metals and alloys are much harder than butter or bread and therefore cannot be cut in this manner. They are so hard that no tool material, with knife-like cutting edges can withstand the high stresses and heat generated during a metal cutting process.

Considering this, it becomes necessary for proper metal-cutting tools "to take the form of a large-angled wedge, which is driven asymmetrically into the work material, to remove a thin layer from the thicker work material body." [92] When the metal-cutting tool is driven into the work material to remove a relatively thin layer, this thin layer is called the chip. Since the primary objective of machining is to generate a new surface on the workpiece that will become the final part, the chip simply becomes a waste product. For this reason, many do not pay much attention to the chip. However, there are many reasons why chip-form is arguably an important aspect of machining performance.

The consumption of energy during the machining process occurs primarily in the overall form and movement of the chip. Since the chip is formed by shear fracture at high strains near the newly generated workpiece surface, knowledge of the chip-form process is necessary for a deeper understanding of the accuracy and quality of a final product. There is also a unique interaction between the chip being formed and the tool that is forming the

chip. Therefore, this interaction should be considered for a deeper understanding of how the chip-form process effects tool-wear and also how tool-wear, in return, effects chip-form during a turning process. As such, many practical and economic problems regarding the machining process should be concerned with chip-form.

4.2   Results and Discussion

Before jumping into the results, this section of Chapter 4 is split up into two separate topics of discussion, cutting forces and chip-form. Cutting forces are of relatively little significance during this work, however that is not to say that they are insignificant to machining. The utility of capturing, interpreting, and applying the cutting force data is limited and will be discussed more in the following section.

In Chapter 2, the commonly used terms *cutting speed, feed,* and *depth of cut* were introduced. The cutting speed, V_c, used during all of the turning experiments performed in this work was 122 m/min. The feed rate, *f*, used during all turning experiments was 0.38 mm/rev. The depth-of-cut, a_p, used during all experiments was 0.51 mm.

These fixed conditions were motivated from an identical set of turning conditions used in the TechSolve study mentioned earlier in this thesis. A specimen that was machined under this same set of experimental conditions during the TechSolve turning study was also later evaluated for machining-induced surface integrity. As such, it was the authors goal during this work to replicate this same set of machining conditions. Doing so would best ensure that the additional knowledge acquired from this work could be integrated with the findings obtained in the previous efforts, thereby providing a robust data set for understanding of turning AF9628 steel in a hardened condition. Finally, careful planning was taken to replicate as many other variables such as the cutting inserts, flood-coolant emulsion type and concentration, tool holder, and workpiece material.

Table 4-1 shows a representation of the test parameters used during experiments. In this table, multiple passes were performed at the fixed processing parameters for cutting speed, feed rate, and depth of cut under dry machining conditions. This particular set of experiments was for high-speed imagery tests using insert 3A. The full set of experimental tables are much longer and repetitive and are therefore not shown in their entirety.

Table 4-1. Representative test parameters for dry machining experiments with a high-speed camera

Pass #	Speed (m/min)	Bar Dia (mm)	Spindle Speed (RPM)	Feed Rate (mmpr)	DOC, a_p (mm)	Cut Length (mm)	Total Cut Length (mm)	Cut Time/ Pass (min)	Total Cut Time (min)	Coolant	Notes
1	122	74.35	522	0.38	0.51	6.35	6	0.032	0.03	dry	high-speed
2	122	74.35	522	0.38	0.51	6.35	13	0.032	0.06	dry	camera tests
3	122	74.35	522	0.38	0.51	6.35	19	0.032	0.10	dry	
4	122	74.35	522	0.38	0.51	6.35	25	0.032	0.13	dry	insert 3A
5	122	74.35	522	0.38	0.51	6.35	32	0.032	0.16	dry	
6	122	74.35	522	0.38	0.51	6.35	38	0.032	0.19	dry	

AF9628 bar (49 HRC)

4.2.1 Cutting Forces

While this chapter is primarily concerned with chip-form, it is necessary to first discuss experimental results that were obtained for cutting forces during the machining experiments. While cutting forces will not be presented nor discussed to great length, they are an important aspect of the machining process. The utility of cutting forces in conjunction with chip-form sheds an interesting light to the process of turning AF9628 alloy that has previously never been seen to the author's knowledge. To this end, cutting forces are included in this work.

Using the dynamometer set up described in Chapter 3, force profiles can be obtained from the cutting process. Figure 4-1 is an example of cutting force profiles, in this case during dry machining, for each of the three machine axes shown in Figure 3-12. From the figure, the top force profile is representative of the force component in the y-axis, F_y, which is referred to as the tangential force that acts downward onto the rake face of the tool. The middle force profile is representative of the force component in the x-axis, F_x, which is referred to as the radial force. The bottom force profile is representative of the force component in the z-axis, F_z, which is referred to as the axial force.

From looking at the force plots in Figure 4-1, it can be observed that the magnitude of each force profile is fairly consistent with respect to the time. This is because a new cutting tool was used and over the relatively short duration of the test, no noticeable tool-wear has occurred. As a tool wears, especially during a significant wear event such as the chipping of a cutting edge, the cutting force measurements will noticeably change. Cutting force profiles can be used meaningfully during machining to inform the operator of tool-wear during machining. It should be noted that the force profiles in Figure 4-1 have been filtered within Kistler DynoWare software with a low-pass filter at 5 Hz to eliminate noise that is typical when acquiring such data.

It should also be noted that for research that is focused on obtaining a ground-truth measure of the cutting forces, more advanced signal analysis must be performed. For the purposes of this work, in which the use of cutting force data is more qualitative than quantitative, the cutting force analysis presented here is sufficient.
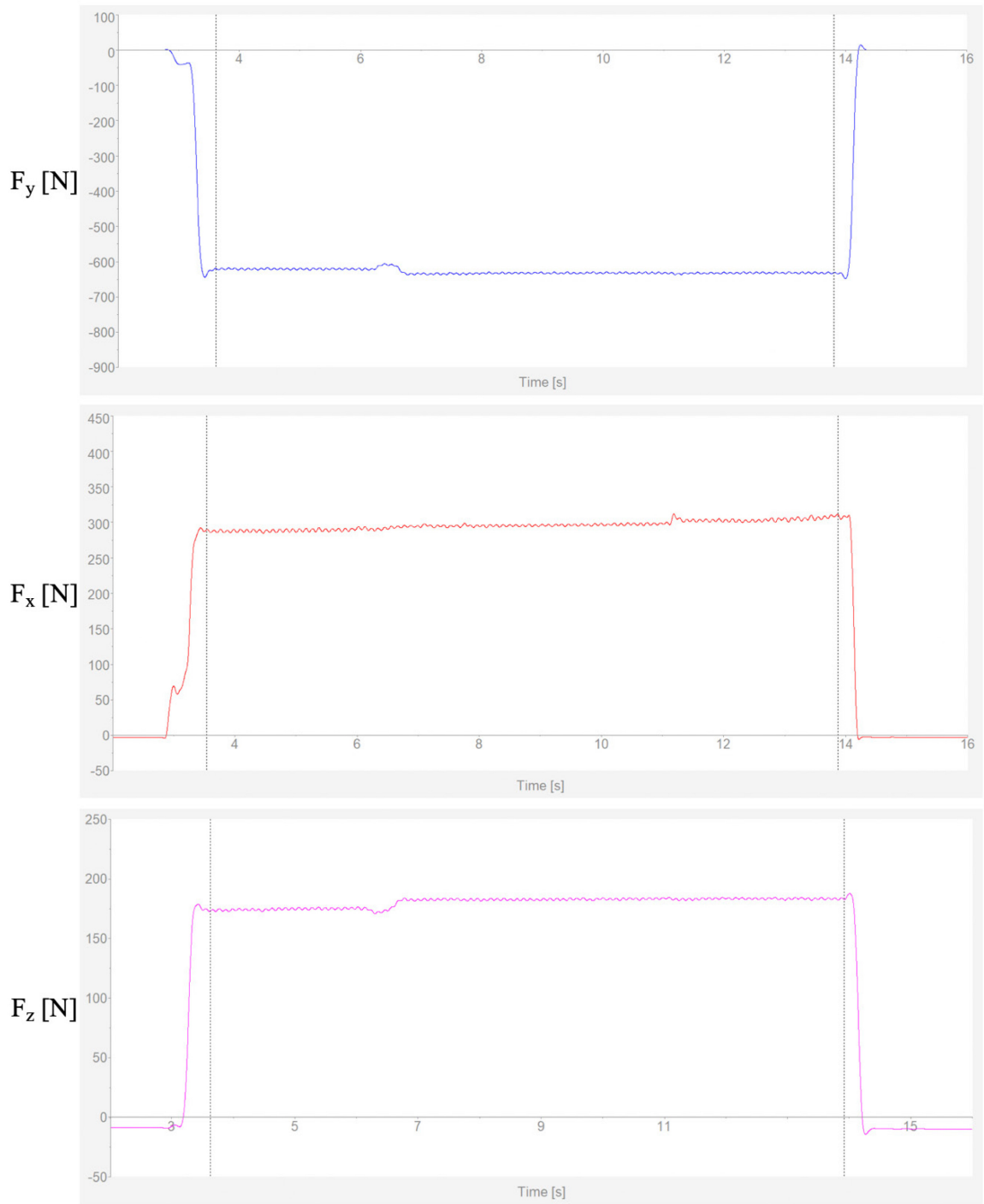
Figure 4-1. Example force plots during dry machining using a new tool (insert 7C). top: F_y, tangential force; middle: F_x, radial force, bottom: F_z, axial force

4.2.2 Chip-form Classification

The resulting chips from the machining process can be widely varied in size and shape. Not all materials can withstand the strain that is induced within the cutting region during machine. Some materials such as gray cast iron produce chips that are always very fragmented. Materials that are more ductile can produce chips in larger segments. However, workpiece material is only one factor that determines how the chip may form and a number of other cutting conditions influence chip-form. Chip-form can be classified into two different categories, those are discontinuous chips and continuous chips. Generally, in industrial operations, discontinuous chips are more favorable as they can be easily cleared from the cutting area and managed for disposal. Both discontinuous and continuous chips can take on many different shapes such as ribbon-like, in the shape of an arc, or a number of different helix types. Table 4-2 illustrates the various chip-form types that can be produced during turning operations with a single-point cutting tool.

During machining operations, chips are formed at extremely high speeds and the region within which they are forming is of relatively small scale. This makes the study of chip formation very difficult at an industrial level. However, in the laboratory, high-speed imaging technology gives us the opportunity to overcome the challenges generally associated with the study of chip formation. Due to the nature of the machining process and the high-speed camera technology, the camera must be positioned very close to the machining process so that it is with in the field of view to capture high-quality images. When operating at 40,000 fps, the camera has enough storage to capture only one-second worth of real-time chip-form phenomenon during machining.

Table 4-2. Chip-form classifications adapted from ISO 3685:1993 (Annex G) [78]
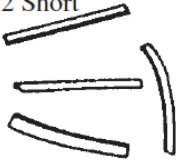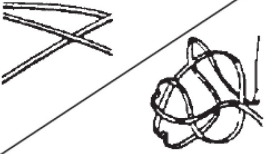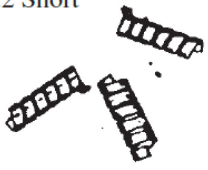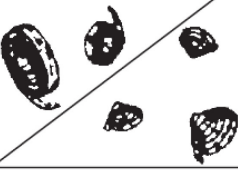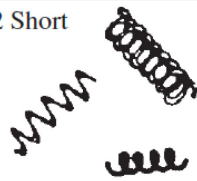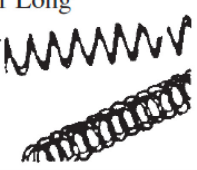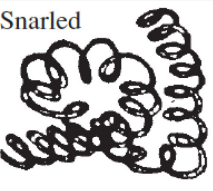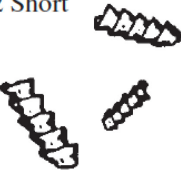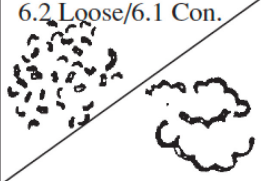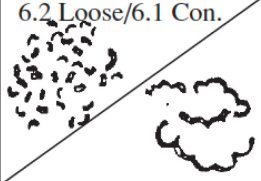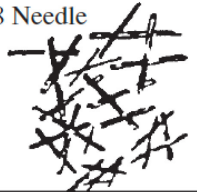
Curling		Favorable	Unfavorable	
Straight	1 Ribbon Chips	1.2 Short		1.1 Long/1.3 Snarled
Mainly Up-Curling	2 Tubular Chips	2.2 Short	2.1 Long	2.3 Snarled
	3 Spiral Chips		3.1 Flat/3.2 Conical	
Mainly Side-Curling	4 Washer type Chips	4.2 Short	4.1 Long	4.3 Snarled
Up- and Side-Curling	5 Conical Helical Chips	5.2 Short	5.1 Long	5.3 Snarled
	6 Arc Chips	6.2 Loose/6.1 Con.		
	7–8 Natural Broken Chips	7 Elemental		8 Needle

Figure 4-2 shows five image tiles at the top of the figure. Each of the images are taken 0.250 ms apart from each other in real-time. To help orient the reader as to what is happening, starting with the left-most image in the figure, the workpiece material is rotating such that the surface being machined is moving from the top of the image towards the bottom of the image as indicated by the arrow and the "workpiece travel direction" label. The cutting tool is traveling from right to left in the image as indicated by the other arrow and the "cutting tool travel direction" label. The orange-colored bubble with the number one inside represents the position number in the image sequence of the chip-form process. We can see that position one is at the tool-workpiece interface, where the chip formation process begins.

Moving now to the image second-from-the-left, we can see that time has advanced by 0.250 ms. During this time, the orange-colored bubble, now with the number two inside, has advanced away from the workpiece surface and along the rake face of the tool. In the middle image, position three, we see that the chip is in the process of curling. This curling action is a result of the cutting tool geometry. More specifically, the chip breaker design and the groove just behind the cutting edge influences the chip to flow into the groove and across the rake face until the flowing material contacts a bump which encourages the upward curling action. It is difficult to observe from the still images, but the high-speed video shows that the chip is primarily up-curl dominated with a little contribution of side-curl in the direction of the cutting tool travel.

Moving now to the image second from the right, we can see (position four) that the chip has continued to curl upwards and is making its way back towards the workpiece surface. Finally, in the right-most image (position five), the chip has continued to curl upwards and has made contact with the workpiece surface. Due to the cyclical nature of the chip formation process during machining in these experiments, one could start back at the left most picture (position one) and follow the chip-form process over and over again.

Before moving onto the next topic of discussion, there are more observations that can be made from the images in Figure 4-2. It is obvious that chips are being formed into an arc shape. Why doesn't the material continue to curl around itself into a long, continuous curly mass? When the chip curls and eventually makes contact with the workpiece (position five) there is a force at position five from that contact. This force is believed to develop a

moment at position one. That moment at position one induces enough strain to sufficiently fracture the chip. This fracture in the chip first becomes visually obvious in the middle image (position three). This cyclical chip-form behavior continues as long as the tool is engaged at a sufficient depth of cut in the material. It should also be noted that the cutting tool used in obtaining these images is new or has minimal wear.

Another interesting observation from Figure 4-2 can be made if we incorporate a corresponding force measurement for this dry machining condition. The magnified insert of the force profile with the five orange-colored bubble positions overlaid on top of the plot shows how the force measurements can capture the fine details of chip-form. It is interesting to note the oscillatory behavior of the force profile. It is also difficult to understand from the images why the chip at position three would correspond to the peak of the force profile. This can be more easily understood from observing the high-speed video footage. In the video footage, it can be seen that as the chip is approaching position three there is sliding contact of the chip across the rake face of the tool such that the chip slides away from the workpiece momentarily before sliding back towards the workpiece before making contact with the workpiece at position five. When this sliding contact occurs, there is an increase in the chip-tool contact area. This increase in the chip-tool contact area consequently results in an increase in the force applied to the tool, which explains why the chip at position three is placed at the peak of the force profile, where the instantaneous force is at a maximum.

The utility of observing both the high-speed images and corresponding force profiles can help us gain an appreciation for the chip formation process and some potential implications this may have on the cutting tool. First, it can be observed from the high-speed images that one (1) half-arc chip formation event takes approximately 1 millisecond to occur. This means that in one second of machining, approximately 100 half-arc chips are formed. The cyclical impact from the frequency of chip formation on the tool, coupled with the sliding contact along the rake face, should be a consideration in tool-wear mechanisms to be discussed in the following chapter. Also, understanding how force profiles can relate to chip-form may be of additional benefit for understanding chip formation in processes when high-speed camera technology is unavailable or inaccessible to the process like in many industrial settings.
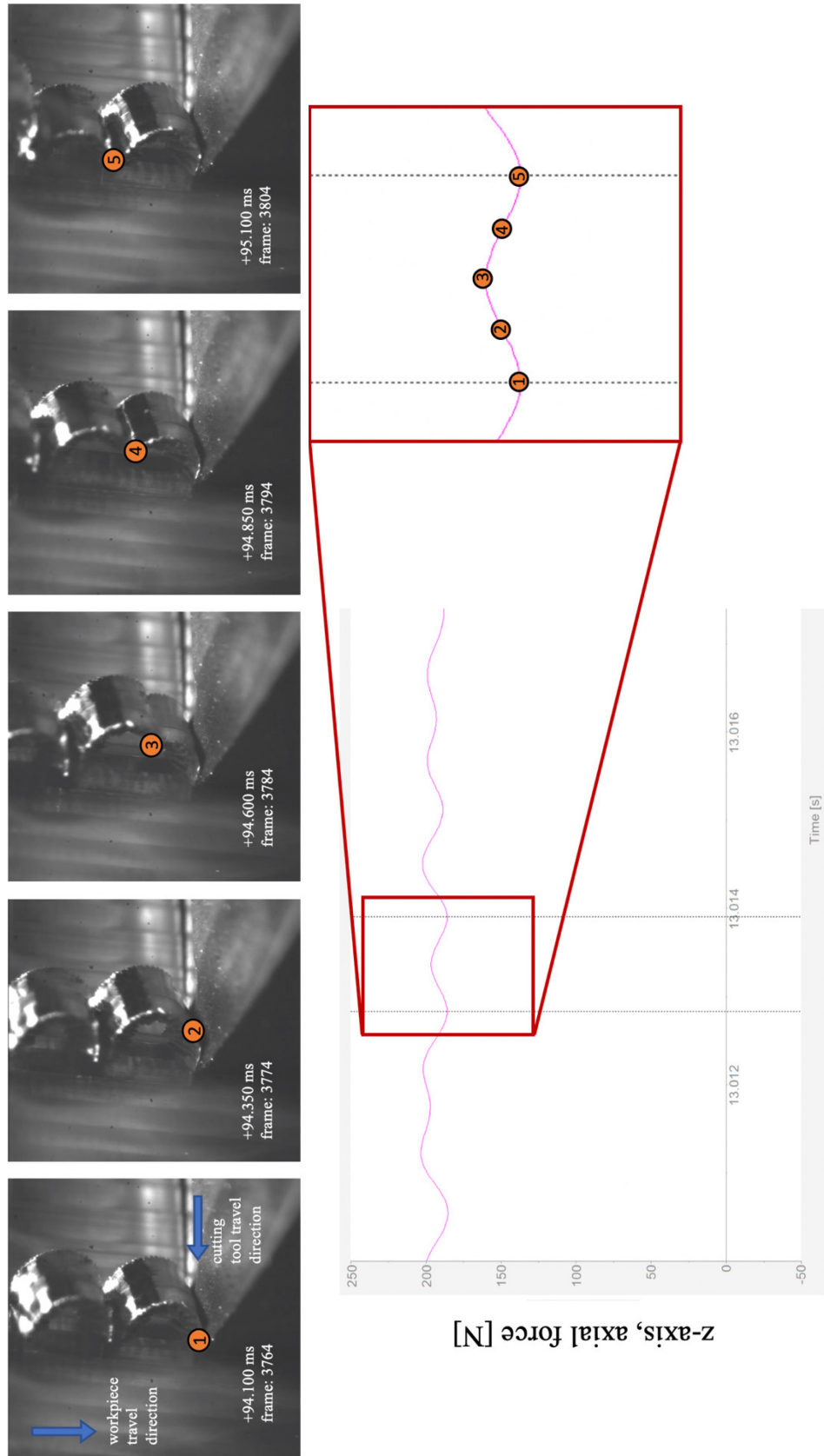
Figure 4-2. High speed camera images of connected arc chip formation and correlation with cutting force data for insert 7C. Images captured with a Photron FASTCAM SA-Z type 2100K-32GB camera at 40,000 fps.

At this point, we have looked at the chip-form process under a dry machining condition with a new tool. Now, we will look at chips produced using the other cooling and lubrication conditions.

First, let's look at chips produced under a flood-cooled condition when the cutting tool is new and when the cutting tool is at the end of its useful life. On the left of Figure 4-3, we can see the familiar arc formation in the chip that was seen during dry machining. What this image shows us, however, that we did not see very clearly from the images in Figure 4-2 is that the arc chips are connected. Generally, these arc chips connect to form a strand of 7 to 10 arcs before the strand is separated and flung away from the cutting area during the machining. The material that connects each arc is very thin and very brittle. If you take a handful of these chips and close your hand, the arcs will break from each other into smaller, loose arcs. Therefore, one may classify these chips as loose, connected arcs.

On the right of Figure 4-3, we see a much different chip-form produced. Here we have long, snarled ribbon chips that are a result of severe wear of the tool. These ribbon chips are certainly not ideal and indicative of a tool that is beyond its useful life. It is not shown in Figure 4-3 but as a tool wears, the arc length of chips can be visibly longer, and radius of curvature can increase. This was not directly measured, but may indicate that as the cutting edge wears, the material flows at a lower point relative to the tool and at a different angle before hitting the bump in the chip breaker design. Thus, the arc length and curvature can change as a result of tool-wear.
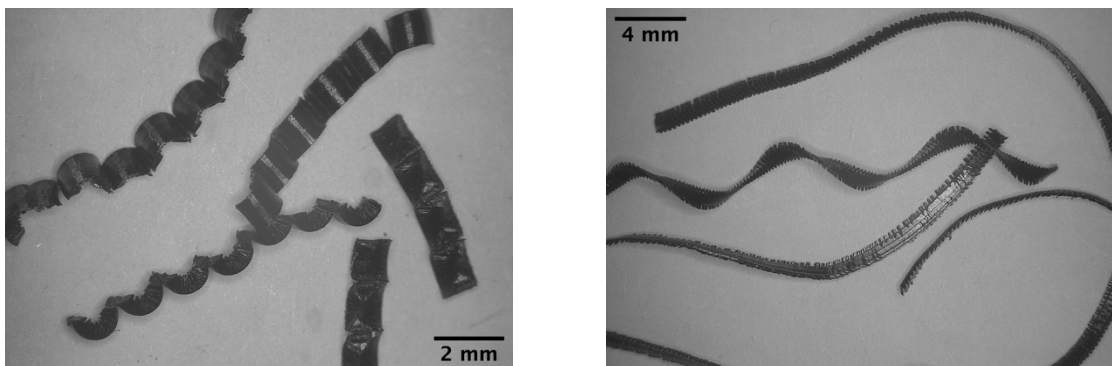
Figure 4-3. Chips produced under flood-cooled conditions with a new tool (left) and a worn tool (right)

Now, let's look at the chips produced with MQL when the cutting tool is new and when the cutting tool is at the end of its useful life. On the left of Figure 4-4, we also see the familiar connected-arc formation in the chip that was seen during dry and flood-cooled machining. On the right of Figure 4-4, we see long, snarled-ribbon chips similar to those from the flood-cooled condition. The snarled-ribbon chips are certainly not ideal and indicative of a tool that is beyond its useful life.
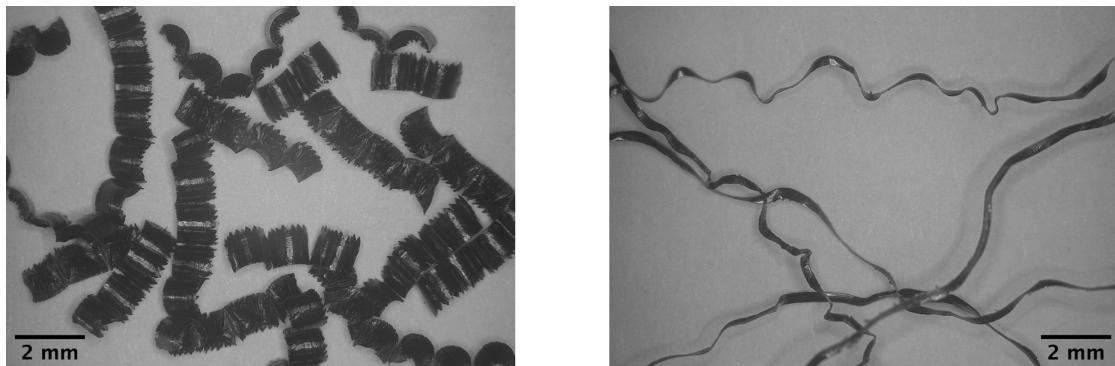
Figure 4-4. Chips produced under MQL conditions with a new tool (left) and a worn tool (right)

Finally, let's look at the chips produced with cryogenic cooling when the cutting tool is new and when the cutting tool is at the end of its useful life. On the left of Figure 4-5, we can see something different has occurred. Instead of the usual connected-arc chip that was observed in the other conditions, we see a more tubular shape of the chip. One of the reasons for this could be due to the way that the cryogenic coolant, LN_2, is being applied to the cutting area. The LN_2 is delivered through a copper tube that is directed at the top of the rake face of the tool. This delivery location is aimed at the chip as it is being formed during cutting. It is possible that the pressure from of the LN_2 delivery is causing the chip to lift slightly off of the bump on the tool that is encouraging the typical chip curl observed in the other conditions. Instead of the chip curling upwards and making contact with the workpiece, the chip continuously curls off to the side of the tool, resulting in continuous, tubular-shaped chips. Figure 4-6 shows this chip-form behavior as it occurred during the cryogenic machining process. As was seen in the flood-cooled and MQL machining conditions, when the tool is worn past its useful life with cryogenic machining snarled-ribbon chips result. This can be seen on the right side of the Figure 4-6.
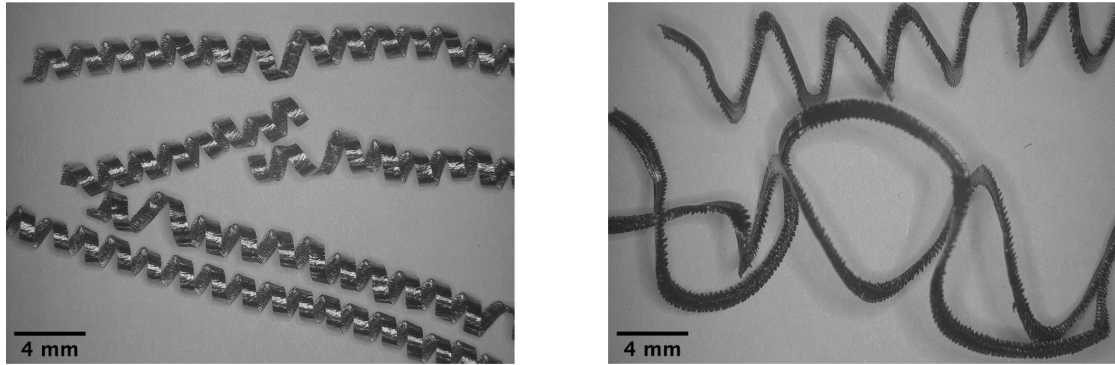
Figure 4-5. Chips produced under cryogenic conditions with a new tool (left) and a worn tool (right)
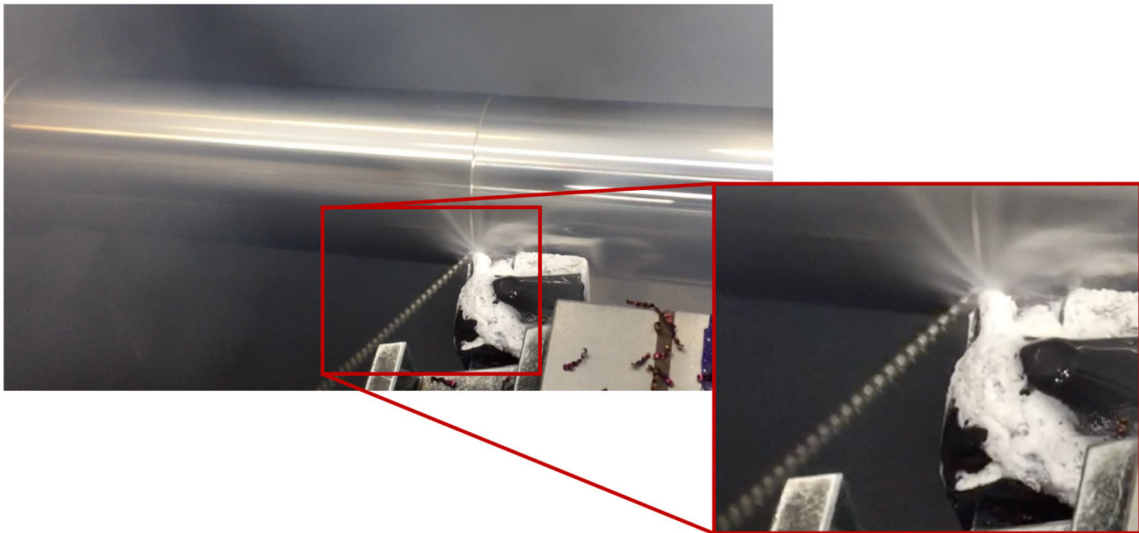
Figure 4-6. Chip formation during cryogenic machining with up-curl and side-curl flow resulting in a continuous tubular-shaped chip

Another observation that can be made from chip observations is that of the "saw-toothed" chip morphology on the inside of the chip and evident near the edge of the chip. This is quite a common phenomenon observed in machining as well as in other material science research areas. n the machining, when a chip is formed so rapidly that the heat generated has no time to flow away from the chip this heating causes the metal to soften, often referred to as thermal softening. Also, during machining, plastic strain caused during

the cutting process in certain conditions can cause a strain hardening effect. A common theory is that if the generated heat causes enough softening of the metal to overcome the strain hardening, shearing becomes localized in a very narrow band of this increasingly high temperature region of the metal. This narrow band is often referred to as shear banding. Under shear banding, periodic localization of plastic flow results in a "saw-tooth" chip morphology. This shear banding can be seen in the chip morphology of a titanium alloy in Figure 4-7.
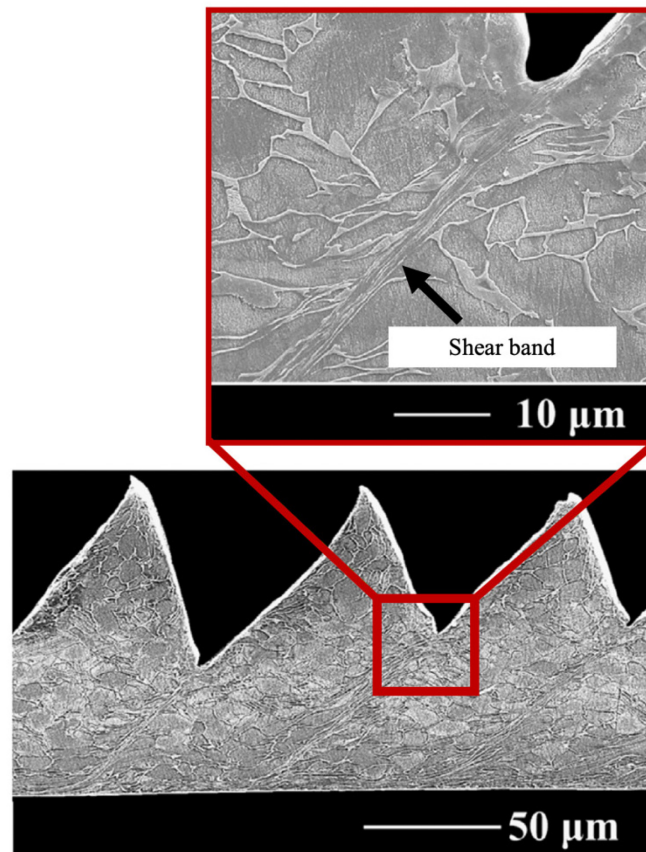
Figure 4-7. Microstructure of chip morphology for *Ti-6Al-4V* at V_c = 4.07 m/s. [104]

Table 4-3 summarizes the chips produced under flood, dry, MQL, and cryogenic machining conditions at varying stages of tool-wear without describing the actual time or length of cut that the tool was in service. Tool-wear and tool-life under the various cooling and lubrication conditions will be discussed more in the following chapter. In Table 4-3

chips produced using a new tool are on the left and as the chips move to the right, the tool is progressing towards the end of life. Analyzing the various shapes and sizes of chips from Table 4-3, it can be seen that favorable chips are formed in the image tiles a, b, d, g, and k, as compared to the chip classifications in Table 4-2. The chips in image tile j could also be considered favorable if the case were that the tubular chips are broken into shorter, more manageable lengths. Since there was a mix of short (< 10 mm) and long, continuous chips, it be considered unfavorable overall.

Up to this point, we have seen the variability of the shape and size of chips produced in a turning operation under various cooling and lubrication conditions. We can also observe the color of the produced chips to try and interpret something else about the process. Table 4-4 is identical to Table 4-3 with the exception of a few select images that are displayed in color. In the table, it was the author's intent to reproduce the non-color images with some degree of transparency so as to draw more attention to the colored images. Starting with the flood-cooled chips, a brownish color can be seen in the chip. During the machining process temperatures can reach into the hundreds of degrees Celsius. When steel is subjected to increases in temperature, a thin oxide layer forms on the surface. Time and temperature have a relationship with the oxide layer thickness that is produced. Different oxide layer thicknesses will reflect different wavelengths of light and therefore affect the color that we see on the surface of the steel. In the case of the flood-cooled chips, despite the application of flood-coolant to the process, the temperature rises enough to produce this brownish, perhaps even auburn-like color.

In the case of the dry machining chips, we can see blue and purple colors dominant in the chip, which is indicative of the higher temperatures that we would expect in this process with the absence of a coolant. Likewise, MQL is considered a technique providing more of a lubrication effect than a cooling effect. As such, we see blue and purple here as we did in the dry machining condition.

The chips produced with cryogenic cooling are much different. They appear more white or faint yellow, which is a result of the chip experiencing lower induced temperatures. Recall from Chapter 3 during the discussion of the cryogenic machining setup. The cooling medium used is liquid nitrogen, which has an approximate temperature

of -196°C (-321°F). The application of this low temperature medium helps explain how heat could be more effectively kept out from the chip.

Table 4-3. Summary of chips produced from flood, dry, MQL, and cryogenic conditions at various stages of tool-wear
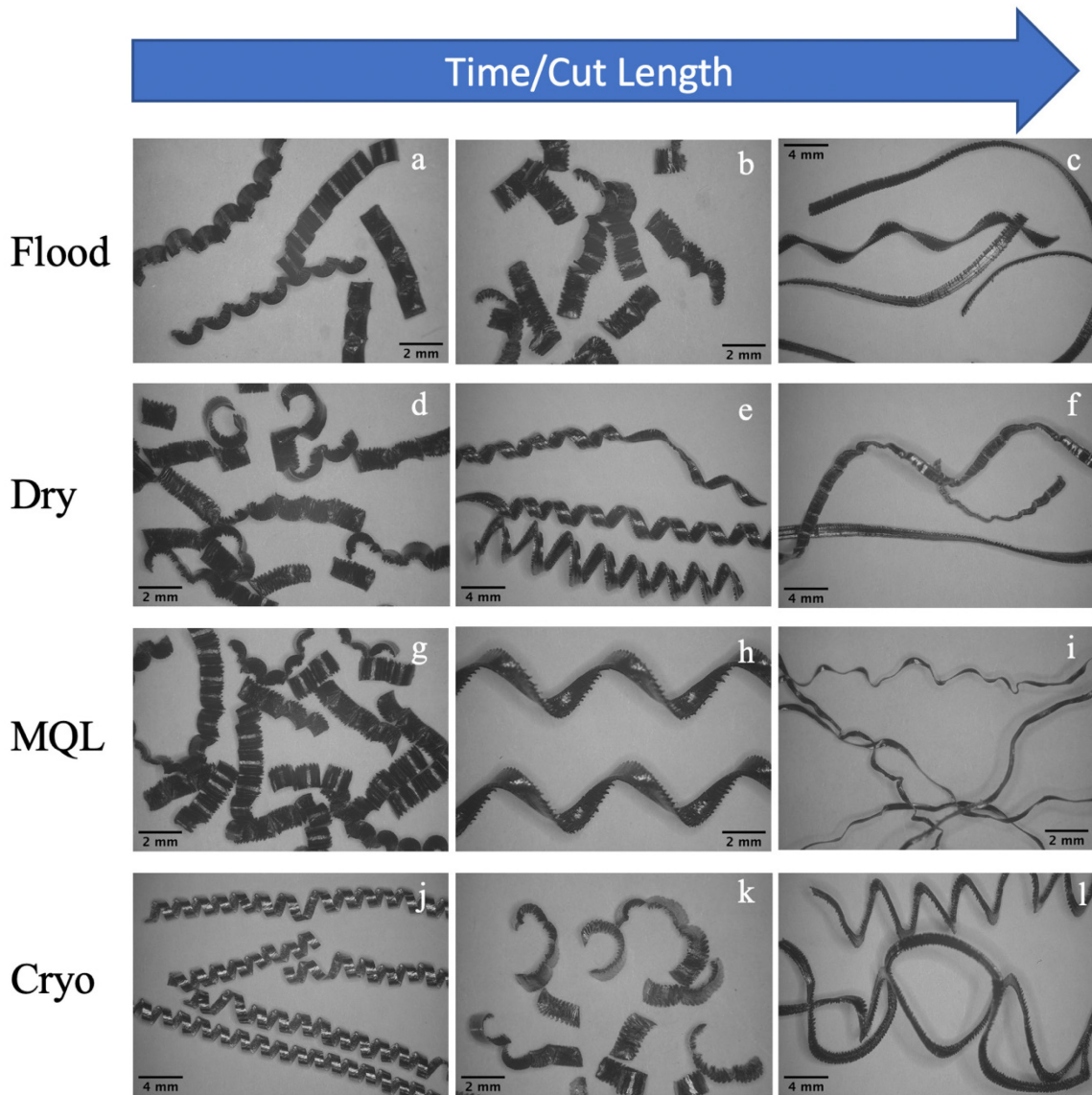
Table 4-4. Chip colors produced from flood, dry, MQL, and cryogenic conditions
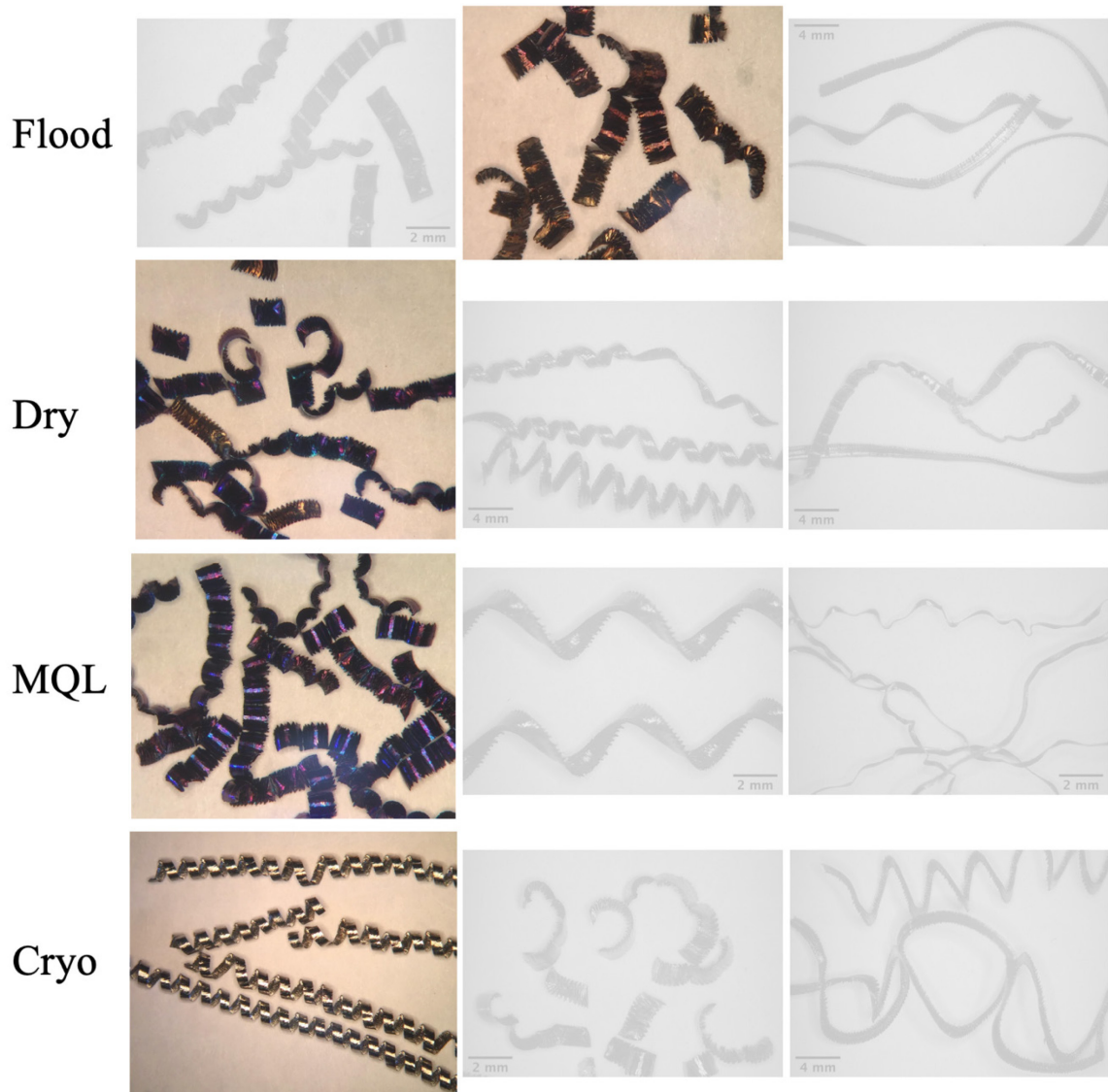
4.3   Concluding Remarks

It has been stated already that since the primary objective of machining is to generate a new surface on the workpiece that will become the final part, the chip simply becomes a waste product. However, chip-form can tell the engineer or machine operator a lot about a process. This chapter analyzed chip-form and classified resulting chips by shape, size, and color under different cooling and lubrication conditions. With new carbide tools, each of the cooling and lubrication conditions demonstrated an ability to produce short chips. Also, each condition demonstrated that as tools progressively wear, the chips can become longer, snarled, and less ideal for an industrial setting.

Other practical considerations regarding chip size and shape that was not previously discussed has to do with part quality and operator safety. A primary reason why long, snarled chips are unfavorable has to do with chip management. With the turning process in mind, long chips can very easily get wrapped up around the rotating workpiece and quickly grow into an uncontrollable mess of hot, sharp metal chips spinning around, ready to grab anything in its path. This poses a great safety risk to the operator and the machine. Not to mention the great likelihood of the occasional chip getting caught between the tool and the workpiece, causing the chip to be extruded and redeposited onto the machined surface, leaving a poor surface quality. Chips that do not clear the work area can also scratch a machined surface. For critical, high-value components used in the aerospace or medical industries, these quality issues must be considered and managed.

The consumption of energy during the machining process occurs largely in forming a chip. The primary shear zone, where a chip is formed by deformation, is where a major part of the energy is converted to heat. Since the chip is formed by shear deformation at high strains near the newly generated workpiece surface, knowledge of the chip-form process is necessary for a deeper understanding of the accuracy and quality of a final product. Something to keep in mind before moving into the following chapter is that, while the higher temperatures generated during machining are evident in the resulting chips, the machining induced temperatures may also have an impact on the cutting tool.

CHAPTER 5

TOOL-WEAR ANALYSIS

You look closely enough, and you'll find everything has a
weak spot where it can break, sooner or later.

- *Anthony Hopkins, "Fracture" film*

5.1   Introduction

Wear is generally an undesirable trait that occurs when two bodies interact by moving relative to one another. Most people are familiar with wear in the case of writing with a pencil on a piece of paper. A sharp, pointy stick of graphite quickly wears down and becomes dull as you write across the page. This may not always be undesirable, but if the goal is to produce consistently crisp lines throughout a written work, then wear is a phenomenon that must be managed by constant re-sharpening. Much like the pencil, cutting tool-wear during machining results in a change in the desired geometry of the machined part. Depending on the geometric tolerances required in the final machined part, the amount of acceptable tool-wear can vary. Regardless, tool-wear must be understood before it can be managed.

With regard to single-point turning tools, wear can be classified into the following major wear mechanisms:

1. Abrasion
2. Adhesion
3. Diffusion
4. Chemical
5. Oxidation

Any one, or combination, of the above wear mechanisms can lead to several types of tool-wear. Attrition is a type of wear associated with adhesion, when workpiece material adheres to the cutting tool as the material flows over the tool creating a built-up edge. When

this built-up edge is overcome with enough force, it will break off the tool taking some of the tool material along. This process repeats many times over resulting in an attrition wear. Diffusion wear at high surface temperatures causes a type of wear called cratering. Carbon atoms and metal from the tool material diffuse into the work material that it sees at the rake face surface. This chemical reaction causes the atoms to be carried away in the chip leaving a crater on the rake face. Abrasive wear can occur when isolated small particles of hard carbides in the workpiece material, or even broken from the tool, are dragged across the tool, consequently ploughing grooves into the tool material. A summary of common tool-wear types, with possible causes and remedies, is listed in Table 5-1.

Table 5-1. Common tool-wear types with possible causes and remedies. Adapted from [58]

Tool-Wear	Possible cause	Remedy
Flank and notch wear (a) Rapid flank wear causing poor surface texture or inconsistency in tolerance. (b) Notch wear causing surface texture and risk of edge breakage.	(a) Cutting speed too high or insufficient wear resistance. (b) Oxidation. (b) Attrition.	Reduce cutting speed. Select a more wear resistant grade. Select an aluminum oxide grade for steel machining. For work-hardening materials, select a larger lead angle or a more wear resistant grade. Reduce the cutting speed.
Crater wear Excessive crater wear causing a weakened edge. Cutting edge break-through on the trailing edge causes poor surface texture.	Diffusion wear due to too high cutting temperatures on the rake face.	Select an aluminum oxide coated grade. Select positive insert geometry. First, Reduce the speed to obtain a lower temperature and secondly, the feed.
Plastic Deformation Plastic deformation (Edge depression (a) or flank impression (b)) leading to poor chip control and poor surface texture. Risk of excessive flank wear leading to insert breakage.	Cutting temperature too high combined with a high pressure.	Select a harder grade with better resistance to plastic deformation. (a) Reduce cutting speed (b) Reduce feed

Tool-Wear	Possible cause	Remedy
Built-up Edge Built-up edge causing poor surface texture and cutting edge frittering when the BUE is torn away	Smearing workpiece material is welded to the insert due to: Low cutting speed. Negative cutting geometry. Very sticky material, such as certain stainless steels and aluminum.	Increase cutting speed or change to coated, tougher P35 grade. Select a positive geometry. Increase cutting speed considerably. If tool-life turns out to be short, apply coolant in large quantities.
Mechanical fatigue cracking Cracks running mainly parallel to cutting edge	Excessive load variations on edge. Heavy shock or vibrations at start of cut.	Select a tougher grade. Reduce feed rate. Change tool approach Improve stability
Chipping Small cutting edge chipping causing poor surface texture and excessive flank wear	Grade too brittle. Insert geometry too weak. Built-up edge.	Select tougher grade. Select an insert with a stronger geometry. Increase cutting speed or select a positive geometry. Reduce feed at beginning of cut. Improve stability.
Thermal cracks small cracks perpendicular to the cutting edge causing chipping and poor surface texture	Thermal cracks from excessive temperature variations caused by: Intermittent machining. Varying coolant supply.	Select a tougher grade with better resistance to thermal shocks. Coolant should be applied copiously or not at all.
Fracture Insert fracture that damages not only the insert but also the shim and workpiece	Grade too brittle. Excessive load on the insert. Insert geometry too weak. Insert too small.	Reduce feed and/or depth of cut. Select a thicker/larger insert. Improve stability.
Chipping from chip hammering Cutting edge, not in cut, is damaged through chip hammering. Both the top side and the support for the insert can be damaged.	The chips are of an excessive length and directed in the wrong direction against the cutting edge.	Change the feed slightly. Select an alternative geometry. Select a tougher grade. Change the lead angle.

Over the last few decades, several groups have worked to develop standard test methods for tool-life testing and produce standards such as the ISO 3685(E) and ASME B94.55M [88, 89]. Tool-life criteria are provided in such standards and various methods exist for the specification of tool-life, such as actual cutting time or volume of material removed. Wear criteria are also used for determining when a cutting tool has reached the end-of life. Most common is the use of data by performing lathe turning tests in continuous cutting and measuring the width of the flank wear land. However, depending on the dominant wear type, other dimensions such as a crater formed on the rake face, for example, can also be measured. In Figure 5-1, a typical crater wear is shown inside the orange outline and a flank wear and notch wear type is shown inside the blue outline.

The summary of tool-wear types in Table 5-1 is more complex, however, and as such, "judgement is required by the investigator on what is significant and what can safely be ignored since tool-wear is seldom as even and clearly defined as is implied by simple models" [92] like the two shown in Figure 5-1. Ideally, the change in shape of a tool will be small and gradual enough that the naked eye cannot accurately discern changes and the use of a microscope will be justified. However, the skill of the machine operator is valuable for determining the end-of-life criterion as it often happens in the real world. That is to say that the criterion can vary from "when the temperature begins to rise and fumes are generated; when the operation becomes excessively noisy or vibration becomes severe; when dimensions or surface finish of the workpiece change" [92] or when the tool shape has changed by some specified amount.
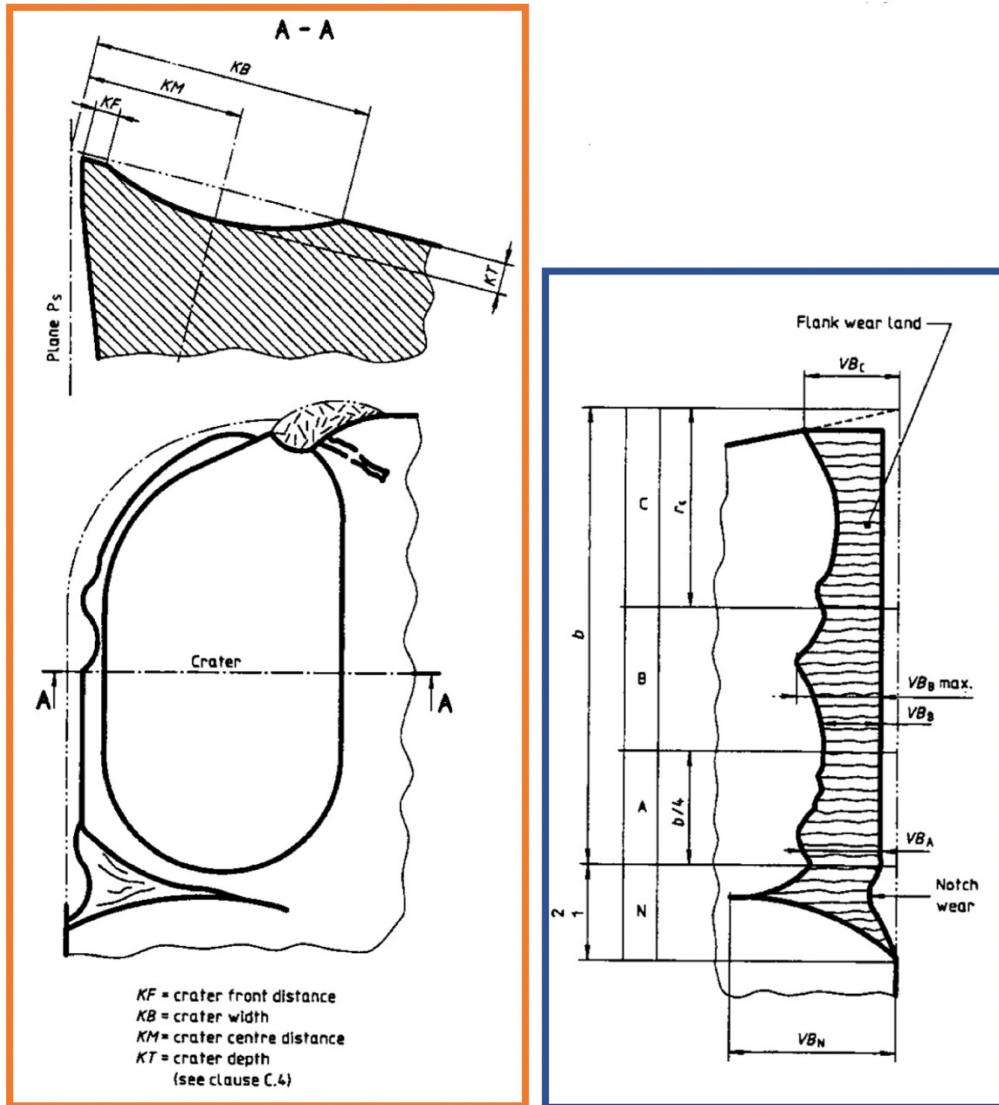
Figure 5-1. Some types of wear on turning tools. Crater wear (left) and flank wear (right).
Adapted from [89]

5.2   Flood-coolant Results and Discussion

The following section will focus on the results from flood-cooled machining experiments, particularly on aspects relating to tool-wear. First, tool-life results from several experiments will be presented. Several types of observed tool-wear will be presented and discussed. Then, the following section will focus on dry, MQL, and cryogenic machining experiment results relating to tool-wear.

88ABW-2019-5923

5.2.1 Tool-life

Common standards for tool-life testing with single point turning tools offer guidelines in accordance with the ISO 3685 standard. The tool-wear criterion, which was discussed briefly in the previous section, was established as being satisfied when the maximum width of the flank wear land, known as VB_{max}, is equal to or greater than 0.30 mm (0.012 in), or if the tool appears to catastrophically fail. VB_{max} is illustrated in the blue outline of Figure 5-1 and the criterion used for this work is consistent with the ISO 3685.

Tool-wear experiments were conducted at fixed parameters for cutting speed, $V_c =$ 122 m/min, feed rate, $f = 0.38$ mm, and depth of cut, $a_p = 0.51$ mm. Continuous passes, or cuts, were made on the outside of the bar at cut lengths for each pass varying from 300-350 mm. The length of continuous cut is limited by the length of the available bars and machine setup. It should be noted that each successive pass is shortened by 0.25 mm than the previous one to avoid making contact at the shoulder, or wall, of material that is created over time as each pass is made. If the cut length was kept constant for each pass, then the hard contact of the tool against this shoulder would cause unnecessary damage to the tool.

After every two passes, the tool is removed from the tool holder and examined under a Nikon stereo microscope to capture images of the rake face, flank face, and nose region of the tool. Images are also captured using the Zygo NewView 7300 scanning white light interferometer (SWLI) for higher fidelity, 3D contour maps of the tool. For tool-life measurements, images from the stereo microscope were analyzed in an image processing software, ImageJ, to measure flank wear as shown in Figure 5-1. While the wear type being measured here is typically considered flank wear, it will be referred to in this work as nose wear, N, which is adopted from the work by Jawahir et al. [42]. The reason for calling it nose wear instead of flank wear is because the nose radius of the cutting tools is 0.8 mm (0.0313 in), and the depth of cut used in the experiments is 0.51 mm (0.02 in). Since the depth of cut is smaller than the nose radius of the tool, the nose is the primary recipient of direct contact with the workpiece during cutting and consequently the primary recipient of tool-wear. Therefore, it is technically more accurate to describe this wear as nose wear.

The nose wear measurement is taken by measuring the widest part of the wear land produced on the nose region of the tool. As the nose wear is measured every couple of

passes, the evolution of nose wear can be plotted with respect to time. Plotting the measured change in nose wear with respect to time generates a tool-life curve. An example measurement of nose wear is shown in Figure 5-2.

In Figure 5-3, it can be seen that images from various stages of the machining experiment have been measured for nose wear and plotted with respect to time. The plot in this figure shows the tool-wear measured along the y-axis and the cumulative cut time along the x-axis. The orange line running horizontal at 0.30mm represent the tool-life criteria established for these experiments. The green curve on the plot is the resulting tool-life curve for a single tool-wear/tool-life experiment. This is an ideal tool-wear curve based on its general profile.

On the tool life curve in Figure 5-3, there are two vertical lines, one placed near the four-minute mark along the x-axis and another placed around the fifteen-minute mark. These vertical lines help distinguish three stages of wear that occur in the idealized tool-wear curve. The initial wear stage starts at the beginning of the test, time equal to zero, and spans the length of time that the tool is in a so-called "break-in" period where it receives a relative quick initial wear. Next, the steady-state wear stage describes the duration of the tool-life in which wear is fairly steady and may increase with time but does not generally make any rapid changes. Finally, the rapid wear stage is where the tool is approaching its end-of-life and quickly breaks down, often times before catastrophically failing. Ideally, tool-wear will be consistent and predictable for a given process so that tool-wear can be managed, and catastrophic failure does not occur during a critical pass along the workpiece, which can have undesirable effects on the quality of the workpiece.

The plot in Figure 5-4 shows the green tool-life curve from the previous figure as well as two more curves from separate tests performed in this work. A similar profile (a result of the three stages of wear) can be seen in all three curves albeit the time until the nose wear reaches the tool-life criteria has shifted to the left slightly. This is not too surprising as tool-life can vary to some degree depending on a number of factors including the machine setup, workpiece material, tool, cutting conditions, etc. The black "X" mark on the plot around the thirteen-minute mark represents the tool-life obtained during the TechSolve study under the same machining conditions. There is excellent agreement in the

measured outcome between the TechSolve data point and the tests performed in this work, particularly the gray and yellow curves, which are less than 10% variance from the TechSolve data. The green curve varies 28% from the TechSolve data point albeit it exhibited a longer tool-life.

It is worth noting that the green curve and the TechSolve data point were both obtained using the AF9628 bar stock at a hardness measurement of 51 HRC. The gray and yellow curves were both obtained using the AF9628 bar stock at a hardness measurement of 49 HRC. The difference in hardness measurement between the two bars is only two points and any significant difference in tool-life would not be expected. If anything, one might expect the harder material to have a worse tool-life.

Another very interesting observation has to do with the tool-life curves and the inserts that were used in each study to generate the curves. The curve with the lowest cumulative cut time before reaching the tool-life criteria is the gray curve with which insert 3D was used during experiments. The curve with the next highest cumulative cut time before reaching the tool-life criteria is the yellow curve with which insert 4A was used during experiments. The curve with the highest cumulative cut time before reaching the tool-life criteria is the green curve with which insert 2A was used during experiments. Referring back to Figure 3-11, the measured edge hone radius for inserts 3D, 4A, and 2A were 40 µm, 37 µm, and 30 µm respectively. This is interesting because it would be expected that the larger edge radius would provide better mechanical strength and therefore have a greater likelihood of lasting longer. However, the opposite is observed. The largest edge hone radius obtained the lowest tool-life and the smallest edge hone radius obtained the highest tool-life.

While it may be tempting, one should not jump quickly to the conclusion that a smaller edge hone radius (i.e. sharper tool) will experience a longer tool-life. A number of reasons could explain this event. First, measuring the edge hone radius in the manner done in this work is a gross over-simplification for characterizing the edge hone. It is assumed that there is a constant radius at any given cross-section and that the radius is consistent at different points along the cutting edge. Both of these assumptions are likely not true and so it would be meaningful to exploring a better edge preparation characterization technique

and to what degree does the edge preparation have on machining performance such as tool-life. More on this general topic will be discussed in the future work section in the following chapter. Next, two different bars were used between these three tests and while both bars were AF9628 steel and of relatively similar hardness, subtle differences in the chemistry and primary processing conditions (e.g. melt process or forging) could be resulting in different tool-life results. Also, the bars were slightly different diameters at the beginning of the tests, with the 51 HRC bar around 55 mm (2.17 in) and the 49 HRC bar around 92 mm (3.62 in). The difference in bar diameter could likely have some effect on how and where the bar, when rotating, contacts the cutting tool including the stability of the cut and effective cutting angles with the rake face and other clearance surfaces on the tool. It should be noted that no chatter or other indication of instability was observed either visually or audibly during any of the experiments.
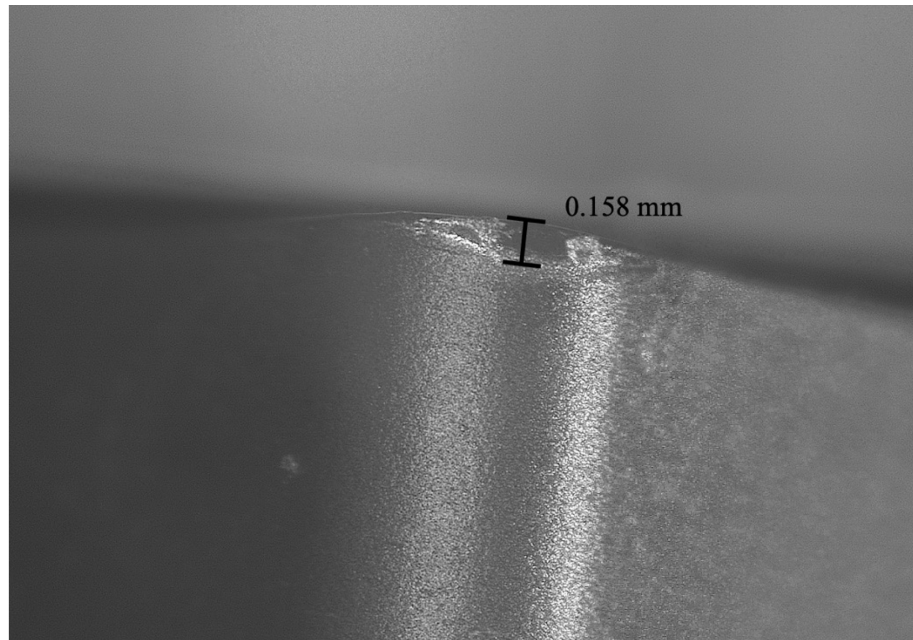
Figure 5-2. Representative measurement of nose wear during flood-cooled machining.
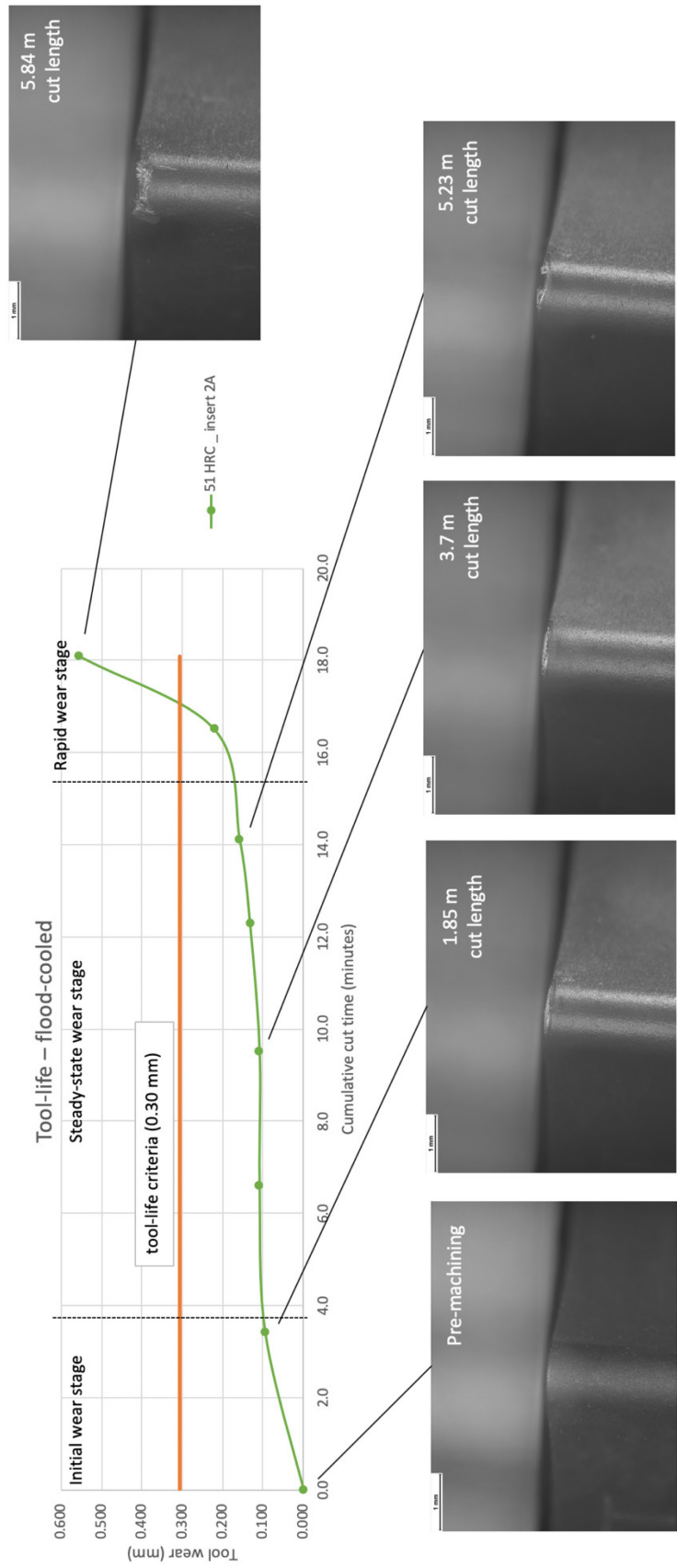
Figure 5-3. Tool-life curve for insert 2A with associated tool images at various stages of wear

88ABW-2019-5923
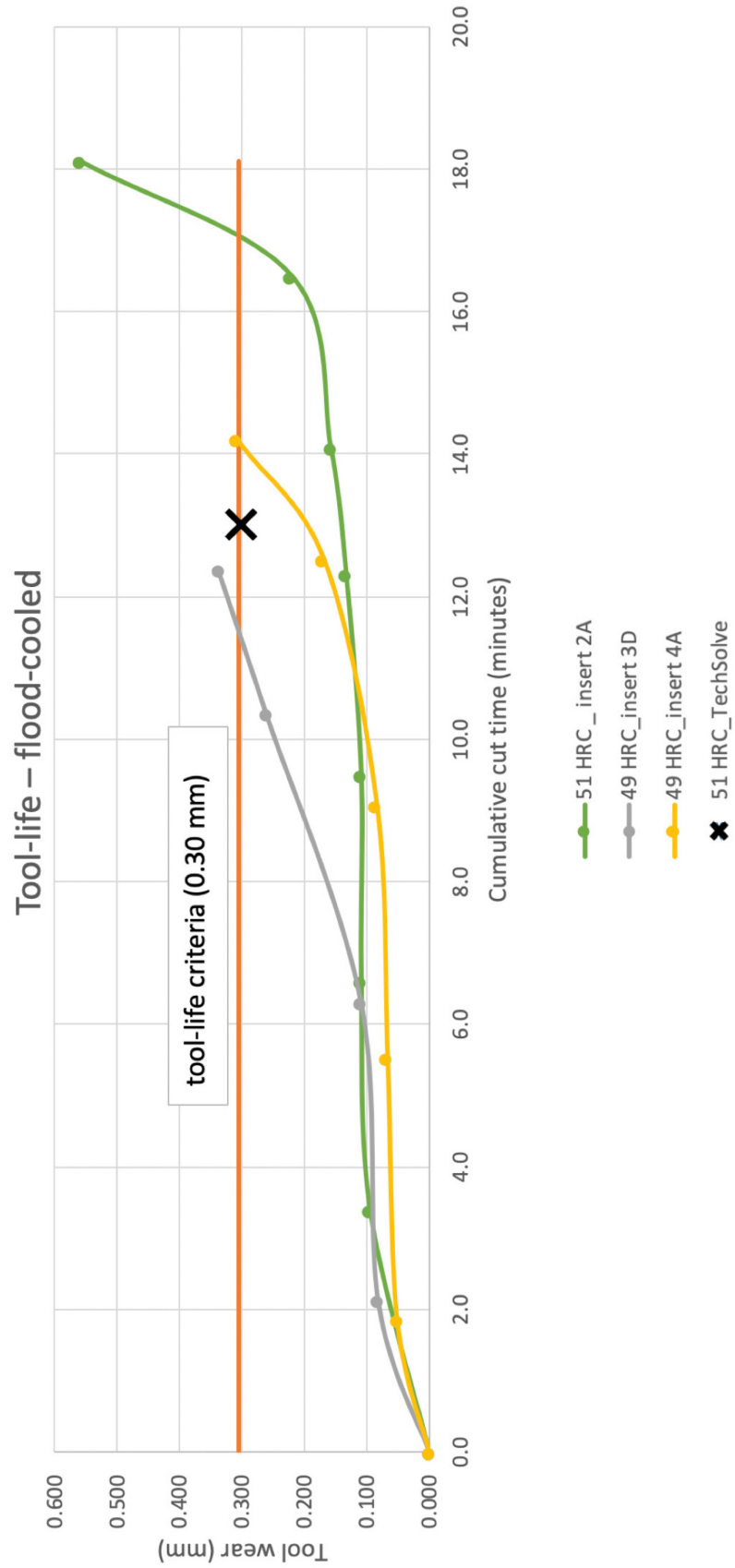
Figure 5-4. Tool-life curve comparison from various tool-wear experiments with multiple inserts

5.2.2 Built-up Edge

So far, nose wear and tool-life have been discussed, but as has been mentioned previously, more than one type of wear generally occurs during most machining processes. Moving further into the analysis of various tool-wear types, the phenomena of a so-called "built-up edge" will be discussed. When workpiece material flows over the tool, sometimes the work material adheres to the tool and separates from the rest of the flowing chip. As more material continues to flow over the tool, more material adheres the initial layer of adhered workpiece material creating a built-up edge (BUE). As the BUE grows in size, it becomes unstable and breaks off. Generally, BUE occurs at relatively lower cutting speeds. The reason for this is because increasing cutting speed will increase the temperature induced into the process. Higher temperatures increase thermal softening of the work material and this lowers flow stress, allowing the chips to more easily flow over the tool without seizing. As such, at lower temperatures, flow stress is higher and work material is more likely to seize or stick to the tool by a sort of pressure welding. BUE is more likely to occur in "sticky" materials such as aluminum, stainless steel, and other low carbon steels.

When BUE breaks off, it often gets extruded between the very tight gap of the tool-workpiece interface and becomes redeposited onto the workpiece surface. Evidence of this redeposited material onto the workpiece surface is shown in Figure 5-5. This image was taken during high-speed camera tests under dry machining conditions, however BUE occurs in flood-cooled machining as well. The redeposition of workpiece material onto the workpiece surface was confirmed during a machining-induced surface integrity study at the University of Kentucky under Air Force contract FA8650-18-F-5573 [5]. The machining-induced surface integrity study was performed on machined specimens using flood-coolant that were produced during the machining study at TechSolve. The investigators of the machining-induced surface integrity study observed evidence of material redeposition during analysis with various microscopy techniques looking at the finish machined surface.

During flood-cooled experiments within this thesis work, evidence of BUE was also captured using the SWLI. From Figure 5-6, BUE can be seen on the cutting edge and was measured to have a peak height of 17 μm (0.0007 in). However, when the BUE

material is redeposited, it gets squeezed between the tool and workpiece as previously stated. Since that gap is very small, the redeposited layer thickness is likely on the order on nanometers. Interestingly, BUE was more likely to be found on newer tools than on tools that were nearing the end of useful life. This needs to be investigated further as it is not well understood what causes this.
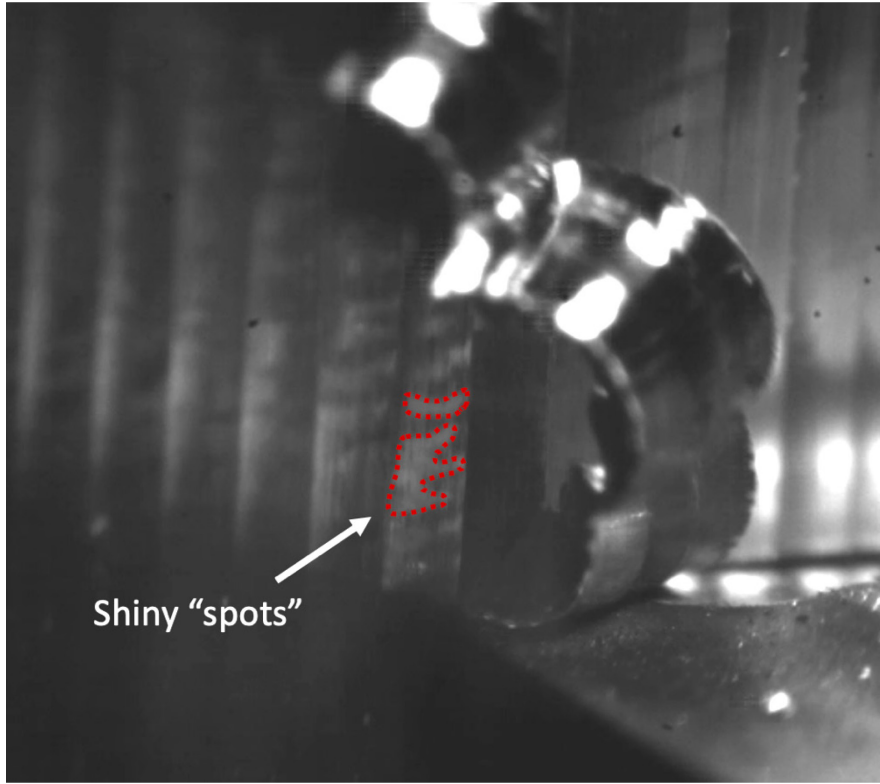
Figure 5-5. Redeposited material, shown as shiny "spots", on the workpiece surface as a result of built-up edge break off

BUE height: ~17 μm
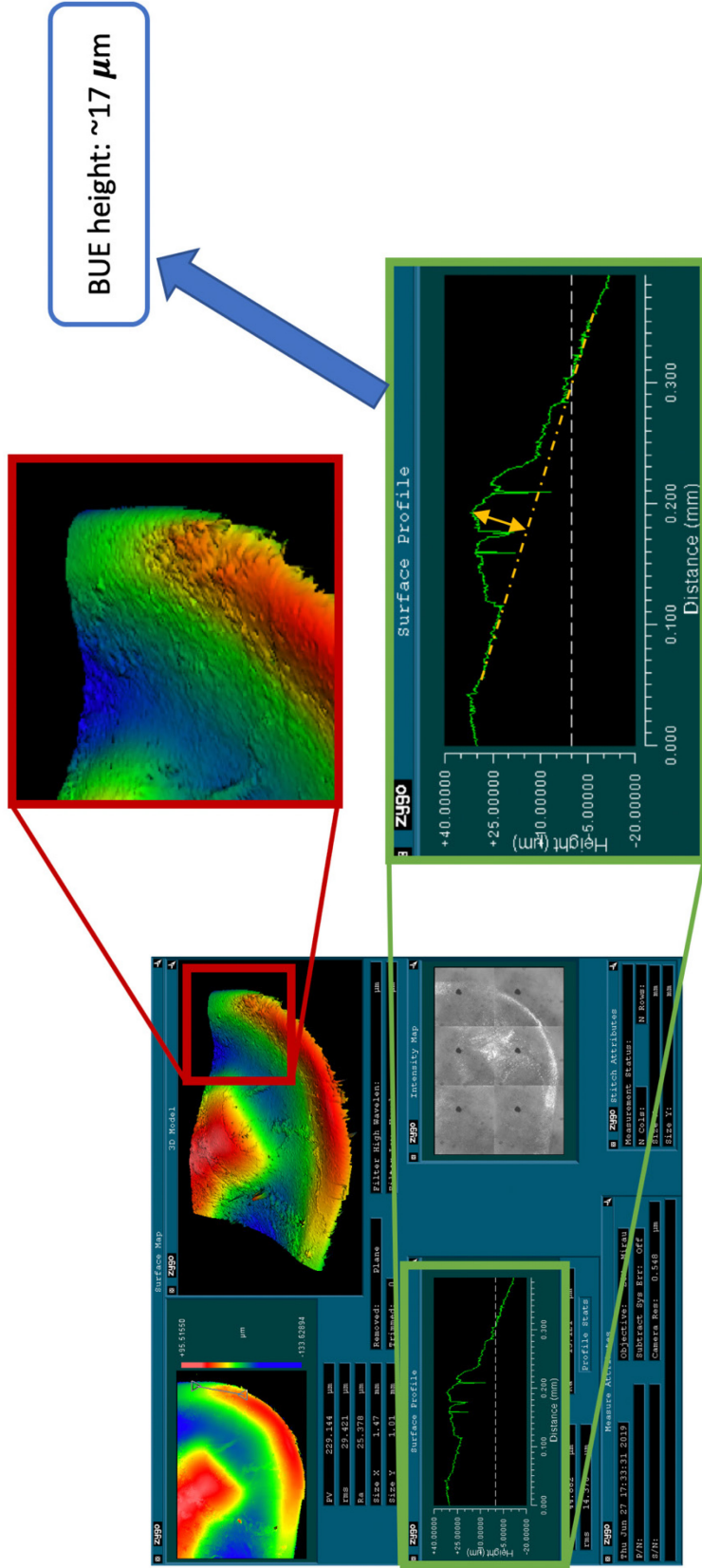
Figure 5-6. Left: Zygo image of rake face (insert 3D). Upper right: zoom-in of BUE on cutting edge of tool. Lower right: surface profile of BUE to quantify height.

5.2.3 Plastic Deformation and Deep Groove Wear

It has been stated many times already that machining can generate high temperatures that effect the cutting tool, chips, and workpiece. When materials reach a certain temperature, they are prone to thermal softening. Carbide tool materials are no exception to this. The combination of thermal softening and compressive stresses from material flow over the cutting tool, results in plastic deformation. Tungsten-carbide cuttings tool are inherently brittle and will therefore chip or fracture due to the low tolerance for bending or plastically deforming to any significant degree.

The cutting tool insert (insert 3D) in Figure 5-7 had a cumulative cut time of 10.4 min when the image was taken. The top-left image in Figure 5-7 shows plastic deformation of the cutting edge as a result of high temperatures and compressive stress. The yellow dotted line represents the original geometry of the cutting tool before plastic deformation occurred. Trent [90] observed similar plastic deformation behavior in carbide tools and found that cracks can generate on the rake face of the tool as a result of the surface being stressed in tension as the edge is depressed.

Deep groove wear can also be observed on the rake face of the carbide tools used in flood-cooled machining experiments. A surface profile of the grooves near the cutting edge shows that the grooves are as wide as 0.1 mm (0.004 in) and as deep as 22 μm (0.0009 in). These grooves are likely to have been formed as a result of the initial cracking from plastic deformation. When the material cracked, small carbide particles from the tool become loose and were dragged across the rake face surface by flow of workpiece material. The combination of nose wear, built-up edge, plastic deformation, and deep groove wear can lead to the ultimate weakening of the tool, causing catastrophic failure.
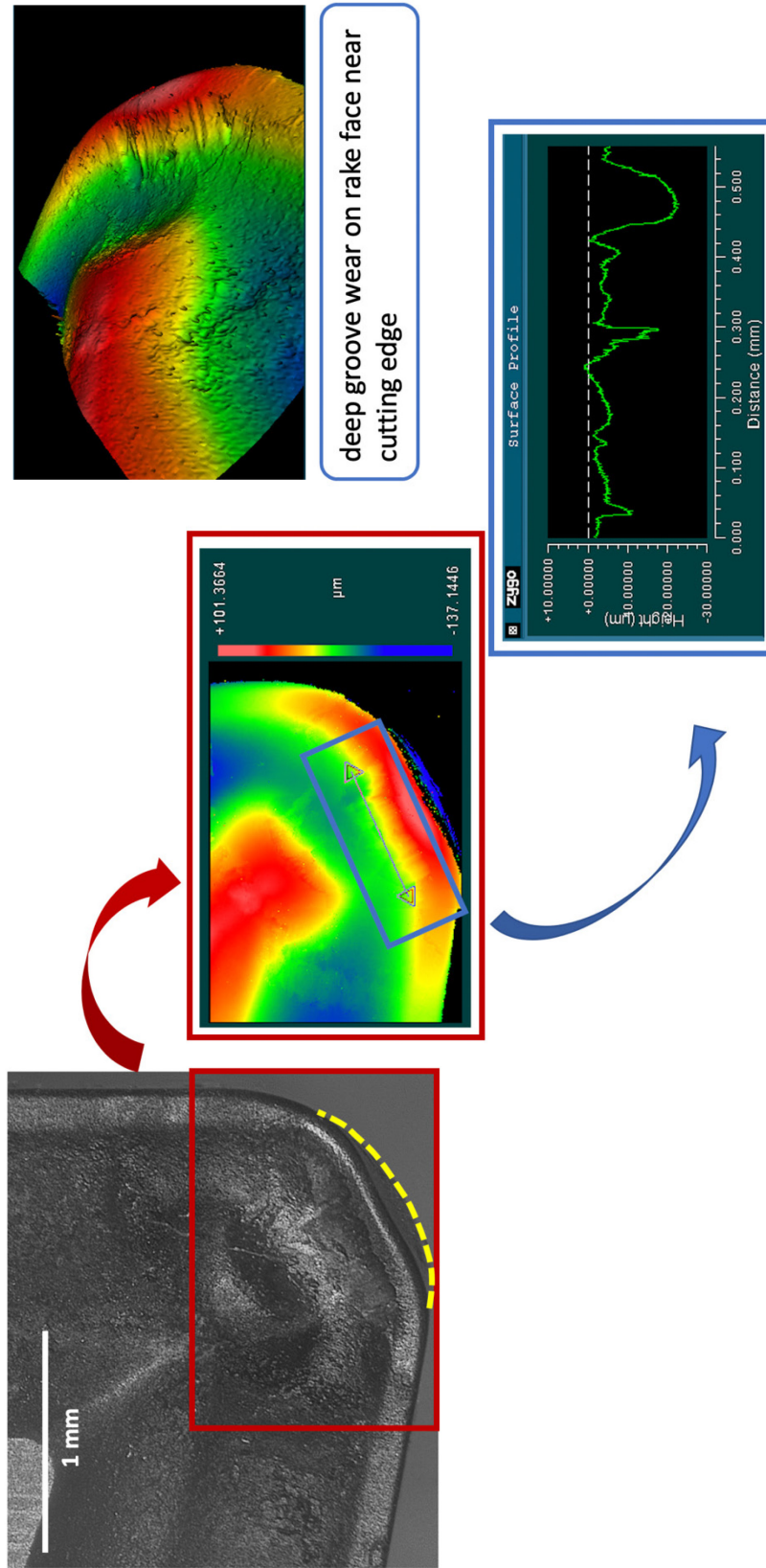
Figure 5-7. Upper left: optical microscope image of cutting tool (insert 3D) rake face. Middle: zygo image of rake face with surface profile (bottom right) quantifying deep groove wear near the cutting edge. Upper right: qualitative zygo image showing detail of deep groove wear on rake face near cutting edge.

5.2.4 Worn Tool and Cutting Forces

Insert 3D can be seen after catastrophic failure in Figure 5-8. The images on the top-right and bottom-right show the rake face and nose region respectively. Using the dynamometer set up described in Chapter 3, force profiles were obtained for insert 3D under flood-coolant. Figure 5-9 shows the cutting force profiles when the tool was new. From the figure, the top force profile is the tangential force F_y, which acts downward onto the rake face of the tool. The middle force profile is the radial force, F_x. The bottom force profile is the axial force, F_z. It should be noted that the force profiles in Figures 5-9 and 5-10 have been filtered in the Kistler DynoWare software with a low-pass filter at 5 Hz to eliminate noise that is typical when acquiring such data.

It can be observed that the magnitude of each force profile it is fairly consistent with respect to the time because a new cutting tool is used, and no noticeable tool-wear has yet occurred. However, Figure 5-10 shows the cutting force profiles when the tool was approaching catastrophic failure. This is evident by the irregular profiles that start approximately around time equal to 15 seconds according to the x-axes of the plots. Around this time, the profiles change magnitude abruptly. This is likely from a major tool-wear event occurring at that time, such as chipping of the cutting edge. Several other abrupt changes in the force magnitude occur due to other major wear events as time moves forward, this is especially clear in the middle plot, which represents the radial force, F_x, perpendicular to the tool travel direction.

The resultant cutting force is calculated by taking the square root of the sum of the squares of each of the three force components. For the new tool, the mean forces for F_x, F_y, and F_z are 310.2 N, -576.5 N, and 162.5 N respectively. Therefore, the resultant cutting force for the new tool is 674.5 N. For the worn tool that is approaching catastrophic failure, the mean forces for F_x, F_y, and F_z are 733.0 N, -732.9 N, and 386.9 N respectively. Therefore, the resultant cutting force for the worn tool is 1106.4 N. The resultant cutting force of the worn tool increased by nearly 64% from when it was new under flood-cooled conditions.

Understanding the interconnectedness between tool-wear and cutting forces can provide significant value to industry. Having insight to the tool-wear during a machining process without having to stop the process to physically measure the wear on a tool, would be a huge time and money saver in a production environment. Imagine for a moment, a scenario where an operator can be informed precisely when the cutting tool is getting too worn out based on the cutting forces being measured from the machine. Processes could be optimized to get the most life out of the tool while producing a part that is within geometric specifications. This would save machined components from having to be reworked or worse, scrapped because of a ruined surface from a tool that catastrophically failed during machining.

Figure 5-8. Insert 3D images of the rake face and nose before dry machining (top-left and bottom-left respectively); images of rake face and nose after catastrophic failure (top-right and bottom-right respectively).
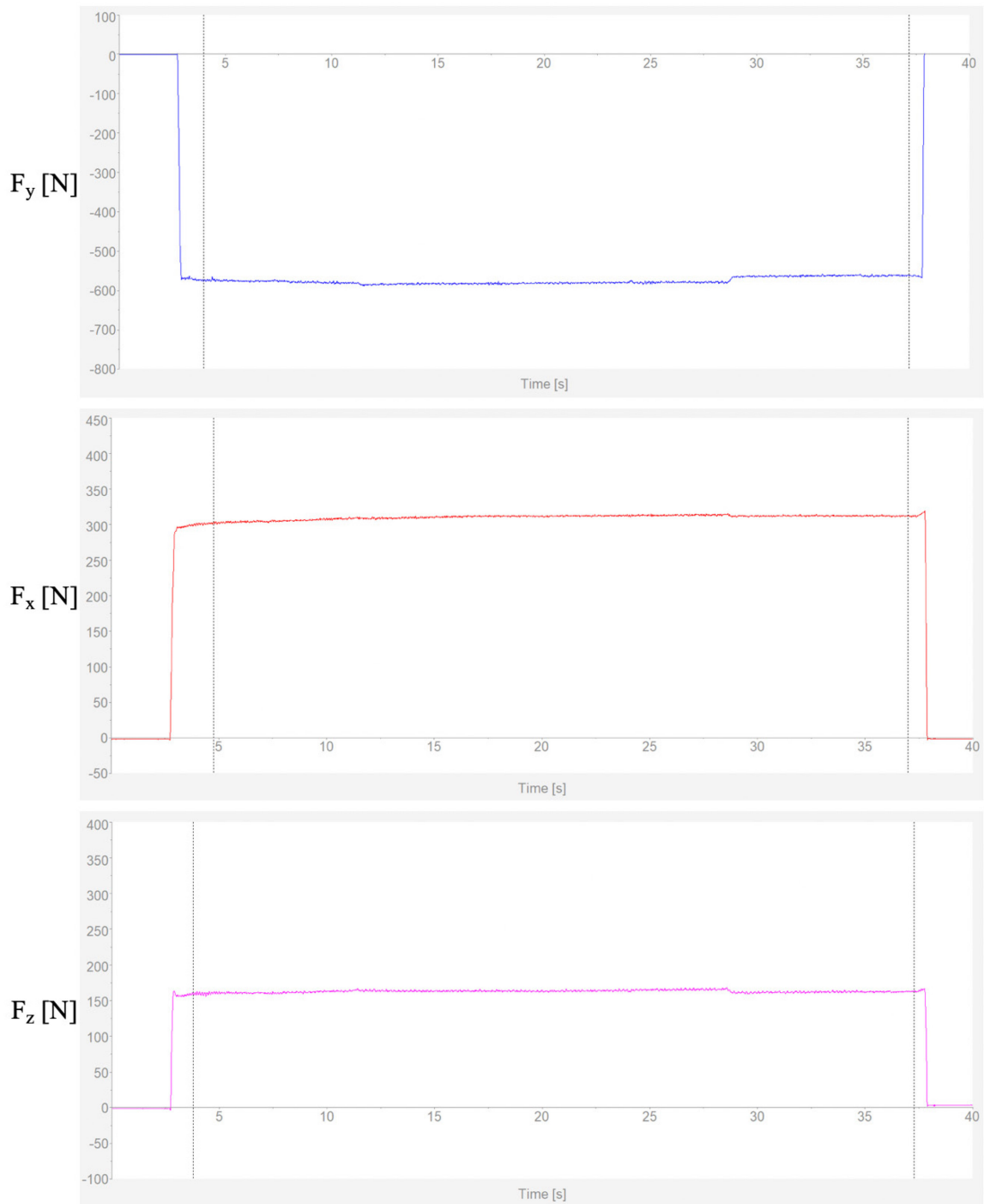
Figure 5-9. Force plots during flood-cooled machining using a new tool (insert 3D). top: F_y, tangential force; middle: F_x, radial force, bottom: F_z, axial force
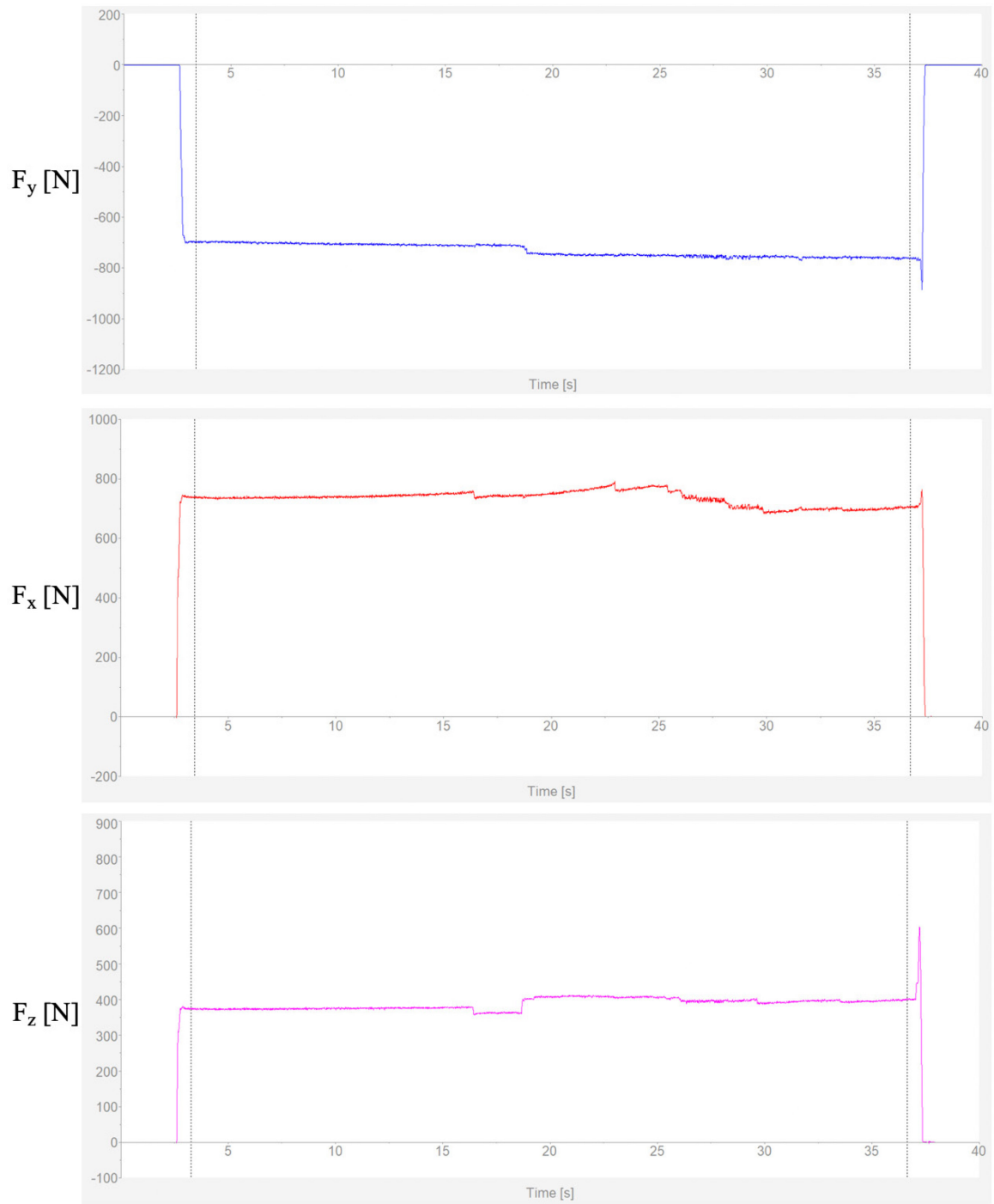
Figure 5-10. Force plots during flood-cooled machining using a worn tool (insert 3D).

top: F_y, tangential force; middle: F_x, radial force, bottom: F_z, axial force

5.3   Dry, MQL, and Cryogenic Cooling Results and Discussion

This section will begin with tool-wear results from dry machining, followed by MQL and then cryogenic machining. Investigative tool-wear experiments under dry machining were conducted in a similar manner as the flood-cooled experiments in the previous section. That is to say, experiments were conducted at fixed parameters for cutting speed, V_c = 122 m/min, feed rate, f = 0.38 mm, and depth of cut, a_p = 0.51 mm. Multiple passes with the cutting tool would be made across the length of the workpiece and after every other pass, the tool would be measured for various tool-wear types until catastrophic failure occurred.

The first test was performed using insert 8A. The two images on the right-hand side of Figure 5-11 show catastrophic failure after approximately one (1) minute of total cut time. Only two passes were made during the test when this occurred. Due to the nature of failure and short life of the tool, tool-wear measurements were not able to be performed properly. It should be noted that the edge hone radius on insert 8A was not measured before the tests.

Due to the unexpected results with insert 8A, three other inserts (3A, 3B, and 3C) were tested under dry conditions. These tests, however, were performed with the high-speed camera setup. The main difference with the high-speed camera setup and the other experiments is that the high-speed camera tests required significantly shorter lengths of cut for each pass to remain in view of the camera. As such, several more passes were able to be made. Regardless, inserts 3A, 3B, and 3C also lasted one to two minutes of cumulative cutting time and experienced the same catastrophic failure. Rather than describing the tool-wear type that occurred during the dry machining, it is more accurate to describe the insert as having experienced catastrophic failure.

The failure of these tools under dry conditions is likely the result of the high cutting temperatures produced during machining without a cooling agent. These high temperatures, as was also seen in the flood-cooled experiments, were enough to cause thermal softening of the tool. The high temperatures combined with high stresses near the cutting edge result in plastic deformation, cracking, and ultimately catastrophic failure of the tool by gross fracture and chipping of the tool. It is also reasonable to expect that a chip

hammering effect due to the cyclical chip-form process caused fatigue in the tool, leading to fracture.

Dry machining experiments with the high-speed camera setup offer interesting insight of the chip-form process at different stages of tool-wear. Plastic deformation can be seen on the tool in the top-left image of Figure 5-12. Despite this, the bottom-left image of that figure shows the chip formation while using the insert in that condition. It is interesting to see the familiar arc shape in the chip. The cumulative cut time on the tool when the two images on the left were taken was 100 seconds.

The two images on the right of Figure 5-12 show the same tool after 104 seconds of cumulative cut time. Catastrophic tool-wear, in the form of mechanical fracture and chipping of the cutting edge, can be seen on the top-right image. The corresponding chip-form can be seen in the bottom-right image. The resulting chip, only four seconds later, is a long ribbon.
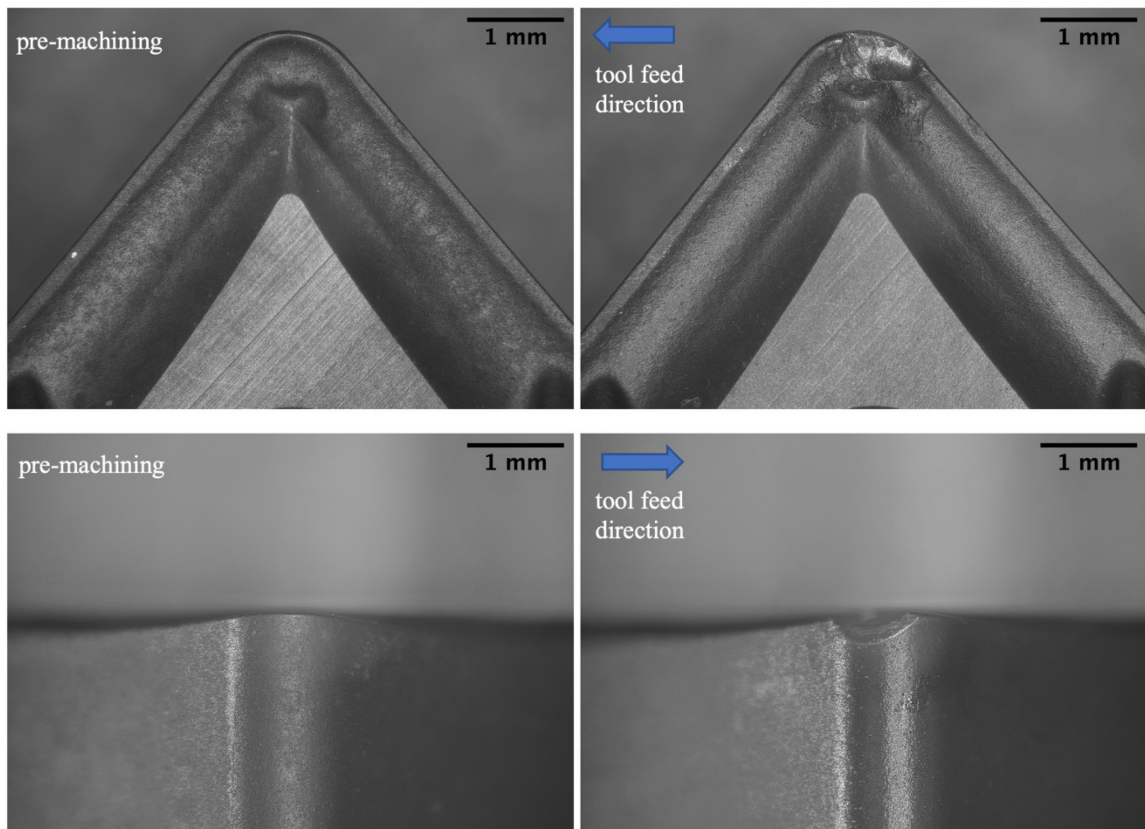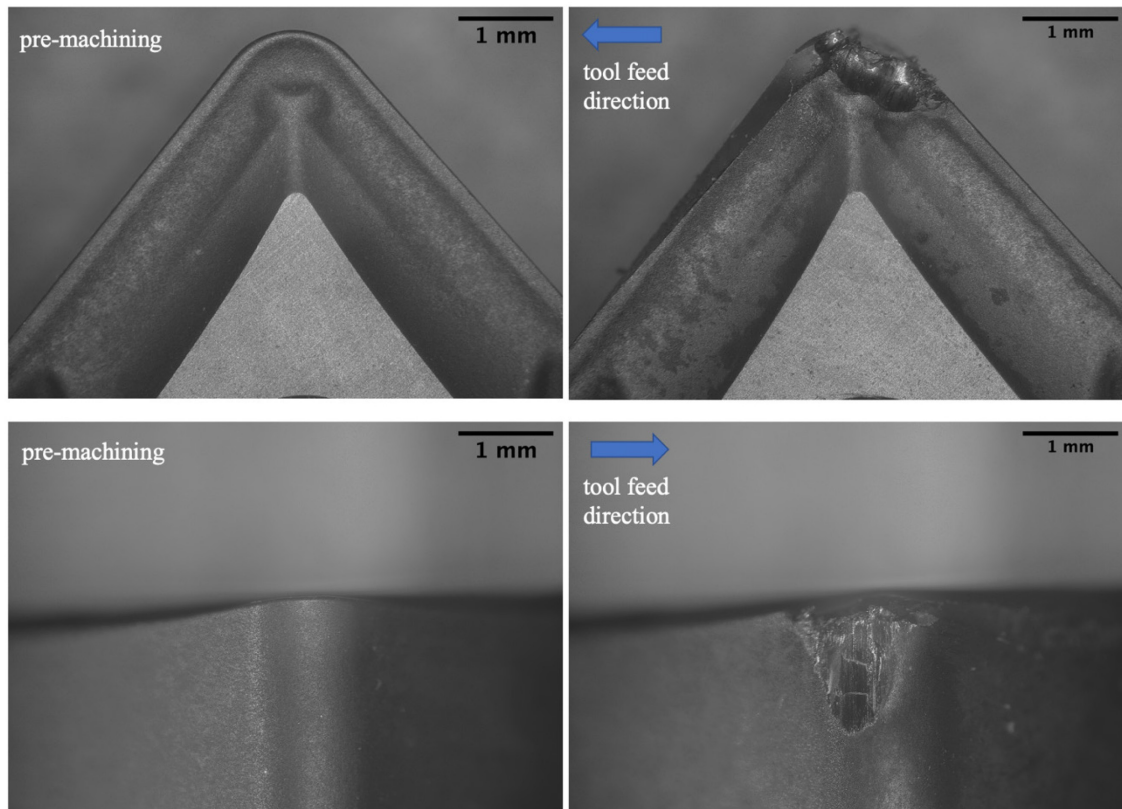

Figure 5-11. Insert 8A images of the rake face and nose before dry machining (top-left and bottom-left respectively); images of rake face and nose after catastrophic failure (top-right and bottom-right respectively).
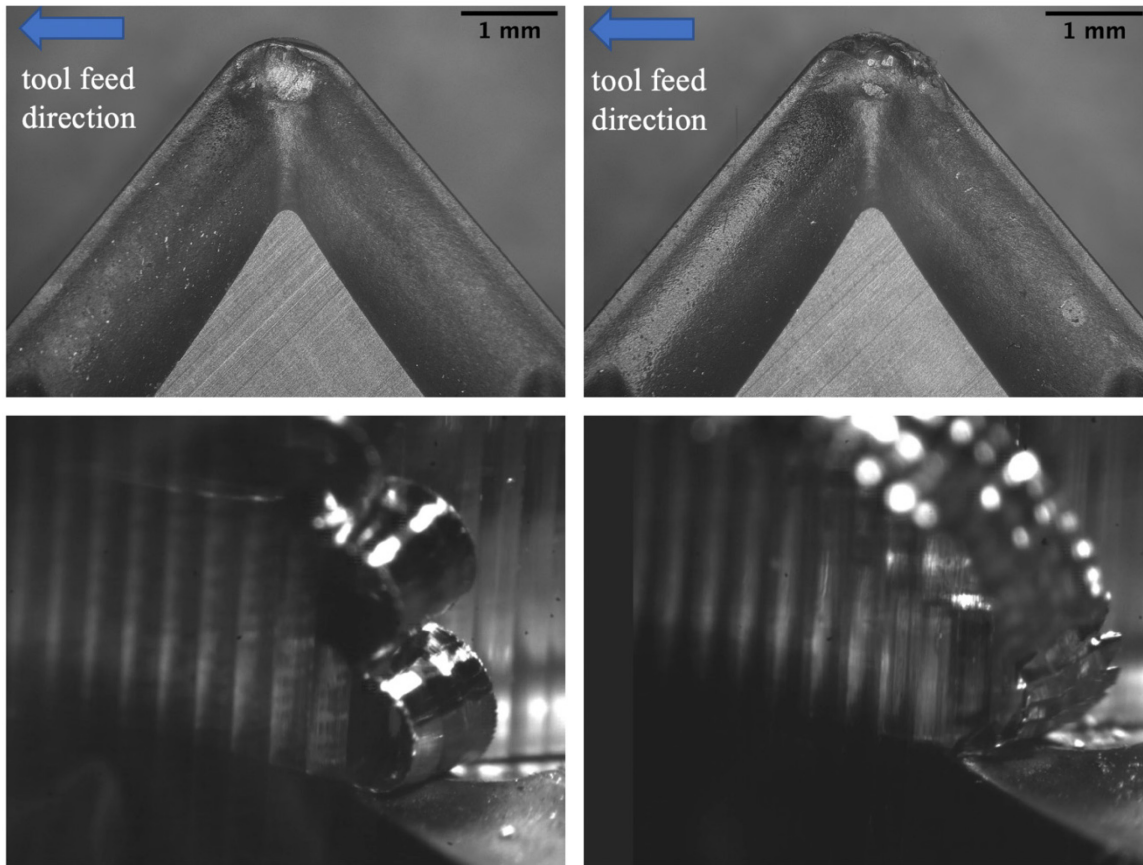
Figure 5-12. Dry machining with high-speed camera. Worn tool (left), forming an arc-shaped chip. Tool after failure (right) forming a ribbon chip

Investigative tool-wear experiments under MQL machining were conducted in a similar manner as the flood-cooled and dry experiments. Cutting speed, V_c = 122 m/min, feed rate, f = 0.38 mm, and depth of cut, a_p = 0.51 mm. Multiple passes with the cutting tool would be made across the length of the workpiece and after every other pass, the tool would be measured for various tool-wear types until catastrophic failure occurred. The first insert used in MQL tests was 2C, and during the first pass, it was obvious, due to the chips being formed and the sound of the process, that the tool was not going to hold up for long. The tool reached catastrophic failure around one minute of cutting as seen in Figure 5-13. To be sure that this was not an unlikely occurrence, another insert (8C) was used under MQL conditions. This insert also did not perform well and catastrophically failed after one minute of cutting.

95

Since MQL is primarily a lubrication technique, with little cooling effect, failure was very similar to that in the dry machining tests. High temperatures, combined with high stresses near the cutting edge, likely resulted in plastic deformation, cracking, and ultimately catastrophic failure of the tool by mechanical fracture and chipping of the cutting edge. Since MQL tests were very short lived, and observations were not made at shorter time intervals, it is difficult to say what other wear types may have been involved. The obvious wear types are mechanical fracture and chipping, which can be observed after each pass of the tool across the workpiece.

Figure 5-13. Tool (insert 2C) used during MQL machining. Top-left and bottom-left: new tool, before machining. Top-right and bottom-right: tool after catastrophic failure

Investigative tool-wear experiments under cryogenic cooling using LN_2 were conducted in a similar manner as the flood-cooled, dry, and MQL experiments. Cutting speed, V_c = 122 m/min, feed rate, f = 0.38 mm, and depth of cut, a_p = 0.51 mm. Multiple passes with the cutting tool would be made across the length of the workpiece and after every other pass, the tool would be measured for various tool-wear types until catastrophic failure occurred.

Insert 1C was used for the initial tests with cryogenic LN_2 applied on the rake face of the tool. After two minutes of cutting, the tool catastrophically failed as shown in Figure 5-14. The wear type from cryogenic machining looks fairly similar to that observed in the case of dry and MQL, where mechanical fracture and chipping of the cutting edge occurred. While this similar wear behavior is observed in the case of cryogenic machining, it is worth considering the super-cool medium being applied to the tool. With an LN_2 application temperature near -196 ºC (-321 ºF), it is plausible that the tool became more brittle and this caused the onset of failure so quickly. To be sure that tool failure under cryogenic conditions was not an unlikely occurrence, another insert (1A) was used under cryogenic conditions with the LN_2 applied on the rake face of the tool. This insert also did not perform well and catastrophically failed after two minutes of cutting.

Previous research in cryogenic machining has applied cryogenic LN_2 in different locations relative to the cutting tool. The first two experiments in this work applied the LN_2 to the rake face of the tool, which is a common application area. Another application area is along the side of the tool flank face, such that the stream of LN_2 is directed at the under-side of the chip as it's being formed. This makes sense as an approach to apply the LN_2 closer to the tip of the cutting tool since there may be less obstruction by the chip that is forming on top of the rake face. Insert 8D was used for this additional test with LN_2 applied along the flank face. After one minute of cutting in this manner, the tool catastrophically failed. Images of inserts 1A and 8D can be seen in Figure 5-15. From the images in Figure 5-15, it can also be seen that workpiece material severely adhered to the tools. This suggests that adhesion could also be a failure mechanism for this tool under cryogenic conditions.

It was stated earlier that adhesion, which is associated with BUE, generally occurs at lower cutting speeds, where temperatures are lower and flow stress is higher. Since

97

cryogenic LN_2 is artificially lowering the temperature near the cutting zone, this could have encouraged a similar material flow behavior, leading to the sever adhesion and ultimate failure.
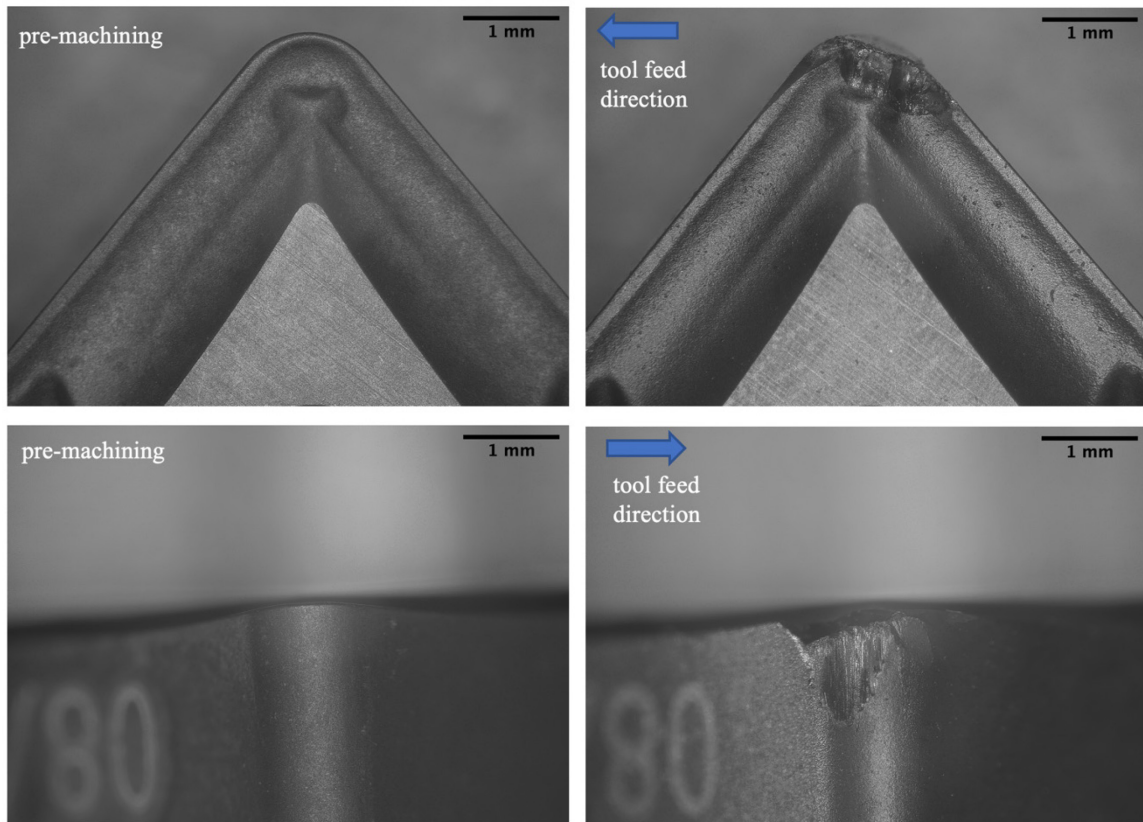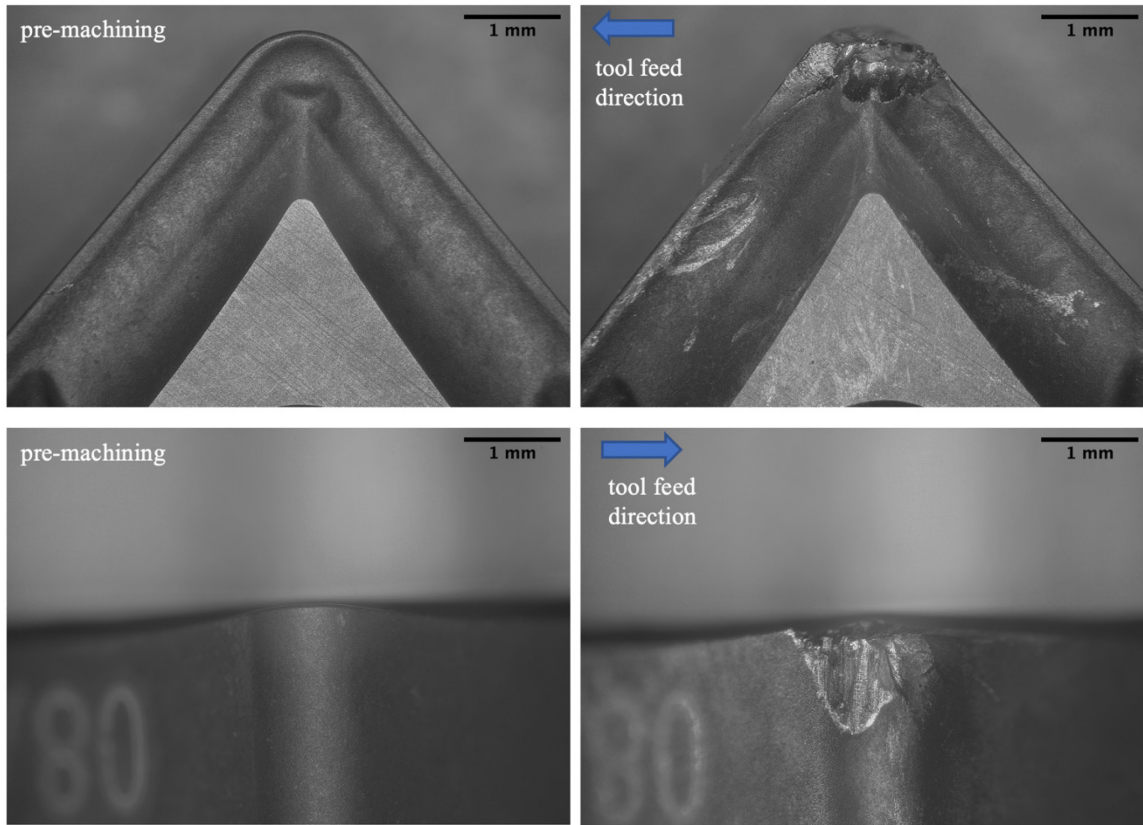

Figure 5-14. Tool (insert 1C) used during cryogenic machining. Top-left and bottom-left: new tool, before machining. Top-right and bottom-right: tool after catastrophic failure
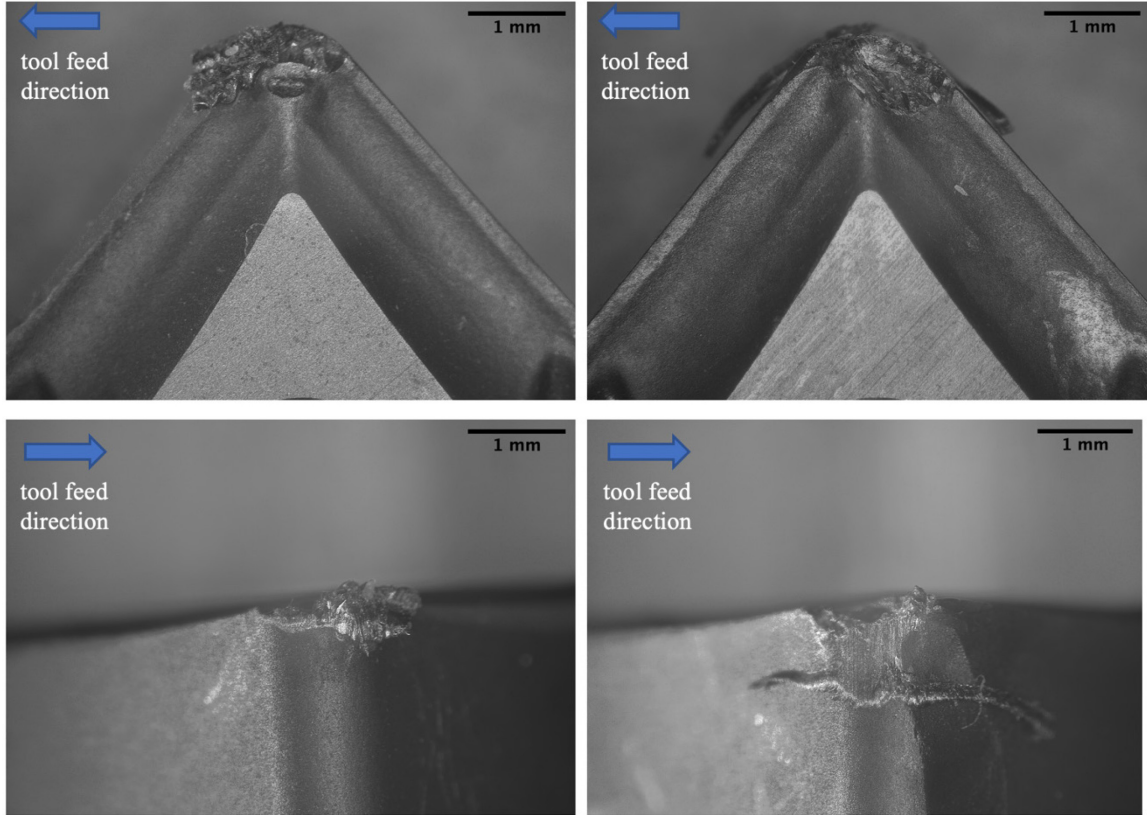
Figure 5-15. Tools used during cryogenic machining showing presence of workpiece material adhesion

5.4   Concluding Remarks

This chapter discussed major wear mechanisms that influence tool-wear during machining. Different tool-wear types, stemming from these major wear mechanisms, were observed during the turning experiments with AF9628. In the case of flood-cooled turning, tool-wear included nose wear, built-up edge, plastic deformation, and groove wear on the rake face of the tool. Nose wear is the result of gradual abrasion of the workpiece material on the nose of the tool. The formation of built-up edge results in the redeposition of material onto the workpiece surface. The temperatures induced during the turning process were high enough to soften the tool material and this, in combination with high compressive stress near the cutting edge, resulted in plastic deformation of the cutting tool. It is believed that this plastic deformation also initiated cracks on the rake face, which may have loosened

carbide particles from the tool material and caused grooves to form on the rake face as they were dragged across the rake face by flowing workpiece material. The combination of nose wear, built-up edge, plastic deformation, and deep groove wear lead to the ultimate weakening of the tool, causing catastrophic failure.

Turning of hardened AF9628 with flood-coolant was the most stable condition explored from a tool-wear perspective. Tool-life curves were generated, and these were ideal. Eventually, chipping of the cutting edge due to mechanical failure resulted in catastrophic failure of the tool. However, in the cases of dry, MQL, and cryogenic machining, sever and rapid tool failure occurred. Tool failure under dry and MQL conditions are likely the result of the high cutting temperatures produced during machining without a cooling agent. These high temperatures, combined with high stresses near the cutting edge, cause thermal softening and result in plastic deformation. As was seen in the flood-cooled tool-wear analysis, cracks likely initiated from the plastic deformation with gross fracture and chipping of the tool following closely after. A chip hammering effect from the cyclical chip-form process may also cause fatigue in the tool, resulting in fracture.

While a similar ultimate tool failure is observed in the case of cryogenic machining, it is worth considering that the tool may became brittle from the super-cool LN_2 being applied. This may have encouraged the onset of mechanical failure such as chipping and fracture. Adhesion of workpiece material on the tool was also observed with cryogenic cooling.

It has been said before that the parameters chosen for chip-form and tool-wear investigation in this study were based on a previous turning study, which only performed flood-cooled machining with carbide tools. Therefore, it is fair to state that the parameters are, to a large degree, designed for flood-cooled turning. As such, the tool-wear results for dry, MQL, and cryogenic cooling under the parameters of this study, and the cutting tool used, are understandably poor. Subsequent studies ought to focus on further investigation of various cutting speeds, feed rates, and depths of cut to determine if turning parameters can be optimized for better tool-life under these alternative cooling and lubrication conditions.

CHAPTER 6
CONCLUSIONS AND FUTURE WORK

If I have seen further, it is by standing upon the shoulders of giants.

- Isaac Newton

6.1   Conclusions

While this work is the first to investigate chip-form and tool-wear in turning of hardened AF9628, there have been many others whom have come before to lay the foundation in understanding these fundamental aspects of machining. This work filled a knowledge gap that existed in classifying chip-form and tool-wear during the turning process of hardened AF9628 alloy and furthermore, discusses the interrelationship to show how chip-form affects tool-wear and how tool-wear consequently affects chip-form.

With regard to chip-form classification, all of the cooling and lubrication conditions explored in this work demonstrated an ability to produce short chips when a new carbide cutting tool is used. Chips were mostly up-curl dominated with new inserts due to the influence of the chip breaker geometry. With regard to tool-wear, flood-cooled turning was the most stable condition investigated under the specific cutting speed, feed rate, and depth-of-cut. Under the flood-cooled turning condition, abrasion and adhesion tool-wear mechanisms were noticeable. Built-up-edge was present on the cutting edge with tools that were relatively new. This was observed with the scanning white light interferometer and during high-speed imaging tests from the appearance of shiny spots, which indicate redeposition of the built-up edge onto the machined surface.

As the flood-cooled tool showed progressive nose wear, the resulting chip-form remained largely unchanged from the mostly up-curl-dominated, arc-shaped chips. However, after several minutes of cutting and chip-flow over the tool, the increasing temperature near the cutting edge caused thermal softening of the tool material. This increase in temperature, along with high stress from the workpiece material flow over the tool, resulted in plastic deformation of the cutting edge. This plastic deformation likely

initiated small cracks on the rake face of the tool. These cracks would loosen carbide particles on the rake face of the tool that the flowing workpiece material could drag across the rake face to create groove wear. The plastic deformation likely increases the tool-chip contact area during turning, which increases the generated heat due to increased friction.

Chip-form appeared largely unchanged once plastic deformation occurred. This was observed in the resulting chips from flood-cooled conditions when plastic deformation occurred in the tool, as well as in dry machining conditions, observed with the high-speed imaging. Since the arc-shaped chips are formed in a cyclical manner, with up to 100 arc-shaped chips being formed every second, this cyclical material flow can cause fatigue near the cutting edge of the tool. This, in combination with the other tool-wear types, resulted in the catastrophic failure of the tool by edge chipping. Cutting force measurements obtained around the time of catastrophic failure of a worn tool (insert 3D) under flood-cooling show that the resultant force increased 64% compared to the resultant force of a new cutting tool under the same condition.

With regard to tool-wear under the alternative conditions of dry, MQL and cryogenic cooling, machining performance was less than desirable. Tool-life in these conditions lasted anywhere from one to two minutes, which is only about one-tenth of the tool-life under flood-coolant. Each cooling and lubrication condition that was investigated in this work, demonstrated that as tools reach the end-of-life due to catastrophic failure, the chips become longer and snarled, which is unfavorable for machining in an industrial setting. The short tool-life experienced under the alternative conditions resulted in limited tool-wear analysis and as such, it is more accurate to describe the tools as having experienced catastrophic failure.

In summary, chip-flow and tool-wear, and the relationship between them, have been investigated, analyzed and discussed under flood-cooled conditions for turning of hardened AF9628. Alternative cooling and lubrication conditions were also investigated, but it was shown that tool-life was less than ideal for practical consideration in an industrial setting. Based on the chip-form and tool-wear observations, further work could be done to investigate different carbide tool grades, coatings, and tool geometry including the chip breaker configurations, etc., which may experience more gradual wear and less likelihood of catastrophic failure. A wider process parameter window could be explored to investigate

how the alternative cooling and lubrication conditions perform under different cutting parameters that may be more properly designed for them. Since tool-wear directly impacts the final geometric tolerances and surface characteristics of the machined workpiece, limiting the types of tool-wear is critical for enhancing final product quality and functional performance of machined components.

6.2   Future Work

The following sub-sections will discuss future work that is related to turning AF9628 and will build upon the findings from this study. As a result of this study and innumerable other prior studies relating to machining performance, future work that need to address much larger machining performance challenges will also be discussed.

6.2.1   Experimentation in a Wider Process Parameter Space

This thesis found that flood-cooled machining is the most effective method for turning AF9628 in a hardened state when compared to dry, MQL, or cryogenic machining under the machining conditions tested with the selected cutting tool. However, it is important to note that machining is a complex process influenced by several factors, many that have not been explored within the scope of this work. A previous machining study performed by TechSolve had varied some of the machining parameters for cutting speed, feed rate, and depth-of-cut, whereas a fixed set of parameters was selected for the current investigation. Also, the parameters during the previous study had only been designed for, and performed under, flood-cooled conditions. As such, it is not a major surprise that flood-cooled machining performed the best in this study.

It is necessary for an extended subsequent work to explore a wider range of these processing parameters (cutting speed, feed rate, and depth-of-cut) that may be better suited for dry, MQL, and cryogenic machining, and using different cutting tools. However, changes to the cutting speed, feed rate, and depth-of-cut will have an effect on productivity and this must be kept in mind. For example, the feed rate used during this study is nearly twice as high as what is used typically in most finish turning operations. Reducing the feed rate by a factor of two will also decrease the productivity (i.e. material removal rate) by a

factor of two. While changing feed rate may improve the tool-life under different conditions, an increased cost due to lost productivity may not outweigh the cost to replace tools twice as often. Experimentation across a wider process parameter space will provide a more complete understanding of the potential benefits of the alternative cooling and lubrication techniques.

6.2.2   Effect of Cutting Tool Edge Geometry on Chip-flow and Tool-wear

The catastrophic failure that was observed during this study was a result of several tool-wear types that ultimately led to chipping of the cutting edge of the tool. In this work, unlike many other machining studies, the cutting tool edge hone radius of several cutting tool edges were measured using scanning white light interferometry prior to experiments to better understand this variable in the cutting tools being used. However, the obtained edge hone radius measurements were an oversimplified characterization since the radius was assumed to be constant, which is rarely the case in reality. Cutting tool geometry, more specifically the cutting edge preparation method and hone geometry that contributes to the overall mechanical strength of the cutting edge, is believed to be an area of tool design that can greatly influence machining aspects such as tool-wear [13, 19] As such, cutting edge geometry characterization has been an area of high interest in the machining research community during the last decade [18, 103]. A robust, high-speed edge geometry characterization technique has recently been developed at the University of Kentucky and this capability should be leveraged in future work [4].

In future work, more advanced characterization of edge hone size and geometry should be performed. To further explore the effect of cutting tool edge geometry on chip-flow and tool-wear in turning AF9628, there exists an alternative cutting tool with the same geometry and chip breaker style as the cutting tool used in this work but with a different carbide grade and coating method and material. The coating method of the alternative tool is chemical vapor deposition (CVD) as opposed to a physical vapor deposition (PVD) coating that was used on the tools in this study. CVD coatings are known to generally be applied to relatively larger edge radii than PVD coatings due to the nature of the coating process. As such, it is hypothesized that the CVD-coated tool, with a larger edge hone

geometry, will exhibit more preferred gradual nose wear and be less likely to experience chipping due to the increased mechanical strength from the larger cutting edge geometry.

6.2.3   Integrated Machining Performance

In 1906, F. W. Taylor published a notable paper entitled "On the Art of Cutting Metals" [86]. In this work, which was the compilation of 26 years of metal cutting experiments by F. W. Taylor, he identified three questions that every machinist who is running a metal-cutting machine must answer every day in the machine shop, namely:

- What tool shall I use?
- What cutting speed shall I use?
- What feed shall I use?

This thesis and the innumerable prior machining studies that have been conducted, clearly demonstrate the need for significant effort and resources. It is common practice when starting a machining research effort to consult with one of many cutting tool manufacturers for recommendations and guidance on proper tool and cutting parameter selection. Then, a process engineer and/or a machine operator spend time on the shop floor, evaluating the many different inserts across a range of cutting speeds, feed rates, depths of cut, and maybe even cooling and lubrication conditions. Eventually, it is determined which cutting tool, and processing parameters work the best based on the application.

As new materials, such as AF9628, are invented and introduced, cutting tool manufacturers develop new tools with more unique geometries that are marketed as being improved versions for the specific application. However, the matter of cutting tool and process parameter selection is complicated and presents a major challenge for industry due to a lack of knowledge on the cutting tool performance for a specified range of machining conditions including coolant/lubrication application. To add to the complexity, many variables that make up a machining system, such as the workpiece material properties, shape and size; the cutting tool material (and coating) properties, runout error, and geometry characteristics, including chip breaker configurations; the machine tool dynamics, power, torque, feed and speed limitations, and the cooling and lubrication medium applied to the process make it more difficult to identify the correct and/or optimal

use of conditions for a given operation. While numerous research groups spend enormous effort into understanding possibly one, or a couple of these basic elements, a serious knowledge gap exists in the ability to understand the total effects of the complex, interconnectedness of these machining system elements.

Interestingly, after over 100 years of machining research, F. W. Taylor's same three questions are still being asked regularly by every process engineer and machinist on the shop floor. Unfortunately, just as these three questions have remained unchanged, the trial-and-error method to answering them has also remained unchanged. Herein lies the problem.

No robust capability exists to help process engineers and machine tool operators identify what insert would be ideal to cut a particular material and under what cutting conditions. A solution to this problem is admittedly very complex. However, even a capability that could provide the 80% solution for determining a good starting place for cutting tool and machining parameter selection would provide immeasurable value to industry and its customers. Therefore, it is of great interest to explore the concept of an integrated machining performance approach that considers the various elements of a machining system.

What will be the answer to Taylor's fundamental, yet complex, questions to move toward a more advanced, future state of machining? It is here that the next chapter is waiting to be written.

REFERENCES

[1]   (n.d.). Retrieved May 21, 2019, from Seco Tools:
        https://www.secotools.com/article/p_02730812?language=en

[2]   Abboud, E., Attia, H., Shi, B., Damir, A., Thomson, V., & Mebrahtu, Y. (2016).
        Residual stresses and surface integrity of Ti-alloys during finish turning –
        guidelines for compressive residual stresses. *Procedia CIRP, 45*, 55-58.

[3]   Abrahams, R. (2016). *U.S. Patent No. 15/160,221.*

[4]   Adeniji, D., Brown, I., & Schoop, J. (draft submitted 12/2019). Robust High-Speed
        Characterization of Asymmetrical Cutting Edge Microgeometries. *Journal of
        Measurement*.

[5]   Adinamis, G., Gorsler, F., & Ontko, N. (2019). Machinability Comparison of
        AF9628 to 4340 Steel for Soft and Hard Turning. *Report No. AFRL-RX-WP-TR-
        2019-0234*. Contract No. FA8650-18-F-5573.

[6]   ASM Handbook. (1991). Volume 4: Heat Treating. *ASM International, 10.*

[7]   Astakhov, V. P. (2005). On the inadequacy of the single-shear plane model of chip
        formation. *International Journal of Mechanical Sciences, 47*(11), 1649-1672.

[8]   Astakhov, V. P. (2010a). Metal cutting theory foundations of near-dry (MQL)
        machining. *International Journal of Machining and Machinability of Materials,
        7*(1/2), 1-16.

[9]   Astakhov, V. P. (2010b). Surface Integrity - Definition and Importance in
        Functional Performance. In *Surface Integrity in Machining* (pp. 1-35). London:
        Springer.

[10]   Bailey, J. A. (1975). Friction in metal machining—mechanical aspects. *Wear,
        31*(2), 243-275.

[11]   Bell, S., Davis, B., Javaid, A., & Essadiqi, E. (2006). Final Report on Refining
        Technologies of Steel. *Technical Report. No. 2004-21(CF)*.

[12]   Bergkamp, L. (2013). *The European Union REACH Regulation for Chemicals:
        Law and Practice.* Oxford: Oxford University Press.

[13]   Bergmann, B., & Grove, T. (2018). Basic principles for the design of cutting edge
        roundings. *CIRP Annals, 67*(1), 73-78.

[14]   Biček, M., Dumont, F., Courbon, C., Pušavec, F., Rech, J., & Kopač, J. (2012).
        Cryogenic machining as an alternative turning process of normalized and hardened
        AISI 52100 bearing steel. *Journal of Materials Processing Technology, 212*(2),
        2609-2618.

[15] Brinksmeier, E., Meyer, D., Huesmann-Cordes, A. G., & Herrmann, C. (2015). Metalworking fluids—mechanisms and performance. *CIRP Annals, 64*(2), 605-628.

[16] Chaudhari, R. G., & Hashimoto, F. (2016). Process controls for surface integrity generated by hard turning. *Procedia CIRP, 45*, 15-18.

[17] de Melo, A. C., Milan, J. C., Silva, M. B., & Machado, Á. R. (2006). Some observations on wear and damages in cemented carbide tools. *Journal of the Brazilian Society of Mechanical Sciences and Engineering, 28*(3), 269-277.

[18] Denkena, B., & Biermann, D. (2014). Cutting edge geometries. *CIRP Annals, 63*(2), 631-653.

[19] Denkena, B., Lucas, A., & Bassett, E. (2011). Effects of the cutting edge microgeometry on tool wear and its thermo-mechanical load. *CIRP annals, 60*(1), 73-76.

[20] Devillez, A., Lesko, S., & Mozer, W. (2004). Cutting tool crater wear measurement with white light interferometry. *Wear, 256*(1-2), 56-65.

[21] Devillez, A., Schneider, F., Dominiak, S., Dudzinski, D., & Larrouquere, D. (2007). Cutting forces and wear in dry machining of Inconel 718 with coated carbide tools. *Wear, 262*(7-8), 931-942.

[22] Dhar, N. R. (2006). Effect of minimum quantity lubrication (MQL) on tool wear and surface roughness in turning AISI-4340 steel. *Journal of materials processing technology, 172*(2), 299-304.

[23] Dilmore, M., & Ruhlman, J. D. (2009). *U.S. Patent No. 7,537,727.*

[24] Emi, T. (2015). Steelmaking Technology for the Last 100 Years: Toward Highly Efficient Mass Production Systems for High Quality Steels. *ISIJ International, 55*(1), 36-66.

[25] Ernst, H. (1938). Physics of metal cutting. *Machining of Metals*, 24.

[26] Fang, N. J. (2001). A universal slip-line model with non-unique solutions for machining with curled chip formation and a restricted contact tool. *International Journal of Mechanical Sciences, 43*(2), 557-580.

[27] Fang, X. D., Fei, J., & Jawahir, I. S. (1996). A hybrid algorithm for predicting chip form/chip breakability in machining. *International Journal of Machine Tools and Manufacture, 36*(10), 1093-1107.

[28] Gerstenmeyer, M., Zanger, F., & Schulze, V. (2016). Complementary Machining–Machining Strategy for Surface Modification. *Procedia CIRP, 45*, 247-250.

[29] Guo, Y. B., Li, W., & Jawahir, I. S. (2009). Surface integrity characterization and prediction in machining of hardened and difficult-to-machine alloys: A state-of-art research review and analysis. *Machining Science and Technology, 13*(4), 437-470.

[30] Han, S., Melkote, S. N., Haluska, M. S., & Watkins, T. R. (2008). White layer formation due to phase transformation in orthogonal machining of AISI 1045 annealed steel. *Materials Science and Engineering: A, 488*(1-2), 195-204.

[31] Hao, Z., Gao, D., Fan, Y., & Han, R. (2011). New observations on tool wear mechanism in dry machining Inconel718. *International Journal of Machine Tools and Manufacture, 51*(12), 973-979.

[32] Hashimoto, F., Chaudhari, R. G., & Melkote, S. N. (2016). Characteristics and Performance of Surfaces Created by Various Finishing Methods. *Procedia CIRP, 45*, 1-6.

[33] Hastings, W. F. (1980). A machining theory for predicting chip geometry, cutting forces etc. from work material properties and cutting conditions. *Proceedings of the Royal Society of London. A. Mathematical and Physical Sciences, 371*(1747), 569-587.

[34] Isakson, S., Sadik, M. I., Malakizadi, A., & Krajnik, P. (2018). Effect of cryogenic cooling and tool wear on surface integrity of turned Ti-6Al-4V. *Procedia CIRP, 71*, 254-259.

[35] Iturbe, A., Hormaetxe, E., Garay, A., & Arrazola, P. J. (2016). Surface integrity analysis when machining inconel 718 with conventional and cryogenic cooling. *Procedia CIRP, 45*, 67-70.

[36] Jawahir, I. S., & Wang, X. (2007). Development of hybrid predictive models and optimization techniques for machining operations. *Journal of Materials Processing Technology, 185*(1-3), 46-59.

[37] Jawahir, I. S., & Zhang, J. P. (1995). An analysis of chip curl development, chip deformation and chip breaking in orthogonal machining. *Transactions-North American Manufacturing Research Institution of SME*, 109-114.

[38] Jawahir, I. S., Attia, H., Biermann, D., Duflou, J., Klocke, F., Meyer, D., . . . Schulze, V. (2016). Cryogenic manufacturing processes. *CIRP annals, 65*(2), 713-736.

[39] Jawahir, I. S., Balaji, A. K., Stevenson, R., & Van Luttervelt, C. A. (1997). Towards predictive modeling and optimization of machining operations. *In Manufacturing Science and Engineering. Proceedings of 1997 ASME International Mechanical Engineering Congress and Exposition*.

[40] Jawahir, I. S., Brinksmeier, E., M'saoubi, R., Aspinwall, D. K., Outeiro, J. C., Meyer, D., . . . Jayal, A. D. (2011). Surface integrity in material removal processes: Recent advances. *CIRP annals, 60*(2), 603-626.

[41]   Jawahir, I. S., Ghosh, R., Fang, X. D., & Li, P. X. (1995). An investigation of the effects of chip flow on tool-wear in machining with complex grooved tools. *Wear, 184*(2), 145-154.

[42]   Jawahir, I. S., Li, P. X., Gosh, R., & Exner, E. L. (1995). A new parametric approach for the assessment of comprehensive tool wear in coated grooved tools. *CIRP annals, 44*(1), 49-54.

[43]   Jawahir, I. S., Puleo, D. A., & Schoop, J. (2016). Cryogenic machining of biomedical implant materials for improved functional performance, life and sustainability. *Procedia CIRP, 46*, 7-14.

[44]   Karasik, B., Maloney, T., Mannan, N., Matysek, M., & Quitter, J. (2019). Manufacturing Technology Innovation for Cost Reduction. *DTIC Accession No. AD1083580*. Contract No. FA8650-14-C-5517.

[45]   Kaynak, Y. (2014). Evaluation of machining performance in cryogenic machining of Inconel 718 and comparison with dry and MQL machining. *The International Journal of Advanced Manufacturing Technology, 72*(5-8), 919-933.

[46]   Kaynak, Y., Karaca, H. E., Noebe, R. D., & Jawahir, I. S. (2013). Tool-wear analysis in cryogenic machining of NiTi shape memory alloys: A comparison of tool-wear performance with dry and MQL machining. *Wear, 306*(1-2), 51-63.

[47]   Kaynak, Y., Robertson, S. W., Karaca, H. E., & Jawahir, I. S. (2015). Progressive tool-wear in machining of room-temperature austenitic NiTi alloys: The influence of cooling/lubricating, melting, and heat treatment conditions. *Journal of Materials Processing Technology, 215*, 95-104.

[48]   Klocke, F., & Eisenblätter, G. (1997). Dry cutting. *Cirp Annals, 46*(2), 519-526.

[49]   Knight, W. A., & Boothroyd, G. (2005). *Fundamentals of Machining and Machine Tools* (3 ed.). Boca Rotan, FL: CRC Press.

[50]   Kopeliovich, D. (2012a). *Electric Arc Furnaces*. Retrieved September 6, 2018, from SubsTech (Substances & Technologies): http://www.substech.com/dokuwiki/doku.php?id=electric_arc_ furnace_eaf

[51]   Kopeliovich, D. (2012b). *Ladle Refining*. Retrieved September 6, 2018, from SubsTech (Substances & Technologies): http://www.substech.com/dokuwiki/doku.php?id=ladle_refining

[52]   Kor, G. J., & Glaws, P. C. (1998). Ladle refining and vacuum degassing. *The Making, Shaping and Treating of Steel, Steelmaking & Refining Volume, 11th Ed.*, 661-713.

[53]   Mabrouki, T., & Rigal, J. F. (2006). A contribution to a qualitative understanding of thermo-mechanical effects during chip formation in hard turning. *Journal of Materials Processing Technology, 176*(1-3), 214-221.

[54] Marksberry, P. W., & Jawahir, I. S. (2008). A comprehensive tool-wear/tool-life performance model in the evaluation of NDM (near dry machining) for sustainable manufacturing. *International Journal of Machine Tools and Manufacture, 48*(7-8), 878-886.

[55] Maruda, R. W., Krolczyk, G. M., Feldshtein, E., Pusavec, F., Szydlowski, M., Legutko, S., & Sobczak-Kupiec, A. (2016). A study on droplets sizes, their distribution and heat exchange for minimum quantity cooling lubrication (MQCL). *International Journal of Machine Tools and Manufacture, 100*, 81-92.

[56] Merchant, M. E. (1945a). Mechanics of the metal cutting process. I. Orthogonal cutting and a type 2 chip. *Journal of applied physics, 16*(5), 267-275.

[57] Merchant, M. E. (1945b). Mechanics of the metal cutting process. II. Plasticity conditions in orthogonal cutting. *Journal of applied physics, 16*(6), 318-324.

[58] *Modern Metal Cutting: A Practical Handbook.* (1996). Sandvik Coromant.

[59] Morehead, M. D., Huang, Y., & Luo, J. (2007). Chip morphology characterization and modeling in machining hardened 52100 steels. *Machining science and technology, 11*(3), 335-354.

[60] M'Saoubi, R., Outeiro, J. C., Chandrasekaran, H., Dillon Jr, O. W., & Jawahir, I. S. (2008). A review of surface integrity in machining and its impact on functional performance and life of machined products. *International Journal of Sustainable Manufacturing, 1*(1-2), 203-236.

[61] Nouari, M., & Ginting, A. (2006). Wear characteristics and performance of multi-layer CVD-coated alloyed carbide tool in dry end milling of titanium alloy. *Surface and Coatings Technology, 200*(18-19), 5663-5676.

[62] Ohashi, N. (1992). Modern steelmaking. *American Scientist, 80*(6), 540-555.

[63] Oxley, P. L. (1998). Development and application of a predictive machining theory. *Machining Science and Technology, 2*(2), 165-189.

[64] Palmer, W. B., & Oxley, P. L. (1959). Mechanics of orthogonal machining. *Proceedings of the Institution of Mechanical Engineers, 173*(1), 623-654.

[65] Piispanen, V. (1937). Lastunmuodostumisen teoriaa. *Teknillinen Aikakauslehti, 27*(9), 315-322.

[66] Piispanen, V. (1948). Theory of formation of metal chips. *Journal of Applied Physics, 19*(10), 876-881.

[67] Poulachon, G. R., & Moisan, A. L. (1999). Hard turning: Chip Formation Mechanisms and Metallurgical Aspects. *J. Manuf. Sci. Eng., 122*(3), 406-412.

[68] Poulachon, G., Moisan, A., & Jawahir, I. S. (2001). On modelling the influence of thermo-mechanical behavior in chip formation during hard turning of 100Cr6 bearing steel. *CIRP Annals, 50*(1), 31-36.

[69] Pu, Z., Outeiro, J. C., Batista, A. C., Dillon, O. W., Puleo, D. A., & Jawahir, I. S. (2011). Surface Integrity in Dry and Cryogenic Machining of AZ31B Mg Alloy with Varying Cutting Edge Radius Tools. *Procedia Engineering, 19*, 282-287.

[70] Ramirez, C., Ismail, A. I., Gendarme, C., Dehmas, M., Aeby-Gautier, E., Poulachon, G., & Rossi, F. (2017). Understanding the diffusion wear mechanisms of WC-10% Co carbide tools during dry machining of titanium alloys. *Wear, 390*, 61-70.

[71] Rech, J., Giovenco, A., Courbon, C., & Cabanettes, F. (2018). Toward a new tribological approach to predict cutting tool wear. *CIRP Annals, 67*(1), 65-68.

[72] Reitz, G. (1919). Die Gro¨sse des geistlichen und ritterschaftlichen Grundbesitzes im ehemaligen Kur-Trier. *Doctoral Thesis*.

[73] Rotella, G., Dillon, O. W., Umbrello, D., Settineri, L., & Jawahir, I. S. (2014). The effects of cooling conditions on surface integrity in machining of Ti6Al4V alloy. *The International Journal of Advanced Manufacturing Technology, 71*(1-4), 47-55.

[74] Schlatter, R. (1972). Melting and Refining Technology of High-Temperature Steels and Superalloys a Review of Recent Process Developments. *Superalloys*, A1-A40.

[75] Schneider, F., Bischof, R., Kirsch, B., Kuhn, C., Müller, R., & Aurich, J. C. (2016). Investigation of Chip Formation and Surface Integrity when micro-cutting cp-Titanium with ultra-fine grain cemented carbide. *Procedia CIRP, 45*, 115-118.

[76] Schoop, J., Ambrosy, F., Zanger, F., Schulze, V., Balk, T. J., & Jawahir, I. S. (2016). Cryogenic machining of porous tungsten for enhanced surface integrity. *Journal of Materials Processing Technology, 229*, 614-621.

[77] Schoop, J., Effgen, M., Balk, T. J., & Jawahir, I. S. (2013). The effects of depth of cut and pre-cooling on surface porosity in cryogenic machining of porous tungsten. *Procedia Cirp, 8*, 357-362.

[78] Shaw, M. C. (2005). *Metal Cutting Principles* (Second ed.). New York: Oxford University Press.

[79] Shaw, M. C., & Vyas, A. (1998). The mechanism of chip formation with hard turning steel. *CIRP Annals, 47*(1), 77-82.

[80] Skerlos, S. J. (2007). Prevention of Metalworking Fluid Pollution: Environmentally Conscious Manufacturing at the Machine Tool. *Environmentally Conscious Manufacturing*, 95-122.

[81] Stanford, M., & Lister, P. M. (2002). The future role of metalworking fluids in metal cutting operations. *Industrial Lubrication and Tribology, 54*(1), 11-19.

[82] *Steel HP 9-4-20*. (n.d.). Retrieved June 19, 2019, from Tech Steel & Materials: https://www.techsteel.net/alloy/steel/hp-9-4-20

[83] Suda, S., Yokota, H., Inasaki, I., & Wakabayashi, T. (2002). A synthetic ester as an optimal cutting fluid for minimal quantity lubrication machining. *CIRP Annals, 51*(1), 95-98.

[84] Sun, Y., Huang, B., Puleo, D. A., & Jawahir, I. S. (2015). Enhanced machinability of Ti-5553 alloy from cryogenic machining: comparison with MQL and flood-cooled machining and modeling. *Procedia Cirp, 31*, 477-482.

[85] Sun, Y., Huang, B., Puleo, D. A., Schoop, J., & Jawahir, I. S. (2016). Improved Surface Integrity from Cryogenic Machining of Ti-6Al-7Nb Alloy for Biomedical Applications. *Procedia CIRP, 45*, 63-66.

[86] Taylor, F. W. (1906). *On the Art of Cutting Metals.* New York: American Society of Mechanical Engineers.

[87] Tolbert, P. E. (1997). Oils and cancer. *Cancer Causes & Control, 8*(3), 386-405.

[88] Tool Life Testing with Single-Point Turning Tools. (1985). ASME, B94.55M.

[89] Tool-life testing with single-point turning Tools. (1993). *2nd Ed*. ISO 3685.

[90] Trent, E. M. (1959). Tool wear and machinability. *Institution of Production Engineers Journal, 38*(3), 105-130.

[91] Trent, E. M. (1988). Metal cutting and the tribology of seizure: I seizure in metal cutting. *Wear, 128*(1), 29-45.

[92] Trent, E. M., & Wright, P. K. (2000). *Metal Cutting.* Woburn, MA: Butterworth-Heinemann.

[93] Umbrello, D., Micari, F., & Jawahir, I. S. (2012). The effects of cryogenic cooling on surface integrity in hard machining: A comparison with dry machining. *CIRP annals, 61*(1), 103-106.

[94] *Vacuum Degassing of Steel*. (2017). Retrieved November 20, 2018, from VAC AERO International: https://vacaero.com/information-resources/vac-aero-training/101401-vacuum-degassing-steel.html

[95] Wang, X., & Jawahir, I. S. (2007). Recent advances in plasticity applications in metal machining: slip-line models for machining with rounded cutting edge restricted contact grooved tools. *International Journal of Machining and Machinability of Materials, 2*(3), 347-360.

[96] Wang, Z. Y., & Rajurkar, K. P. (2000). Cryogenic machining of hard-to-cut materials. *Wear, 239*(2), 168-175.

[97]   Wegman, D. D. (2009). *An Introduction to Premium Melting.* Retrieved September 6, 2018, from Carpenter Technology Corporation: https://www.cartech.com/globalassets/literature-files/carpenterintrotopremiummelting_whitepaper.pdf

[98]   Weinert, K., Inasaki, I., Sutherland, J. W., & Wakabayashi, T. (2004). Dry machining and minimum quantity lubrication. *CIRP annals, 53*(2), 511-537.

[99]   Werda, S., Duchosal, A., Le Quilliec, G., Morandeau, A., & Leroy, R. (2016). Minimum Quantity Lubrication: Influence of the oil nature on surface integrity. *Procedia CIRP, 45*, 287-290.

[100] Whittaker, D. A. (1988). The Effects of Ladle Refining, With and Without Vacuum, on Bearing Steel Quality. *Effect of Steel Manufacturing Processes on the Quality of Bearing Steels. ASTM International.*, 331-347.

[101] Wolf, J., Saldana, C., Maloney, T., Quitter, J., & Von Roemer, J. (2018). Machining Performance and Microstructure Evolution in Milling Advanced Low-Alloy Military-Grade Steel. *In ASME 2018 13th International Manufacturing Science and Engineering Conference.* American Society of Mechanical Engineers Digital Collection.

[102] Wu-Singel, J. (2017). *Low Alloy, High Impact Toughness Steel*. Retrieved June 20, 2019, from TechLink: https://techlinkcenter.org/technologies/low-alloy-high-impact-toughness-steel/

[103] Wyen, C. F., Knapp, W., & Wegener, K. (2012). A new method for the characterisation of rounded cutting edges. *The International Journal of Advanced Manufacturing Technology, 59*(9-12), 899-914.

[104] Ye, G. G., Chen, Y., Xue, S. F., & Dai, L. H. (2014). Critical cutting speed for onset of serrated chip flow in high speed machining. *International Journal of Machine Tools and Manufacture, 86*, 18-33.

VITA

Jason Wolf graduated Cum Laude in 2015, earning a Bachelor's degree with a major in Mechanical Engineering and a minor in Physics, from Cleveland State University in Cleveland, OH, USA. As a non-traditional student during most of his undergraduate studies, Jason worked full-time for three and a half years as a Tool & Die Maker Apprentice at Exact Tool & Die in Cleveland, OH and one and a half years as an Apprentice at the NASA Glenn Research Center also in Cleveland, OH. In 2016, he relocated to southwest Ohio where he has since been a Mechanical Engineer at the Air Force Research Laboratory, Wright-Patterson Air Force Base. In 2018, Jason began graduate studies in the Manufacturing Systems Engineering program at the University of Kentucky in Lexington, KY, USA. In that same year, the Society for Manufacturing Engineers recognized Jason as a 30 under 30 honoree for his early-career contributions as a leader in manufacturing.

LIST OF PUBLICATIONS AND PRESENTATIONS

1. **Wolf, J.**, Saldana, C., Maloney, T., Quitter, J., & Von Roemer, J. (2018). "**Machining Performance and Microstructure Evolution in Milling Advanced Low-Alloy Military-Grade Steel.**" Paper presented at the *ASME 2018 13th International Manufacturing Science and Engineering Conference*. American Society of Mechanical Engineers, College Station, TX.

2. **Wolf, J.**, Shelley, E., & Stralka, D. (2016). "**Design of an Engine Air Particle Separator for Unmanned Aerial Vehicle Applications.**" Paper presented at the *54th AIAA Aerospace Sciences Meeting*, San Diego, CA.

3. **Wolf, J.**, & Zhang, W. (2015). "**Visualization of Air Particle Dynamics in an Engine Inertial Particle Separator.**" Presentation at the *APS Division of Fluid Dynamics Meeting*, Boston, MA.